Fundamental Studies on the Extraction of Rare Earth Elements from Ion Adsorption Clays

Oznur Onel

Dissertation submitted to the faculty of the Virginia Polytechnic Institute and State University in partial fulfillment of the requirements for the degree of

Doctor of Philosophy
In
Mining Engineering

Roe-Hoan Yoon, Chair
Christopher A. Noble
Bahareh Nojabaei
Kaiwu Huang

September 20, 2023
Blacksburg, Virginia

Keywords: rare earth elements, ion adsorption clays, ion exchange leaching, kaolinite, surface force

Fundamental Studies on the Extraction of Rare Earth Elements from Ion Adsorption Clays

Oznur Onel

ABSTRACT

Rare earth elements (REEs) are critically important for high-tech, renewable energy and defense industries. However, rare earth minerals (REMs) are stable compounds, requiring aggressive conditions to decompose them for their extraction and use. One exception is the ion-adsorption clays (IACs) that are mined in South China. They were formed in nature *via* the adsorption of the REE ions on clay minerals; therefore, they can be readily extracted into solution under mild conditions using the ion-exchange leaching process using $(NH_4)_2SO_4$ as lixiviant. It also happens that IACs are the largest source of the heavy rare earth elements (HREEs) that are critical, especially for the defense industry. At present, more than 80% of the HREEs are produced commercially from the IACs mined in Southeast Asia.

The objective of the present research was to study the fundamental mechanisms involved in the formation and processing of IACs using the ion-change leaching process. The first part of the project was the synthesis of IACs by contacting kaolinite samples with known concentrations of rare earth chloride ($REECl_3$) solutions at different pHs and analyzing the synthetic IACs for XPS studies. It was found that the REE adsorption on kaolinite stays constant in acidic pHs. At pH 7 and above, adsorption density increases sharply, possibly due to the formation of $REE(OH)_3$ and/or REE(OOH). The IACs formed under these conditions responded well to the ion-exchange leaching process by reducing the pH to below 7.

In the second part of the study, the effect of iron (Fe^{3+}) species co-adsorbing with REEs on the kaolinite surface was studied. Unlike the colloidal phases of IACs formed at pH > 7, the synthetic IACs formed in the presence of iron did not respond to the ion-exchange leaching process using $(NH_4)_2SO_4$ as lixiviant. This problem has been solved by subjecting the synthetic IACs to a reducing condition to convert the Fe^{3+} to soluble Fe^{2+} species at pH < 7.

The driving force for the standard exchange leaching process is the large differences between the hydration enthalpies of the Ln^{3+} ions that are in the range of -3,400 kJ/mole and that of the NH_4^+ ions (-320 kJ/mole). In the present work, alkylammonium ions ($C_nH_{2n}NH_4^+$) of varying chain lengths were used as novel lixiviants and obtained excellent results. Since these are surface active species, their concentrations in the vicinity of the clay minerals that are negatively charged would be substantially higher than in the bulk. As a result, it was possible to achieve the same level of leaching efficiencies as obtained using ammonium sulfate at approximately ten times lower reagent dosages.

One of the problems associated with extracting REEs from coal-based clays is that the REE concentrations are typically in the range of 300 to 600 ppm, which makes it difficult to extract the critical materials economically using ion-exchange leaching and other processes. As a means to overcome this issue, the REE-bearing particles, including IACs and REMs, were liberated by blunging and subsequently upgraded using the hydrophobic-hydrophilic separation (HHS) process. The results showed that blunging outperformed grinding in liberating the REE-bearing particles from the clayey materials in coal. It was shown that one can improve blunging by increasing the disjoining in the thin liquid films present between clay and other minerals by controlling the double-layer (EDL) forces. These findings should enhance our understanding of the fundamental mechanisms involved in upgrading critical materials and thereby increase the economic viability of REE recovery from coal-based materials.

Fundamental Studies on the Extraction of Rare Earth Elements from Ion Adsorption Clays

Oznur Onel

GENERAL AUDIENCE ABSTRACT

Rare earth elements (REEs) play a vital role in numerous modern industries, advanced technological applications, and defense industries. The United States accounts for about 15 % of the global demand for REEs. However, the country heavily relies on imported Chinese raw materials, creating vulnerability in the U.S. supply chain. REEs are rarely found in concentrations suitable for mining, and in certain cases, extracting and processing conventional REE deposits come with significant environmental hazards. The limited availability of rare earth elements (REEs) raises concerns regarding their production despite their critical role in high-tech industries. Consequently, various federal agencies and private enterprises have recently attempted to identify promising alternative resources due to these complex challenges. REEs have been found in several major coal basins and are evidenced to be associated with coal byproducts such as kaolinite clays–one of the major host materials of IACs.

This research investigates the recovery of rare earth elements (REEs) from clayey materials through various processes. Emphasis is placed on the synthesis of ion-adsorption clays from kaolinite, and the factors influencing the ion-exchange leaching process are being studied. Furthermore, the impact of iron co-adsorption on REE binding to kaolinite is being examined, and reductive leaching is being evaluated as a means to overcome the hindrance caused by iron passivating layers. Novel lixiviants are being tested as alternatives to conventional lixiviant ($(NH_4)_2SO_4$) for REE extraction. The application of hydrophobic-hydrophilic separation techniques for extracting REE-bearing particles from coal clay samples is also being explored, with a comparison made between grinding and blunging processes. Overall, valuable insights into the efficient recovery of REEs from clay minerals are being obtained, contributing to the development of cost-effective and novel approaches for their extraction.

ACKNOWLEDGEMENTS

I am deeply grateful to my supervisor, Dr. Roe-Hoan Yoon, for his unwavering support, guidance, and encouragement throughout my PhD journey. His expert knowledge and insights have been invaluable in helping me to develop as a researcher and to complete this dissertation. I am also grateful to the members of my supervisory committee, Dr. Aaron Noble, Dr. Bahareh Nojabaei and Dr. Kaiwu Huang, for their helpful comments and suggestions.

I am thankful to the professors and researchers at Virginia Tech who have supported me throughout my studies. I would like to express my gratitude to Dr. Emily Sarver for her guidance and support. I am also grateful to Annie Hassall Lawrence who has helped and supported me throughout my time here.

I am grateful to the Department of Energy for providing the financial support that made this research possible. I would also like to thank the participants in my research for their time and willingness to contribute to my work.

I would like to express my appreciation to my colleagues and fellow graduate students who have provided support and friendship during my time at Virginia Tech. I have learned so much from all of you and am grateful to have had the opportunity to work and grow alongside such talented and inspiring individuals.

I will always express my gratitude to my chosen family in the United States, Wayne and Betty Coleman, for their genuine affection and unwavering assistance.

Finally, I would like to acknowledge my beloved family, Nebahat & Dursun Ali Önel and Eylem & Önder Önel, whose unwavering love and support have been the guiding lights of my life. Their belief in my abilities and their encouragement to pursue my passions have been instrumental in helping me reach this point.

Thank you all for your contributions to my research and for helping me complete this journey. I am grateful for the opportunity to pursue my Ph.D. and for all the support and guidance I have received along the way.

Table of Contents

List of Figures

List of Tables

Attributions

Some section of Chapter 2 in this dissertation has been previously published as Feng, X., Onel, O., Council-Troche, M., Noble, A., Yoon, R. H., & Morris, J. R. (2021). A study of rare earth ion-adsorption clays: The speciation of rare earth elements on kaolinite at basic pH. Applied Clay Science, 201, 105920.

Contribution: I was responsible for preparation of all test samples for XPS and leaching tests, designing and running the leaching tests, data analysis, and manuscript composition. Dr. Xu Feng conducted XPS measurements and manuscript composition. McAlister Council-Troche conducted ICP-MS measurements. Dr. Roe-Hoan Yoon, Dr. Aaron Noble and Dr. John Morris were the supervisory authors and were involved in concept formation and manuscript composition.

Some section of Chapter 3 in this dissertation has been previously published as Feng, X., Onel, O., Council-Troche, M., MacCormac, B. L., Noble, A., Yoon, R. H., & Morris, J. R. (2023). Rare earth ion-adsorption clays in the presence of iron at basic pH: Adsorption mechanism and extraction method. Applied Clay Science, 231, 106744.

Contribution: I was responsible for preparation of all test samples for XPS and leaching tests, designing and running the leaching tests, data analysis, and manuscript composition. Dr. Xu Feng conducted XPS measurements and manuscript composition. McAlister Council-Troche conducted ICP-MS measurements. Dr. Roe-Hoan Yoon, Dr. Aaron Noble and Dr. John Morris were the supervisory authors and were involved in concept formation and manuscript composition.

Chapter 5- Concentrate Rare Earth Elements from Coal Clay Using Blunging and Hydrophobic-Hydrophilic Separation Process

Contribution: I was responsible for preparation of the test samples, running of the Blunging and HHS tests and chemical analysis. Dr. Kaiwu Huang conducted to HHS and SEM tests.

Chapters 1, 4, 5 and 6 are unpublished.

Chapter 1. Introduction

1.1 General

Rare earth elements (REEs) are regarded as the vitamins of modern industry. In the periodic table, rare earth elements, also known as lanthanides, are composed of 15 elements identified by their atomic number 57 to 71. The elements scandium and yttrium, which have atomic numbers of 27 and 39, respectively, are also considered rare earth elements due to their similar physical and chemical properties (Feng et al., 2021; Rim et al., 2013; Jorjani and Shahbazi, 2016; Anderson et al., 2017; Zhou et al., 2018; Bryan et al., 2015).

A wide variety of industries rely on REEs, including aerospace and defense, healthcare, clean energy, electronics, transportation, and vehicles, as well as oil refining and chemical manufacturing (Feng et al., 2020; Binnemans et al., 2013; Wang et al., 2017). In the 21st century, rare earth elements have been in growing demand globally. In 2021, the global mine production of rare earth oxides (REOs) was 280,000 metric tons, of which China accounted for 60 %, followed by the U.S. (15.36%), Burma (9.3%), Australia (7.8%), and other countries (7.54%) (USGS Mineral Commodity Summary, 2022). A single country, China, controls more than 80% of global production due to the fact that U.S. mines and many products are shipped to this country for processing.

The rare earth mineral (REM) sources with the highest REE content, such as bastnaesite, monazite, and xenotime, are distributed around the globe. High-grade carbonate and phosphate sources for rare earth elements (REEs) come with elevated recovery costs due to the challenges of mining, separation, beneficiation, and the need for aggressive conditions to dissolve REEs. Bastnasite is typically leached with concentrated H_2SO_4 or HCl, while monazite/xenotime concentrates require baking in either 98% H_2SO_4 or 70% NaOH to render REEs soluble. Alternatively, the ion adsorption clays (IACs) have lower REE content (0.05–0.3% rare earth oxides), but the cost of extracting REE from IACs is relatively low due to the simplicity of the overall process (Feng et al., 2021, Moldoveanu and Papangelakis, 2012; Zhang et al., 2016). Additionally, the main source of heavy rare earth elements (HREE) is ion-adsorption clays found in the regolith formed by weathering of granite (Bao and Zhao, 2008, Sanematsu and Watanabe, 2016). It has been estimated that 40-90% of the REEs are physically adsorbed on layer-structured minerals. Thus, they can be readily extracted with simple ion-exchange leaching without being

subjected to the aggressive conditions required to process rare earth minerals (REMs). A large portion of the world's HREEs is produced from the ion adsorption clays mined in South China (Foley and Ayuso,2015a; Foley and Ayuso,2015b).

Recent studies have identified coal and coal byproducts as potential sources of rare earth elements, alongside the primary sources (bastnaesite, monazite, and xenotime) (Seredin, 1996; McLellan et al., 2014; Hower et al., 2016; Zhang and Honaker, 2018; Huang et al., 2018). Considering the vast amount of coal reserves available and the volumes of byproducts generated during coal mining and processing, coal can be utilized in a way that has the potential to contribute to the U.S. economy and overcome the challenges the rare earth industry faces. Due to the absence of a domestic supply chain, the U.S. is prone to international market interruptions. In this regard, it is extremely important for the United States to establish a rare earth supply chain. In many ways, the limited nature of the current supply chain threatens long-term viability. Upon a nationwide survey of feasible domestic REE sources in the U.S., REEs with grades up to 1,500 ppm have been found in several major coal basins and are evidenced to be associated with coal byproducts such as kaolinite clays–one of the major host materials of IACs (Bryan et al., 2015).

Therefore, in this thesis, we hypothesized that by-products from U.S. coal preparation plants can serve as viable sources of IACs. However, the nature of REE-bearing clays in U.S. coal basins is still poorly understood, which is crucial for the development of targeted extraction processes. The primary objective of the proposed thesis is to investigate the rare earth species on clay surface at various pH values and utilize novel chemicals to recover rare earth elements (REEs) from coal refuse material, specifically clay. In addition, hydrophobic-hydrophilic separation (HHS) tests were conducted to recover REE-bearing particles from a coal clay sample, employing grinding and blunging processes to enhance particle liberation. The results indicate the superiority of blunging over grinding in liberating REE-bearing particles from the clay sample. Analysis of the disjoining pressure isotherm highlights the significant role of the strongly repulsive electrical double-layer (EDL) force in particle liberation during blunging. These findings contribute to our understanding of the mechanisms involved in blunging processes and their efficacy in the recovery of REE-bearing particles from coal clay samples.

1.2 Literature Review

1.2.1 Occurrence and Utilizations of Rare Earth Elements (REEs)

Rare earth elements (REEs) are a group of 17 metallic elements, including 15 lanthanides from lanthanum to lutetium (La–Lu), whose atomic numbers range from 57 to 71, as well as scandium and yttrium, which share similar chemical properties, having the atomic numbers 27 and 39, respectively (Feng et all, 2021; Rim et al., 2013; Jorjani and Shahbazi, 2016; Anderson et al., 2017; Zhou et al., 2018, Zhang et al., 2015).

Table 1.1 Chemical properties of rare earth elements and their applications (Van Gosen et al., 2019).

Element	Symbol	Atomic Number	Example application
Light rare earth elements			
Lanthanum	La	57	Optical glass, nickel-metal-hydride batteries
Cerium	Ce	58	Colored glass (flat panel displays), automobile catalytic converters
Praseodymium	Pr	59	Super-strong magnets, metal alloys, specialty glass, lasers
Neodymium	Nd	60	Permanent magnets
Samarium	Sm	62	Permanent magnets, nuclear reactor control rods, lasers
Europium	Eu	63	Optical fibers, visual displays, lighting
Gadolinium	Gd	64	Shielding in nuclear reactors, X-ray and magnetic resonance imaging scanning systems
Heavy rare earth elements			
Terbium	Tb	65	Visual displays, fuel cells, lighting
Dysprosium	Dy	66	Permanent magnets, lighting
Holmium	Ho	67	Lasers, high-strength magnets, glass coloring
Erbium	Er	68	Glass coloring, fiber optic cables
Thulium	Tm	69	Lasers, portable X-ray machines
Ytterbium	Yb	70	Stainless steel, lasers
Lutetium	Lu	71	Petroleum refining
Yttrium	Y	39	Metal alloys, visual displays, lasers, lighting
Scandium	Sc	21	Aluminium-scandium alloys for aerospace components, radioactive tracing agent in oil refineries

Despite their names, rare earth elements are more abundant than many elements found in the earth's crust (Jordens, 2016; Van Gosen et al., 2017). Although thulium and lutetium are the rarest of rare earth elements, they have an abundance of crystals approximately hundreds of times greater than precious metals. Cerium, yttrium, lanthanum, and neodymium are the most abundant rare earths, contrary to thulium and lutetium. Despite the fact that there are limited amounts of concentrated deposits of rare earths, this results in an inefficient and uneconomical method of production (Fouquet and Martel-Jantin, 2014; McLellan et al., 2014, Talan.,2021).

As a result of their atomic weight, rare earths fall into two distinct groups. Light rare earths (LREEs) consist of elements between lanthanum and gadolinium, while the rest are classified as heavy rare earths (HREEs). HREEs are more valuable than LREEs due to their strategic importance (Van Gosen et al., 2019). On the basis of its similar characteristics to other heavy rare earths, yttrium is included in the heavy rare earth group despite its atomic number of 39. A detailed list of heavy and light rare earths and example applications for each of the rare earth elements are provided in Table 1.1.

As summarized in Table 1.1, rare earth elements can be used for a variety of purposes due to their magnetic, optical, and electrical properties. The rare earths are used for the production of night-vision goggles, communications devices, and GPS systems for the military. In addition, they are used in the development of missile guidance systems, jet engines, and satellites for defense (Van Gosen et al., 2019). The production of computers, cell phones, electric vehicle batteries, and many other electronic devices heavily relies on rare earth elements. Besides being crucial to modern technology, energy, defense, and military industries, they are also highly utilized in glass, oil, automotive, medical, and ceramic industries (Banda et al., 2012; Yoon et al., 2016).

The petroleum and automotive industries commonly utilize lanthanum-based and cerium-based catalysts, while the glass industry utilizes cerium oxide, lanthanum, and lutetium for polishing, color, and optical properties (Van Gosen et al., 2017). The production of permanent magnets from rare earth alloys is an accelerating field, with neodymium being used to produce the strongest magnet, called neodymium iron boron magnet (Uda et al., 2000). Additionally, permanent magnets are used to produce electric motors for hybrid vehicles and wind turbines. Also, gadolinium phosphorous is used for X-ray imaging and medical applications such as MRI,

while yttrium, lanthanum, and praseodymium are used as pigments in ceramics (Akdogan and Ghosh, 2014).

Numerous research studies have provided comprehensive summaries of the occurrence and extraction methods of rare earth elements (Kuzmin et al., 2012; Seredin and Dai, 2012; Zhang et al., 2015; Van phosphorite, 2017; Arbuzov et al., 2018). Rare earths are formed in a variety of ways. Unlike native elemental metals, these metals occur as components of host minerals, such as halides, carbonates, oxides, phosphates, and silicates (Rim et al., 2013; Suli et al., 2017). There are currently more than two hundred rare earth-bearing minerals identified in nature. Considering their REE contents and economic feasibility, bastnaesite, monazite, xenotime and ion-adsorption clays are considered primary sources of rare earth, accounting for over 95% of total rare earth production (Amaral and Morais, 2010; Hidayah and Abidin, 2017; Kanazawa and Kamitani, 2006).

The world's two largest rare earth deposits, located in Mountain Pass (USA) and Bayan Obo (China), are renowned for their abundant reserves of bastnaesite, a mineral known for its high concentration of light rare earth elements. Monazite is generally found in sedimentary rocks, especially in coastal deposits. In South Africa, Australia, Brazil, India, Malaysia, and China, monazite is the most abundant mineral. Brazilian and Indian east coasts are currently the main extraction areas (Van Gosen et al., 2017, Talan, 2021). Xenotime, on the other hand, is extremely rich in heavy rare earths and yttrium (Alex et al., 1998). A large amount of heavy rare earths is also found in Ion Adsorption Clays (typically 300 ppm), which differs from mineral deposits (bastnaesite, monazite, and xenotime), found in granite weathering crust in Southern China in the late 1960s (Wang et al., 2018). The remaining secondary sources are apatite, cheralite, eudialyte, loparite, and phosphorite (Dutta et al., 2016).

1.2.2 Rare Earth Elements Demand in the US and Alternative Resources

Due to the growing population worldwide and the expansion of applications of rare earth elements, their demand is increasing despite decreasing requirements for individual products. It became a major issue in 2011 when rare earth prices almost doubled (Paul and Campbell, 2011; Paulick and Machacek, 2017). Aside from this, as the majority of rare earth deposits are located in China, this poses a serious concern for many countries. In terms of global reserves, China holds approximately 37% while the U.S., India, and Australia hold 1.5%, 5.75%, and 3.3%, respectively

(USGS Mineral Commodity Summary, 2022). In the context of increasing trade tensions between the United States and China, such a high reliance on REE supply from China is extremely detrimental. In this regard, even minor changes to China's REE export policy can result in immeasurable losses for the U.S.

In 2022, the USGS mineral commodity summary estimated the world's rare earth metal reserves at 120 million metric tons, while industrial demand is expected to grow. As of 2019, the rare earth market was valued at $9 billion; by 2024, it is predicted to be worth more than $20 billion (Talan, 2021). A demand increases of 2600% is predicted for some elements, such as dysprosium (Honaker et al., 2018). Neodymium (Nd), terbium (Tb), yttrium (Y), dysprosium (Dy), and europium (Eu) are recognized as critical rare earths by the US Department of Energy for their importance in multiple industries (Bauer et al. 2010; Chu, 2011; Quinn et al., 2015; European Commission, 2020). In response to the depletion of rare earth resources, environmental apprehensions regarding rare earth mining, and China's export restrictions, countries have embarked on research projects aimed at recycling, developing substitutes, and exploring alternative sources. These endeavors are driven by a commitment to comply with environmental regulations while ensuring a sustainable supply of rare earth elements (U.S. Department of Energy, 2011; McLellan et al., 2014; Das et al., 2018; Talan,2021). As a result, the importance of research and development studies has increased significantly.

New operations have been started in India, Brazil, and Vietnam to produce rare earth elements as a byproduct of rutile and zircon production in order to fulfill the demands of the rare earth market (Paulick and Machacek, 2017). A number of new deposits have been discovered, including in Canada, Estonia, and Greenland (Suli et al., 2017). According to Schreiber et al., (2016), 0.59% of total rare earth oxide has been identified in Sweden. During the same period, the Russians began to extract rare earths from magnesia plants while Malaysia extracted REEs from cassiterite (Van Gosen et al., 2017).

Moreover, Mountain Pass in the U.S. and Mount Weld in Australia have been reopened in an effort to boost rare earth production. The U.S. Department of Energy as well as the U.S. Critical Materials Institute support multiple initiatives to develop substitutes for rare earths and other critical materials. Also, bauxite residues (red mud) contain a significant amount of rare earth elements, primarily scandium (Binnemans et al., 2015).

Many research projects are currently being sponsored by the European Union with a particular focus on recycling rare earth metals from permanent magnets, discarded metal alloys, and fluid catalytic cracking catalysts. For instance, rare earth metals are recycled from nickel-metal-hydride batteries by a Belgian company. Similar efforts are being made by the German and French governments to recycle rare earth elements as part of the European supply chain (Van Gosen et al., 2017, Talan.,2021). As an alternative source of rare earth elements, scientists have examined coal and coal byproducts in recent years (Noble and Yoon, 2020; Akdogan and Ghosh, 2014; Hower et al., 2016; Kolker et al., 2017; Das et al., 2018; Huang et al., 2018; Lanzerstorfer, 2018; Lin et al., 2018; Valentim et al., 2019).

1.2.2.1 Rare Earth Elements in the U.S. Coal and Coal By-products

In 2012, NETL determined reserves of REEs in four U.S. coal basins using USGS statistics and other data submitted by state geological surveys. A review of the coal basins identified in the study indicated that the REEs reserves may reach at least 2 million tons, of which over 25% are heavy REEs (Ekmann, 2012). Reports have indicated that coal-based REEs were blindly mined during the coal mining process, and the annual production of mined REEs exceeded 40,000 tons in 2010, almost four times the amount consumed by the US in 2018. Based on these results, US coal might be an attractive option for extracting REEs from coal.

The presence of trace amounts of rare earth elements (REEs) in coal has been established for several decades (Goldschmidt, 1935). Extensive studies have investigated the occurrence and mineralogy of REEs in coal, including notable works by Dai and Finkelman (2018), Seredin and Dai (2012), and Zhang et al. (2015). Concentrations of REEs in coal and coal byproducts range from 300 to 1500 ppm (Blissett et al., 2014; Das et al., 2018). Studies across diverse geological regions report an average REE content of 69 ppm in coal (Eskanazy, 1987; Ketris and Yudovich, 2009; Karayigit et al., 2000; Hu et al., 2006; Wagner and Matiane, 2018; Huang et al., 2019). Furthermore, Das et al. (2018) examined 86 coal ash samples from the United States, revealing a total rare earth concentration ranging between 95 and 520 ppm. Supporting this observation, Lin et al. (2018) and Ekmann (2012) suggest that the Appalachian region holds potential as a rare earth recovery area. Additionally, Yang et al. (2020) found coal refuse piles spanning over 10,000 acres to contain rare earth concentrations ranging from 200 to 500 ppm.

Akdogan and Ghosh (2014) conducted a study on Alaskan coals and ash samples, revealing that the inorganic component of the samples exhibited higher concentrations of rare earth elements (REEs) compared to the organic component. Honaker et al. (2016) further investigated REE distributions in coal and found a correlation between REEs and the incombustible material rather than the combustible carbon. In another study, Honaker et al. (2014) identified monazite, xenotime, and bastnaesite as carriers of REEs in coal, with particle sizes ranging from 1 to 10 microns.

Dai et al. (2014) categorized REEs in coal into five types, including ion-exchangeable, water-soluble, carbonates, aluminum-silicates, and organic matter. Huang et al. (2019) examined various Colombian coal samples and observed significant variations in rare earth element content related to the chemical conditions during coal formation. Additionally, a positive relationship was found between rare earth content and ash content in their study. Pan et al. (2019) investigated coal fly ash samples from China and noted a strong association between the Si/Al ratio and rare earth elements. These studies contribute to our understanding of the distribution and characteristics of REEs in coal, highlighting the varying behavior of REEs in different coal samples and their correlation with specific components and chemical settings.

Harnessing coal by-products for rare earth element manufacturing offers a chance to create a circular economy, transforming discarded materials from one sector into precious assets for another. This strategy advocates for sustainability and optimized resource utilization (Das et al., 2018; Zhou et al., 2018). REEs can be found in coal through various mechanisms, including micro-dispersed minerals, ion-adsorption clays, and chemical bonding with carboxyl and carbonyl groups (Jordens et al., 2013; Zhang et al., 2017; Finkelman et al., 2018). Notably, Finkelman et al. (2018) reported that clay minerals in low-rank coals contain a significant portion of rare earth elements, ranging from 50 to 60%. Additionally, Zhang and Honaker (2019a) observed the presence of a small quantity of ion-exchangeable REEs in bituminous coal samples.

In 2020, Montross et al. investigated REEs in the Central Appalachian coal seam underclay following a series of acid digestion and leaching experiments. As a result of the ion exchange leaching test by using ammonium sulfate, REEs recovered at a maximum rate of 7.5%. Following acid digestion with 1 M HCl, an additional 10-30% of REEs were recovered, while a maximum of 20 % of REEs can be recovered after sulfuric acid leaching subjected to filtrate at 1.2 M. Based on

these results, hydrometallurgy techniques typically employ acid or ion exchange leaching systems for REE recovery (Eterigho-Ikelegbe, et al., 2021; Hamza, H. et al., 2022).

A sustainable process for extracting and recovering REEs from coal or coal byproducts is also essential (Navarro and Zhao, 2014; Valkov et al., 2014). The environmental impact of rare earth mining was not adequately considered until recent years. Nevertheless, modern mining operations and many other industries are increasingly concerned with developing cleaner production (Paul and Campbell, 2011). In this case, ion exchange leaching from IACs is still a better option than traditional acid leaching, as it reduces acid consumption, costs, and environmental issues associated with the mobilization of radioactive materials.

1.2.3 The Formation Process of Ion-Adsorption Clay Deposits

1.2.3.1 REE Enrichment Mechanisms in Clay Minerals

Ion-adsorption clay deposits originate from the chemical weathering of granite, a prominent silicate rock covering approximately 25% of the Earth's surface (Oliva et al., 2003). During this process, the weathering of potassium feldspar in granite by meteoric water containing dissolved CO_2 leads to the formation of kaolinite, as depicted by the following reaction:

$$2KAlSi_3O_8 + 2CO_2 + H_2O \rightarrow Al_2Si_2O_5(OH)_4 + 4K^+ + 4HCO_3^- + 4SiO_2 \quad [1.1]$$

Kaolinite, being the final product, exhibits high stability and constitutes a significant portion of the regolith. Silica released from feldspar is transported by groundwater and accumulates in chert and nodules, or disperses into the oceans where it contributes to the formation of microscopic animal shells. Quartz, another major component of granite, exhibits exceptional resistance to weathering and remains largely unchanged, except for fragmentation. Other constituents of granite, such as muscovite and biotite, undergo chemical transformations to convert into different clay minerals (Velde, 2008).

In warm climates, minerals containing rare earth metals, called accessory minerals, are weathered by meteoric water, releasing lanthanide ions (Ln^{3+}) into soil water. There are some accessory minerals, such as bastnaesite, gadolinite-(Y), dolerite, and apatite, that weather more readily than others, such as fergusonite, monazite, and alunite. The most resistant minerals to weathering are xenotime and zircon (Bao and Zhao, 2008). While most of the REY in ion-

adsorption clays is obtained from the accessory minerals, about 24-28% of REY in granite is obtained directly from the rock-forming minerals.

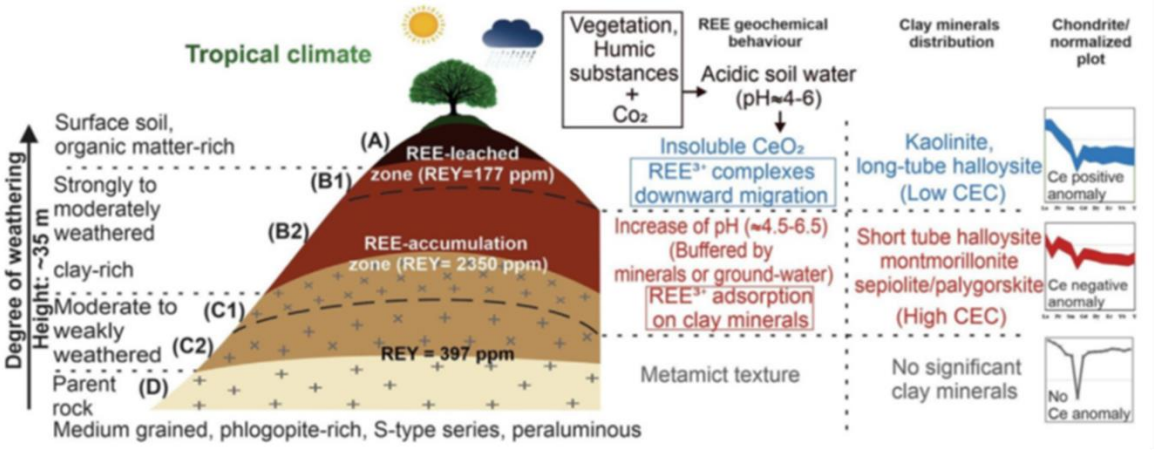

Figure 1.1 Weathering profile of regolith-hosted ion-adsorption clay ore deposit (Sobri et al.,2023) Used under the fair use, 2023.

Figure 1.1 illustrates the typical weathering profile of an ion-adsorption ore deposit hosted within regolith. The profile consists of four different horizons depending on the level of weathering: (Soil) thin humic layer with a thickness of 0-2 m for 25 m thick regolith. It has a dark color and is rich in organic matter and clay minerals. (REE-leached zone) a fully weathered layer, 5-10 m thick. It is of mottled yellowish and orangish red in color, rich in clay minerals (80%) and unaltered minerals (quartz, micas, etc.), (REE-accumulation zone) strongly weathered layer of 2-3 m thick, formed of clay minerals and rock-forming minerals of spotted white and pinkish brown color, (weakly weathered granite) weathering front, interfacing unweathered bedrock (Sobri et al., 2023; Sanematsu and Watanabe 2016, Li et al., 2017, Yang, 1987; Wu et al., 1989; Bao, 1992; Qiu and Bao, 1992).

Furthermore, Figure 1.1 illustrates changes in REE concentration along the profile depth. As shown, the REE concentration in soil zone is low due to the lanthanide (Ln^{3+}) ions being transported to the lower section of the regolith layer by rainwater. The presence of the HCO_3^{2-} ions, and F-ions may act as complexing agents and help the Ln^{3+} ions stay liberated from the rare earth-bearing minerals. Ln^{3+} ions preferentially adsorb on negatively charged substrates with large surface areas offered by clay minerals formed *via* Eq. [1.1] during meteoric water flow through the regolith layer (Li et al., 2017). The particle sizes of the kaolinite and halloysite are in the range of 1-2 μm and 0.5-2μm, respectively (Bao and Zhao, 2008). Chemically, the halloysite is similar

to kaolinite, however, the 1:1 layers are separated by water molecules; hence, its structural formula is $Al(OH)_4Si_2O_5 \cdot nH_2O$.

Kaolinite has a point of zero charge below pH 3 (Wang et al, 2008). Above this pH, Ln^{3+} ions should adsorb on mineral surfaces *via* electrostatic interaction. In the clay mineral, there are two adsorption sites, including i) the basal Si-O-Si surface that is negatively charged due to the isomorphic substitution of the Si^{4+} ions by the Al^{3+} ions, and ii) the Al-OH and Si-OH sites exposed on the edge surfaces. Adsorption of OH^- is possible at the latter sites as follows,

$$Al\text{-}OH + OH^- \rightarrow Al\text{-}(OH)_2^- \quad [1.2]$$

and

$$Si\text{-}OH + OH^- \rightarrow Si\text{-}(OH)_2^+ \quad [1.3]$$

to adopt negative charges at elevated pH levels, the latter sites maintain permanent charges that are unaffected by pH due to their inherent structural characteristics (Velde, 2008).

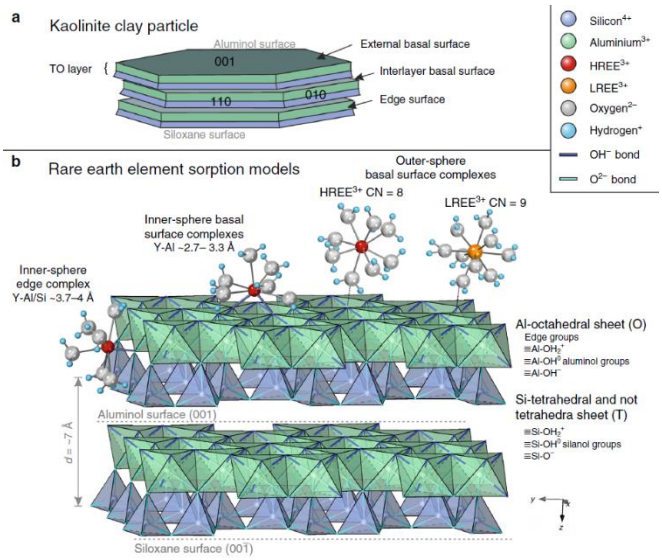

Figure 1.2 A model for REE adsorption on the basal and edge surfaces of kaolinite (Borst et al, 2020) Used under the fair use, 2023.

In 2020, Borst et al. investigated Nd and Y adsorption onto kaolinite using x-ray absorption spectroscopy (XAS) and found that heavy and light Ln^{3+} ions adsorb on the basal surfaces as fully-hydrated ions with eight and nine water molecules, respectively as given in Figure 1.2. The outer-sphere complexes, which are fully hydrated ions, adhere to the basal surfaces of the $AlO_4(OH)_2$ octahedra and the SiO_4 tetrahedra through electrostatic interactions. This interaction makes them

susceptible to displacement by appropriate lixiviants like NH_4^+, as indicated in Equation [1.4]. On the edge surfaces of kaolinite, Ln^{3+} ions can attach as partially hydrated ions to the Al-OH_2^+ and Si-OH_2^+ groups, forming inner-sphere complexes, as described by Velde in 2008. The extraction of inner-sphere complexes through an ion-exchange mechanism is challenging, as noted by Borst et al.

$$\text{Clay-}Ln^{3+} + 3NH_4^+ \rightarrow \text{Clay-}3NH_4^+ + Ln^{3+} \quad [1.4]$$

Previously, it was established that in solutions with a slightly acidic or neutral nature (pH < 6.5-6.8), the majority of ion-exchangeable rare earth elements bind to clay minerals as straightforward cations or hydrated cations, forming species known as 'clay-REE' or 'clay-REE (H_2O_n)' (Bradbury and Baeyens, 2002; Piasecki and Sverjensky, 2008). Conversely, when the pH > 7, the adsorption transpires in the form of 'clay-O-REE^{2+}' species, characterized by irreversible chemisorption (Moldoveanu and Papangelakis, 2016). Consequently, ion exchange leaching procedures are typically conducted within a pH range of 4.0-5.5.

1.2.3.2 REE Fractionation: Mechanisms and Implications

The HREEs are generally considered to be more capable of forming inner-sphere complexes than the LREEs. This is due to the smaller ionic radius associated with lanthanide contraction, particularly at higher pH levels, lower lanthanide concentrations, and lower ionic strengths (Mukai et al., 2020). The adsorption of a full spectrum of REEs on halloysite was investigated by Yang et al. (2019). The findings clearly demonstrated a noteworthy surge in the concentration of ion-exchangeable REEs, escalating from 355 to 775 ppm as the depth increased from 12.6 to 14.9 meters. This trend could be ascribed to factors such as elevated pH, increasing atomic number, and the presence of halloysite within the sample. Conversely, the decline in ion-exchangeable REE concentration observed at greater depths could be attributed to the inclination of these elements to form inner-sphere REE complexes along the edges of clay minerals. These complexes are established through mono- or bidentate oxygen ligands, rendering them more resistant to the process of ion-exchange leaching.

Mukai et al. (2020) employed laser abrasion inductively coupled plasma mass spectrometry (LA-IP-MS) to examine the ion-adsorption clay deposit within the regolith. Within their research, they analyzed individual mineral particles, specifically clay particles, both prior to and following ion-exchange leaching tests. These tests were conducted using a standard lixiviant, $(NH_4)_2SO_4$ at

a concentration of 0.5 M. As a result of the formation of inner-sphere complexes on the edges of clay minerals, nearly half (45.5%) of the REEs remained in the kaolinitic particles after the leaching. Additionally, the study revealed a consistent pattern with the findings of Yang et al. (2019), indicating that the removal of Heavy Rare Earth Elements (HREEs) posed a greater challenge compared to Light Rare Earth Elements (LREEs).

The ratio of LREE/HREE in many IAC ore deposits is known to decrease with increasing depth. This phenomenon has been explained by the fact that LREEs have a greater tendency to bind with clay minerals, enabling smaller HREEs to migrate deeper into the regolith, resulting in fractionation. This theory was first proposed by Bao and Zhao in 2008. However, there appears to be some inconsistency, which could be due to the stronger bonding of HREEs to inorganic and organic ligands, leading to their depletion in the regolith and increased concentration in soil water. Conversely, LREEs tend to hydrolyze at shallower depths and form REE oxides/hydroxides. Consequently, HREEs tend to migrate deeper and adsorb onto clays, as suggested by Li et al. in 2017 and Fu et al. in 2019.

In their 2008 study, Bao and Zhao discovered that the concentration of cerium is greater in the shallow area (0-0.7 m) as opposed to the deeper region (3-4 m). This is attributed to the oxidation of Ce^{3+} to Ce^{4+} ions, which subsequently leads to the creation of a non-soluble mineral known as cerite, resulting in the positive cerium anomaly. Furthermore, the concentration of REE+Y in the B horizon of the regolith-containing IAC ore deposit is 3-4 times higher compared to the original rock, highlighting the significance of IACs as valuable resources.

Physically displacing the outer-sphere Ln^{3+} complex from clay mineral basal surfaces would require only a fraction of the energy required for REE extraction from IACs. As discussed in the previous section, displacing the inner-sphere Ln^{3+} complexes adsorbed to edge surfaces and those chemisorbed at pH > 7 would be more challenging. Borst et al. (2020) reported that at elevated pH values, inner sphere complexes may develop on the Al-OH groups found on the basal surface of kaolinite.

To produce rare earth oxalate precipitates, Ln^{3+} ions are extracted into a solution and precipitated with oxalic acid,

$$2Ln^{3+} + 3H_2C_2O_2 \rightarrow Ln_2(C_2O_4)_3 + 6H^+ \quad [1.5]$$

which is subsequently roasted at 900 ^{o}C,

$$Ln_2(C_2O_4)_3 \rightarrow Ln_2O_3 + 3CO + 3CO_2 \quad [1.6]$$

to attain Ln_2O_3 or rare earth oxides (REO). The equations presented in Eq. [1.4], [1.5]- [1.6] are relatively uncomplicated and do not entail aggressive reactions. In comparison to rare earth minerals like bastnaesite and monazite, ion adsorption clays exhibit a higher prevalence of heavy rare earth elements due to the enrichment mechanisms discussed earlier. Notably, during ion exchange leaching, there is minimal dissolution of thorium (Th) into the solution. As a result of these factors—reduced processing expenses, valuable final products, and the low concentration of Th in the leach solution—IACs contribute to more than 80% of the global production of HREEs. Remarkably, despite comprising merely 1% of the world's rare earth oxide resources, which are estimated at 480 million metric tons according to Zhou et al. (2017), IACs persistently maintain their dominance in HREE production due to the aforementioned benefits.

1.2.4 REE Extraction Technique: Method and Advance

1.2.4.1 Ion-Exchange Leaching Method

REEs have been extracted from ion-adsorption clays using a variety of leaching methods, such as heap leaching, tank leaching, and in-situ leaching (Yang XJ, et al.,2013). Heap leaching is the most common method used for extraction, and involves the use of large piles of ore that are treated with a leaching solution (Papangelakis and Moldoveanu, 2014). Tank leaching is used when ore particles are too small for heap leaching and involves mixing ore with a leaching solution in large tanks (Yang, XJ et al., 2013). In-situ leaching involves injecting a leaching solution into the ore deposit and allowing it to soak into the ore. Currently, in-situ leaching is the most prevalent method of mining due to its ability to perform the process on-site, and requirement to remove less topsoil (Chi et al., 2005; Schüler et al., 2011).

As previously noted, ion adsorption clays form through in-situ weathering of rare earth-rich host rocks like granite. Clay minerals, such as kaolinite, consist of layers with silica (SiO_2) tetrahedra and alumina (Al_2O_3) octahedra. During their formation, some Si^{4+} and Al^{3+} ions in the interconnected polyhedra are substituted by cations with lower formal charges, like Al^{3+} for Si^{4+} and Fe^{2+} for Al^{3+}. This substitution causes the basal surfaces of clay particles to adopt negative charges when immersed in water (Meunier, 2005). In the presence of trivalent rare earth ions like

RE^{3+} in the same water, they bind to the negatively charged basal surfaces, creating ion-adsorption clays rich in rare earth elements. This adsorption process relies on coulombic attractions, allowing them to be easily replaced by other cations based on the charge densities, chemical potentials, and ionic radii of the ions involved (Noble and Yoon, 2020).

In the Jiangxi province, a mining operation was initiated to extract IAC ores, wherein NaCl was utilized as a lixiviant to extract Ln^{3+} ions through the mechanism of ion exchange. The deposits having substantial levels of yttrium content (> 65% of the REEs) have already been extracted. Presently, the mining of ore deposits in the Jiangxi provinces involves yttrium content ranging from 20-30% (Schultze et al., 2017).

The extraction efficiencies (%E) ranged from 40-80%, which correlates with the proportion of ion-exchangeable REEs projected by Chi and Tian (2008). The efficiencies decreased as the atomic number increased, which can be ascribed to the reduction in ionic radii of Ln^{3+} ions owing to lanthanide contraction, thereby resulting in enhanced reactivity. The efficiencies for Ce are particularly low because of the conversion of Ce (III) to Ce (IV) that occurs during the process of weathering.

As demonstrated by the adsorption model in Figure 1.2, Ln^{3+} ions that create outer-sphere complexes on the basal surfaces of clay minerals are easily exchangeable as they are adsorbed physically. On the other hand, those that attach to the edge surfaces by forming inner-sphere complexes are hard to recover because they are chemically adsorbed.

According to Moldoveanu and Papangelakis (2012), the ion-exchange mechanism is based on the enthalpy of hydration (H_{hyd}) data given in Table 1.2. The hydration enthalpies of monovalent cations, such as Li^+, Na^+, NH_4^+, and Cs^+, are nearly ten times less negative than those of Ln^{3+} ions. This suggests that the monovalent ions can displace Ln^{3+} ions from the surface of clay minerals because the hydration enthalpy decreases with increasing cation valence. Moreover, Na^+ ions have a more negative ΔH_{hyd} than NH_4^+ ions. This explains why NH_4^+ ions were preferred as a lixiviant in the early 1980s for ion exchange leaching (Noble and Yoon, 2020).

According to Table 1.2, the radii of the RE^{3+} ions decrease with increasing atomic number, thus resulting in the charge densities of the lanthanide ions increasing (Marcus, 1985). As a result, there exists a stronger inclination for heavier RE^{3+} ions to adhere to clay mineral surfaces compared to lighter counterparts. This phenomenon is the key reason why ion-adsorption clays

serve as the primary reservoir for HREEs. Essentially, clay minerals have persistently acted as discerning attractors for heavy rare earth elements over geological epochs.

Table 1.2 Ionic radii and enthalpies of hydration of cations (Marcus, 1985) Used under the fair use, 2023.

Cation	Ionic Radius (Å)	ΔH_{hyd} (kJ/mol)
La^{3+}	1.06	-3285
Ce^{3+}	1.03	-3340
Pr^{3+}	1.01	-3384
Nd^{3+}	0.99	-3420
Pm^{3+}	0.98	-3445
Sm^{3+}	0.96	-3465
Eu^{3+}	0.95	-3508
Gd^{3+}	0.94	-3522
Tb^{3+}	0.92	-3553
Dy^{3+}	0.91	-3577
Ho^{3+}	0.89	-3621
Er^{3+}	0.88	-3647
Tm^{3+}	0.87	-3668
Yb^{3+}	0.86	-3715
Lu^{3+}	0.85	-3668
Li^{+}	0.68	-520
Na^{+}	0.95	-406
NH_4^{+}	1.48	-322
Cs^{+}	1.69	-276

In the 1970s, ion-adsorption clay ores were processed using 1 M NaCl solutions and the recovered RE^{3+} ions were precipitated with oxalic acid. However, a major issue with this approach was that the quality of the final product was poor, with REO content being less than 70%, primarily due to the co-precipitation of sodium oxalate. During the early 1980s, the mining industry started using 0.3 M $(NH_4)_2SO_4$ as a substitute for 1 M NaCl to extract the RE^{3+} ions from ion-adsorption clay ores. This change in lixiviant resulted in a significant improvement in product quality, with a percentage of > 92% REO, leading to the widespread adoption of the new technique. To minimize water pollution and landslides, the industry has turned to in-situ leaching after decades of intensive

and largely uncontrolled use of $(NH_4)_2SO_4$ in heap and pond leaching (Moldoveanu and Papangelakis, 2016).

According to Xiao et al. (2015), the concentrations of $(NH_4)_2SO_4$ in surface water and groundwater were 3,500-4,000 ppm and 80-160 ppm, respectively, which may be predictable since 7-9 tons of the reagent is used per ton of REO produced. Many investigators are investigating greener lixiviants, which include $MgSO_4$ and $Al_2(SO_4)_3$. In 2020, Noble and Yoon also studied several novel lixiviants as an alternative to $(NH_4)_2SO_4$ to extract heavy and critical REEs from clay and shale associated with coal material.

1.2.4.2 Colloid phase

The rare earths found in the IAC ores in China can be classified into four distinct phases: water-soluble, ion-exchangeable, colloidal sediment (oxides), and mineral phases (Chi et al., 2005). The water-soluble phase is found in extremely low quantities, while the ion-exchangeable phase constitutes approximately 80% of the total rare earths. The remaining rare earths are distributed between the colloid and mineral phases, which together make up approximately 20% of the total rare earths.

The Longnan IAC ore contains a high proportion of HREEs (87%), whereas the Xingfeng and Ninghua ores have lower percentages (44% and 41%, respectively). The colloidal phase of the Longnan ore comprises chemisorbed Ln^{3+} ions that are not eliminated by ion exchange leaching with a 2% $(NH_4)_2SO_4$ solution. Chi et al. described a process that involves leaching the residue of the first step in a 2M HCl solution with a strong reducing agent to identify the colloidal phase. The residue from the second step is roasted at 900 ^oC to transform REMs, like monazite, to Ln_2O_3, then leached with HCl. Finally, the entire ore can be analyzed for comparison after roasting it at 900 ^oC in the presence of Na_2O_2 and NaOH (Chi et al., 2005).

Yanfei et al. (2018) conducted a study to determine the distribution of rare earth elements (REEs) in three different phases of an ion-adsorption clay (IAC) ore sample from the Liutang mine in China. The three phases were residual minerals, colloidal, and ion-exchangeable. The authors used a sequential leaching procedure and analyzed the leach solutions using ICP-IES. They found that the ion-exchangeable phase had the highest concentration of REEs, followed by the residual minerals and colloidal phases. The Ce (IV) compounds in the colloidal phase were insoluble in water, leading to a limited partitioning of Ce (III) into the ion-exchangeable phase. This

phenomenon is referred to as the negative Ce anomaly, as discussed in the previous section. The study suggests that REEs can be extracted from the colloidal phase by using a reducing agent. Overall, their study provides insights into the distribution and potential extraction of REEs in different phases of ore samples (Yanfei et al., 2016; Lai et al., 2018).

The ways in which rare earth elements (REEs) are linked with kaolinite could be similar to those explained earlier for ion-adsorption clays in general. Based on the conducted research, experiments involving ion-exchange leaching were carried out on coal byproducts derived from the Upper Kittanning seam coal waste. The results indicated that employing 1 M $(NH_4)_2SO_4$ as the lixiviant yielded REE recoveries ranging from 72-89 % (Rozelle et al., 2016). Corresponding with Reaction [1.4], the possibility of hydrolysis occurring on the rare earth ions adsorbed onto the clay was observed.

The RE^{3+} ions adhering through coulombic attraction can be readily substituted by Na^+ and NH_4^+ ions via ion exchange. However, replacement with the hydrolysis byproduct, $RE(OH)_3$, isn't feasible. This byproduct constitutes a "colloidal phase" of adsorbed rare earths, exclusively recoverable through acidic leaching, as noted by Moldoveanu and Papangelakis in 2016. Typically, this colloidal phase emerges when the pH surpasses 6-7, with variations dependent on the specific rare earth ions studied. As a result, the optimal pH for traditional ion-exchange leaching is confined to the pH 5.0-5.5 range.

The degree of hydrolysis and the quantity of colloidal phase produced on clay surfaces are likely to differ based on a variety of factors, including weathering conditions, host rock characteristics, pH levels, temperature, pressure, and redox conditions. The ion-exchange clays present in American coals and their accompanying mineral matter may have been formed under distinct conditions compared to those found in the ion adsorption clays of South China.

Voßenkaul and colleagues in 2015 presented a model that demonstrated the different ways in which rare earth elements (REEs) are distributed. The model showed that RE^{3+} ions can be adsorbed by coulombic attraction and can therefore be easily extracted using NH_4^+ ions through simple ion-exchange leaching. The model also illustrated that RE^{3+} ions can form a colloidal phase through hydrolysis and can be present in a crystal lattice, which makes them unable to be extracted by ion-exchange leaching (Voßenkaul et al., 2015).

The presence of alkaline minerals like limestone and dolomite is a common feature in Central Appalachian coals, which implies that the RE^{3+} ions found on the coexisting clay minerals could have undergone hydrolysis. This process would result in the formation of colloidal REEs, which would make it challenging to extract REEs using conventional ion-exchange leaching techniques.

In two separate papers by Lai et al. (2018a and 2018b), ascorbic acid was utilized as a reducing agent to dissolve the colloidal REEs and enhance the efficiency of REE leaching. The mechanism presented in the papers suggests that the colloidal-phase REEs are attached to either iron oxides or cerium oxides/hydroxides. Iron and cerium oxides exhibit varying valences, leading to their solubility being influenced by both pH and Eh. Unlike most other lanthanides that possess a single valence, cerium stands out in this aspect. The Pourbaix diagrams presented in Figure 1.3 by Lai et al. (2018b) demonstrate this occurrence for iron and cerium.

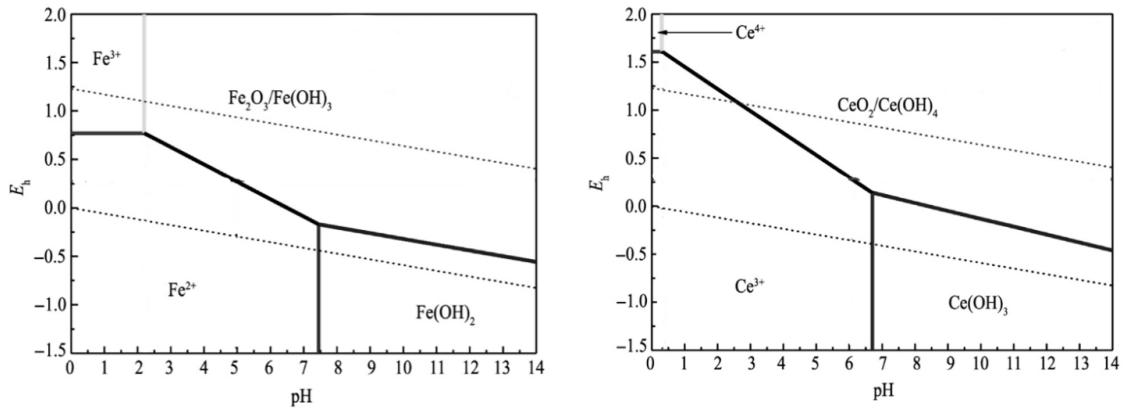

Figure 1.3 pH-Eh diagram for Fe-Ce. (Lai et al., 2018) Used under the fair use, 2023.

The diagrams show that the Fe^{3+} and Ce^{4+} oxides and hydroxides, which are not soluble, can be transformed into their more soluble forms, Fe^{2+} and Ce^{3+}, at pH levels below 6.5. The research papers reveal that ascorbic acid is used to bring about this reduction, and it has been found to substantially enhance the extraction efficiency of REEs from the colloidal sediment phase. In certain instances, the inclusion of ascorbic acid can enhance the extraction efficiency of REEs by 15% to 20% when compared to using only an ion exchange lixiviant (Lai et al., 2018).

1.2.4.3 Effect of Fe

REEs in the ion exchange phase accounts for 60-90% of the total REEs in IACs and can be exchanged on the clay surface by monovalent cations such as NH_4^+ following the Eq. [1.4]. Two main types of colloidal phase have been found on IACs, i.e. REEs bound to FeMn oxides or hydroxides by coordination, and RE oxides or hydroxides that are bonded with or deposited on cerium (IV) oxide (CeO_2) (Chi et al., 2005; Chi et al., 2000; Lai et al., 2018; Xiao et al., 2016; Xiao et al., 2017). The RE^{3+}-Fe/Mn colloid can be effectively dissolved by direct acid leaching or reductive leaching using sulfur dioxide (SO_2) or sodium sulfite (Na_2SO_3) (Chi et al., 2000), while RE^{3+}-CeO_2 only responds to reducing agents such as ferric sulfate ($FeSO_4$) and ascorbic acid (Lai et al., 2018; Xiao et al., 2016; Xiao et al., 2017).

The mineral phase requires more aggressive treatments such as NaOH roasting to liberate REEs into a leaching solution (Chi et al., 2005). Among those elements that co-exist with REEs in U.S. eastern coal and coal byproducts, Fe draws the most interest as it accounts for 1.7 - 9.0 wt. % (17,000 - 90,000 ppm) of the eastern coal waste materials on a dry ash basis (Montross et al., 2020; Zhang and Honaker, 2019).

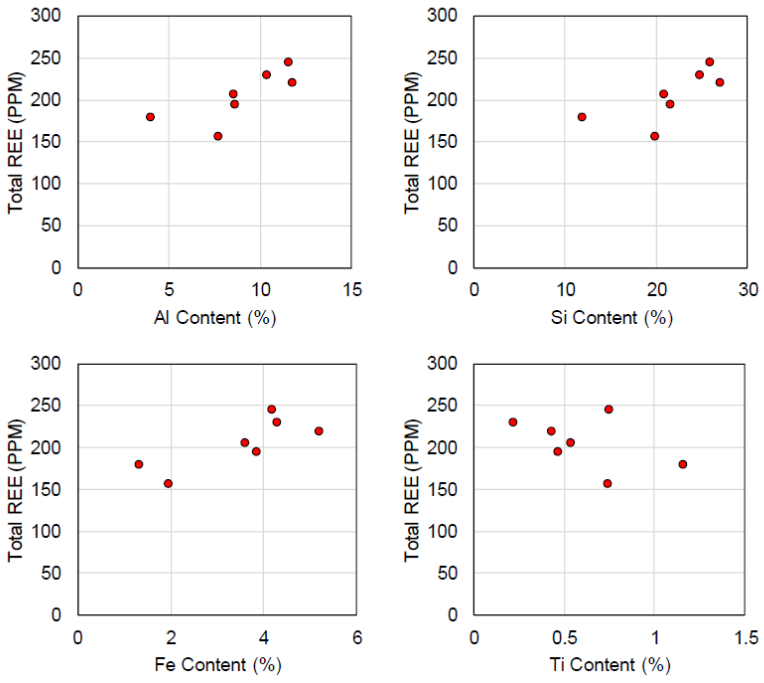

Figure 1.4 Relationship between total REE content and other major constituents (Noble and Yoon, 2020) Used under the fair use, 2023.

The correlation between the total REE content and the content of the four main constituents is illustrated in Figure 1.4. The results indicate that there is a robust positive correlation between REE content and Al, Si, and Fe, whereas a weak negative correlation is observed for Ti, as reported by Noble and Yoon (2020).

1.2.5 Environmental Issues

The majority of heavy rare earth production worldwide is sourced from IAC ores mined in China, but the ore grades have been decreasing, and environmental concerns are growing due to intensive mining. Recovery enhancement and finding nitrogen-free lixiviants have been the focus of research and development efforts to address these issues. The industry achieved high REY recoveries (85-90%) with the heap or pond leaching, but in-situ leaching, which is mandated in South China to minimize environmental impacts, has reduced recoveries to 40-70% (Schulze et al., 2017). The low recoveries observed in ion-exchange leaching may be due to the presence of species that are not ion-exchangeable, including residual and secondary minerals, oxides in the colloidal phase, and those adsorbed via chemisorption (Mukai et al., 2020).

This study explores novel lixiviants to eliminate nitrogen pollution and minimize the generation of Al^{3+} ions in leach liquor, addressing environmental concerns about $(NH_4)_2SO_4$ use. Additionally, ion exchange leaching tests are applied at nearly natural/mid-acidic pH values, reducing acid consumption compared to conventional leaching processes.

1.3 Research Objectives

The main objectives of these studies are to examine the RE-species on the clay surface at various pH values and address the problem caused by colloidal phases. In addition to that application of novel lixiviants on ion exchange leaching from ion adsorption clays was investigated. The dispersive liberation techniques and mechanism of REE-bearing particles was explained.

The specific objectives for this research were as follows:

Chapter 1- Introduction

Chapter 1 gave a brief introduction of the background information and a comprehensive review of the occurrence and application of rare earth elements, the current status of recovering REEs from

coal and coal byproducts, the formation of ion adsorption clay deposits, and the background of the REEs extraction process.

Chapter 2 - A study of rare earth ion-adsorption clays: The speciation of rare earth elements on kaolinite at various pH (some parts of this chapter published in 2021)

Chapter 2 serves as a fundamental study into REE adsorption and speciation on model clay surfaces under acidic/basic pH conditions without the introduction of other ligands and metals that are commonly found on the clay minerals in U.S. coal basins. Kaolinite was used as the model clay for REE adsorption because it is the most common clay mineral found in the U.S. coal basins and one of the primary REE-bearing materials in global IAC deposits.

Besides, Chapter 2 provides a fundamental study into REE adsorption and speciation on kaolinite clay surfaces under basic pH conditions. As well as XPS data, thermodynamic data was used in order to explain the mechanism and a model was proposed to explain ion exchange leaching.

Chapter 3 - A study of rare earth ion-adsorption clays: The effect of iron co-adsorption at various pH (some parts of this chapter published in 2022); SME/MPD Poster Presentation Contest-First Place)

The presence of common co-existing elements in U.S. eastern coal and coal byproducts, such as iron (Fe), calcium (Ca), manganese (Mn) and phosphorus (P) could greatly impact the uptake mechanism and speciation of REEs on clays. So, in Chapter 3, the co-adsorption of Fe with REEs on kaolinite at acidic/basic pH conditions was studied. Powder X-ray diffraction (PXRD), inductively coupled plasma mass spectrometry (ICP-MS), and X-ray photoelectron spectroscopy (XPS) were used to characterize the influence of Fe on the REE adsorption behavior on kaolinite at basic pH and provide insights into the speciation of co-adsorption products on the synthesized REE-Fe-kaolinite. Reductive leaching tests was performed on the REE-Fe-kaolinite to overcome the harmful effect of Fe.

Chapter 4- Effect of Novel Lixiviants on the Leaching Process of Ion Adsorption Type Rare Earth Ore (SME/PCMIA Student Short Presentation Contest -First Place)

Chapter 4, investigated the ion-exchange leaching technology that utilizes novel lixiviants to extract REEs from kaolinite clay. As an alternative to ammonium sulfate, the industry-standard

ion exchange lixiviant, this study explored the usage of alkylammonium ions with varying chain lengths for the ion exchange leaching tests.

Chapter 5- Concentrate Rare Earth Elements from Coal Clay Using Blunging and Hydrophobic-Hydrophilic Separation Process

The objective of the Chapter 5 is to conduct a comprehensive series of bench-scale blunging and hydrophobic-hydrophilic separation (HHS) tests using a decarbonized clay sample obtained from a coal preparation plant. The aim is to investigate the effect of blunging in enhancing the liberation of rare earth element (REE)-bearing particles from gangue minerals.

Chapter 6- Provided a summary of the present work

Bibliography

Anderson, C., Taylor, P., & Anderson, C. (2017). Rare Earth Flotation Fundamentals: A Review. *American Journal of Engineering Research*, 155-166.

Alex, P., Suri, A., & Gupta, C. (1998). Processing of Xenotime Concentrate. *Hydrometallurgy*, 331-338.

Arbuzov, S., Maslov, S., Finkelman, R., Mezhibor, A., Ilenok, S., Blokhin, M., & Peregudina, E. (2018). Modes of Occurrence of Rare Earth Elements in Peat from Western Siberia. *Journal of Geochemical Exploration*, 40-48.

Amaral, J., & Morais, C. (2010). Thorium and Uranium Extraction from Rare Earth Elements in Monazite Sulfuric Acid Liquor Through Solvent Extraction. *Minerals Engineering*, 498-503.

Akdogan, G., & Ghosh, T. (2014). Identification of REE in Soma Alaskan Coal and Ash Samples. Mineral Industry Research Laboratory (MIRL) Institute of Northern Engineering, University of Alaska Fairbanks.

Bao, Z., Zhao, Z., 2008. Geochemistry of mineralization with exchangeable REY in the weathering crusts of granitic rocks in South China. Ore Geol. Rev. 33, 519–535.

Banda, R., Jeon, H., & Lee, M. (2012). Solvent Extraction Separation of Pr and Nd from Chloride Solution Containing La using Cyanex 272 and Its Mixture with Other Extractants. *Separation and Purification Technology*, 481-487.

Bauer, D., Diamond, D., Li, J., Sandalow, D., Telleen, P., Wanner, B., U.S. Department of Energy critical materials strategy. United States: N. p., 2010. Web. doi:10.2172/ 1000846.

Bao, Z.W., 1992. A geochemical study of the granitoid weatheringcrust in Southeast China. Geochimica 21, 166–174 (in Chinesewith English abstract).

Binnemans, K., Jones, P., Blanpain, B., Gerven, T., Yang, Y., Walton, A., & Buchert, M. (2013). Recycling of Rare Earths: A Critical Review. Journal of Cleaner Production, 1-22.

Blissett RS, Smalley N, Rowson NA. An investigation into six coal fly ashes from the United Kingdom and Poland to evaluate rare earth element content. Fuel. 2014 Mar 1; 119:236-9.

Borst, A. M., Smith, M. P., Finch, A. A., Estrade, G., Villanova-de-Benavent, C., Nason, P., and Geraki, K. (2020). Adsorption of rare earth elements in regolith-hosted clay deposits. *Nature communications*, *11*(1), 1-15.

Bradbury, M. H., & Baeyens, B. (2002). Sorption of Eu on Na-and Ca-montmorillonites: experimental investigations and modelling with cation exchange and surface complexation. *Geochimica et Cosmochimica Acta*, *66*(13), 2325-2334.

Bryan, R. C., Richers, D., Andersen, H. T., & Gray, T. (2015). Assessment of rare earth elemental contents in select United States coal basins. *United States National Energy Technology Laboratory*.

Chu S, editor. Critical materials strategy. Diane Publishing; 2011.

Chi, R., & Tian, J. (2008). *Weathered crust elution-deposited rare earth ores*. Nova Science Publishers.

Chi, R., Tian, J., Zhongjun, L., Cui, P., Yuanxin, W., Shirong, L., & Zhiang, Z. (2005). Existing State and Partitioning of Rare Earth on Weathered Ores. *Journal of rare earths*, *23*(6), 756.

Chi, R., Zhu, G., Zhou, Z., Xu, Z., 2000. A novel process for recovering rare earth from weathered black earth. Metall Mater Trans B 31, 191-196.

Das, S., Gaustad, G., Sekar, A., & Williams, E. (2018). Techno-Economic Analysis of Supercritical Extraction of Rare Earth Elements from Coal Ash. *Journal of Cleaner Production*.

Dai, S., & Finkelman, R. (2018). Coal as A Promising Source of Critical Elements: Progress and Future Prospects. *International Journal of Coal Geology*, 155-164.

Dai, S., Seredin, V., Ward, C., Jiang, J., Hower, J., Song, X., Zhao, C. (2014). Composition and Modes of Occurrence of Minerals and Elements in Coal Combustion Products Derived from High-Ge Coals. *International Journal of Coal Geology*, 79-97.

Dutta, T., Kim, K., Uchimiya, M., Kwon, E., Jeon, B., Deep, A., & Yun, S. (2016). Global Demand for Rare Earth Resources and Strategies for Green Mining. Environmental Research, 182-190.

Ekmann, J. (2012). Rare Earth Elements in Coal Deposits - A Prospectivity Analysis. *Search and Discovery*.

Eskanazy, G. (1987). Rare Earth Elements and Yttrium in Lithotypes of Bulgarian Coals. *Org. Geochem.*, 83-89.

Eterigho-Ikelegbe, O., Harrar, H., & Bada, S. (2021). Rare earth elements from coal and coal discard–A review. *Minerals Engineering*, *173*, 107187.

European Commission, 2020. "European Commission, Study on the EU's list of critical raw materials - Final report (2020)".

Feng, X., Onel, O., Council-Troche, M., Noble, A., Yoon, R. H., & Morris, J. R. (2021). A study of rare earth ion-adsorption clays: The speciation of rare earth elements on kaolinite at basic pH. *Applied Clay Science*, *201*, 105920.

Finkelman, R.B., Palmer, C.A., Wang, P., 2018. Quantification of the modes of occurrence of 42 elements in coal. Int. J. Coal Geol. 185, 138–160.

Foley, N., & Ayuso, R. (2015a). REE enrichment in granite-derived regolith deposits of the Southeastern United States: prospective source rocks and accumulation processes. *Geol. Surv. Pap*, *3*, 131-138.

Foley, N., Ayuso, R., Hubbard, B., Bern, C., & Shah, A. (2015b). Geochemical and mineralogical characteristics of REE in granite derived regolith of the Southeastern United States. In *Mineral resources in a sustainable world. Proceedings of the 13th Biennial SGA Meeting* (Vol. 2, pp. 725-729).

Fouquet, Y., & Martel-Jantin, B. (2014). Rare and Strategic Metals. In Y. Fouquet, & D. Lacroix, *Deep Marine Mineral Resources* (pp. 55-64). Springer.

Fu, W., Li, X., Feng, Y., Feng, M., Peng, Z., Yu, H., & Lin, H. (2019). Chemical weathering of S-type granite and formation of rare earth element (REE)-rich regolith in South China: critical control of lithology. *Chemical Geology, 520,* 33-51.

Goldschmidt VM. Rare elements in coal ashes. Industrial & Engineering Chemistry. 1935 Sep;27(9):1100-2.

Hamza, H., Eterigho-Ikelegbe, O., Jibril, A., & Bada, S. O. (2022). Application of the Response Surface Methodology to Optimise the Leaching Process and Recovery of Rare Earth Elements from Discard and Run of Mine Coal. *Minerals*, *12*(8), 938. https://doi.org/10.3390/min12080938

Hidayah, N., & Abidin, S. (2017). The Evolution of Mineral Processing in Extraction of Rare Earth Elements Using Solid-Liquid Extraction over Liquid-Liquid Extraction - A Review. *Minerals Engineering*, 103-113.

Hower, J., Granite, E., Mayfield, D., Lewis, A., & Finkelman, R. (2016). Notes on Contributions to the Science of Rare Earth Element Enrichment in Coal and Coal Combustion Byproducts. *Minerals*, 1-9.

Honaker, R., Zhang, W., Yang, X., & Razaee, M. (2018). Conception of An Integrated Flowsheet for Rare Earth Elements Recovery from Coal Coarse Refuse. Minerals Engineering, 233-240.

Honaker, R., Groppo, J., Bhagavatula, A., Razaee, M., & Zhang, W. (2016). Recovery of Rare Earth Minerals and Elements from Coal and Coal Byproducts. Louisville, KY.

Honaker, R., Hower, J., Eble, C., Weisenfluh, J., Groppo, J., Rezaee, M., & Bhagavatula, A. (2014). Laboratory and Bench-Scale Testing for Rare Earth Elements, Final Project Report.

Hower, J., Granite, E., Mayfield, D., Lewis, A., & Finkelman, R. (2016). Notes on Contributions to the Science of Rare Earth Element Enrichment in Coal and Coal Combustion Byproducts. *Minerals*, 1-9.

Huang, Q., Noble, A., Herbst, J., & Honaker, R. (2018). Liberation and Release of Rare Earth Minerals from Middle Kittanning, Fire Clay, and West Kentucky No. 13 Coal Sources. *Powder Technology*, 242-252.

Huang, Q., Talan, D., Restrepo, J., Baena, O., Kecojevic, V., & Noble, A. (2019). Characterization Study of Rare Earths, Yttrium, and Scandium from Various Colombian Coal Samples and Non-Coal Lithologies. *International Journal of Coal Geology*, 14-26.

Huang, K., & Yoon, R. H. (2019). Surface Forces in the Thin Liquid Films (TLFs) of Water Confined between n-Alkane Drops and Hydrophobic Gold Surfaces. *Langmuir*, *35*(48), 15681-15691.

Hu, J., Zheng, B., Finkelman, R., Wang, B., Wang, M., Li, S., & Wu, D. (2006). Concentration and Distribution of Sixty-One Elements in Coals from DPR Korea. *Fuel*, 679-688.

Jordens A, Cheng YP, Waters KE. A review of the beneficiation of rare earth element bearing minerals. Minerals Engineering. 2013 Feb 1; 41:97-114.

Jordens, A. (2016). *The Beneficiation of Rare Earth Element-Bearing Minerals.* Montreal: Thesis, McGill University.

Kanazawa Y, Kamitani M. Rare earth minerals and resources in the world. Journal of alloys and compounds. 2006 Feb 9; 408:1339-43.

Karayigit, A., Gayer, R., Querol, X., & Onacak, T. (2000). Contents of Major and Trace Elements in Feed Coals from Turkish Coal-Fired Power Plants. *International Journal of Coal Geology*, 169-184.

Ketris, M., & Yudovich, Y. (2009). Estimations of Clarkes for Carbonaceous Biolithes: World Averages for Trace Element Contents in Black Shales and Coals. *International Journal of Coal Geology*, 135-148.

Kuzmin, V., Pashkov, G., Lomaev, V., Voskresenskaya, E., & Kuzmina, V. (2012). Combined Approaches for Comprehensive Processing of Rare Earth Metal Ores. *Hydrometallurgy*, 1-6.

Kolker, A., Scott, C., Hower, J., Vazquez, J., Lopano, C., & Dai, S. (2017). Distribution of Rare Earth Elements in Coal Combustion Fly Ash, Determined by SHRIMP-RG Ion Microprobe. *International Journal of Coal Geology*, 1-10.

Lai, F.G., Huang, L., Gao, G.H., Yang, R., Xiao, Y.F., 2018. Recovery of rare earths from ion-absorbed rare earths ore with MgSO4-ascorbic acid compound leaching agent. Journal of Rare Earths 36, 521-527.

Lanzerstorfer, C. (2018). Pre-processing of Coal Combustion Fly Ash by Classification for Enrichment of Rare Earth Elements. *Energy Reports*, 660-663.

Li, Y. H. M., Zhao, W. W., & Zhou, M. F. (2017). Nature of parent rocks, mineralization styles and ore genesis of regolith-hosted REE deposits in South China: an integrated genetic model. *Journal of Asian Earth Sciences*, *148*, 65-95.

Lin, R., Soong, Y., & Granite, E. (2018). Evaluation of Trace Elements in U.S. Coals Using the USGS COALQUAL Database Version 3.0. Part I: Rare Earth Elements and Yttrium (REY). *International Journal of Coal Geology*, 1-13.

Marcus, Y. (1985). Ion Solvation John Wiley.

McLellan, B., Corder, G., Golev, A., & Ali, S. (2014). Sustainability of the Rare Earths Industry. *Procedia Environmental Sciences*, 280-287.

Meunier, A. (2005). Clays. In Clays. https://doi.org/10.1007/b138672

Montross, Scott. N., Yang, J., Britton, J., McKoy, M., Verba, C., 2020. Leaching of Rare Earth Elements from Central Appalachian Coal Seam Underclays. Minerals 10, 1–20.

Moldoveanu, G. A., Papangelakis, V. G. (2016). An overview of rare-earth recovery by ion-exchange leaching from ion-adsorption clays of various origins. *Mineralogical Magazine*, *80*(1), 63-76.

Moldoveanu, G.A., Papangelakis, V.G., 2012. Recovery of rare earth elements adsorbed on clay minerals: I. Desorption mechanism. Hydrometallurgy 117-118, 71-78.

Mukai, H., Kon, Y., Sanematsu, K., Takahashi, Y., & Ito, M. (2020). Microscopic analyses of weathered granite in ion-adsorption rare earth deposit of Jianxi Province, China. *Scientific reports*, *10*(1), 1-11.

Navarro, J., Zhao, F. (2014). *Life-Cycle Assessment of the Production of Rare Earth Elements for Energy Applications: A Review.* Retrieved from Frontiers in Energy Research: https://www.frontiersin.org/articles/10.3389/fenrg.2014.00045/full

Noble, A., Yoon, R. H. (2020). *Development of a Cost-Effective Extraction Process for the Recovery of Heavy and Critical Rare Earth Elements from the Clays and Shales Associated with Coal* (No. DOE-Virginia Tech-31523). Virginia Tech.

Oliva, P., Viers, J., & Dupré, B. (2003). Chemical weathering in granitic environments. *Chemical geology*, *202*(3-4), 225-256.

Pan, J., Zhou, C., Tang, M., Cao, S., Liu, C., Zhang, N., Ji, W. (2019). Study on the Modes of Occurrence of Rare Earth Elements in Coal Fly Ash by Statistics and A Sequential Chemical Extraction Process. Fuel, 555-565.

Pan, L., Yoon, R. H. (2016). Measurement of hydrophobic forces in thin liquid films of water between bubbles and xanthate-treated gold surfaces. *Minerals Engineering*, *98*, 240-250.

Paul, J., Campbell, G. (2011). *Investigating Rare Earth Element Mine Development in EPA Region 8 and Potential Environmental Impacts.* The United States Environmental Protection Agency.

Papangelakis VG, Moldoveanu G (2014) Recovery of Rare Earth Elements from Clay Minerals. 1st European Rare Earth Resources Conference, pp. 191-202.

Paulick, H., Machacek, E. (2017). The Global Rare Earth Element Exploration Boom: An Analysis of Resources Outside of China and Discussion of Development Perspectives. *Resources Policy*, 134-153.

Piasecki, W., Sverjensky, D. A. (2008). Speciation of adsorbed yttrium and rare earth elements on oxide surfaces. *Geochimica et Cosmochimica Acta*, *72*(16), 3964-3979.

Quinn, J., Soldenhoff, K., Stevens, G., & Lengkeek, N. (2015). Solvent Extraction of Rare Earth Elements Using Phosphonic/Phosphinic Acid Mixtures. *Hydrometallurgy*, 298-305.

Qiu, Y.Z., Bao, Z.W., 1992. Two types of REE mineralization in theweathering crust of Huashan and Guposhan granites, NE Guangxi,China. In: Tu, G.Z., Xu, K.Q., Qiu, Y.Z. (Eds.), Petrogenesis and Mineralization of Granitoids—Proceedings of 1987 Guangzhou International Symposium. Science Press, Beijing, pp. 1149–1158.

Raghavan S, Fuerstenau DW. On the wettability and flotation concentration of submicron hematite particles with octylhydroxamate as collector. In Advances in interfacial phenomena of particulate/solution/gas systems; applications to flotation research. 1975; 150(71):59-67.

Rim, K., Koo, K., & Park, J. (2013). Toxicological Evaluations of Rare Earths and Their Health Impacts to Workers: A Literature Review. *Saf. Health Work*, 12-26.

Sanematsu, K., Kon, Y., Imai, A., 2015. Influence of phosphate on mobility and adsorption of REEs during weathering of granites in Thailand. J. Asian Earth Sci. 111, 14–30.

Sanematsu, K., Watanabe, Y. (2016). Characteristics and genesis of ion adsorption-type rare earth element deposits. Reviews in Economic Geology 18: 55–79.

Schulze, R., Lartigue-Peyrou, F., Ding, J., Schebek, L., & Buchert, M. (2017). Developing a life cycle inventory for rare earth oxides from ion-adsorption deposits: key impacts and further research needs. *Journal of Sustainable Metallurgy*, *3*(4), 753-771.

Schüler D, Buchert M, Liu R, Dittrich S, Merz C (2011) Study on rare earths and their recycling. 49: 30-40.

Sennett P, Olivier JP, inventors; Plant F Sulphur Co, assignee. Process for treating clay. United States patent US 3,446,348. 1969 May 27.

Seredin, V., & Dai, S. (2012). Coal Deposits as Potential Alternative Sources for Lanthanides and Yttrium. *International Journal of Coal Geology*, 67-93.

Seredin, V. (1996). Rare Earth Element-Bearing Coals from the Russian Far East Deposit. *International Journal of Coal Geology*, 101-129.

Sheludko, A. (1962). Certain peculiarities of foam lamellas, Parts I–III. In *Proc. Koninkl. Ned. Akad. Wetenschap. B* (Vol. 65, pp. 76-108).

Suli, L., Ibrahim, W., Aziz, B., Deraman, M., & Ismail, N. (2017). A Review of Rare Earth Mineral Processing Technology. *Chemical Engineering Research Bulletin*, 20-35.

Sobri, N. A., Yunus, M. Y. B. M., & Harun, N. (2023). A review of ion adsorption clay as a high potential source of rare earth minerals in Malaysia. Materials Today: Proceedings.

Song, G., Yuan, W., Zhu, X., Wang, X., Zhang, C., Li, J., & Wang, J. (2017). Improvement in Rare Earth Element Recovery from Waste Trichromatic Phosphors by Mechanical Activation. *J. Clean. Prod.*, 361-370.

Talan, D. (2021). *Evaluation of Various Separation Techniques for the Removal of Actinides from A Rare Earth-Containing Solution Generated from Coarse Coal Refuse*. West Virginia University.

USGS. (2022). Mineral Commodity Summary

Uda, T., Jacob, K., & Hirasawa, M. (2000). Technique for Enhanced Rare Earth Separation. *Science*, 2326-2329.

U.S. Department of Energy. (2011). *Critical Materials Strategy.*

Van Gosen, B., Verplanck, P., Seal, R. I., Long, K., & Gambogi, J. (2017). *Rare-Earth Elements, Chap. O Schulz, K.J, DeYoung, J.H. Jr, Seal, R.R., II, and Bradley, D.C., eds. Critical Mineral Resources of United States-Economic and Environmental Geology and Prospects for Future Supply: U.S. Geological Survey Professional Paper.* Retrieved from https://doi.org/10.3133/pp1802O

Van Gosen , B., Vernplanck, P., & Emsbo, P. (2019). *Rare Earth Element Mineral Deposits in the United States.* U.S.Geological Survey Circular 1454.

Valentim, B., Abagiu, A., Anghelescu, L., Flores, D., French, D., Goncalves, P., Ward, C. (2019). Assessment of Bottom Ash Landfilled at Ceplea Valley (Romania) As A Source of Rare Earth Elements. *International Journal of Coal Geology*, 109-126.

Valkov, A., Sergievskiy, V., Sofronov, V., Kalaev, M., & Ermakova, Y. (2014). Studies in the Field of Rare Earth Elements. *Procedia Chemistry*, 171-175.

Velde, B. B., & Meunier, A. (2008). *The origin of clay minerals in soils and weathered rocks*. Springer Science & Business Media.

Voßenkaul, D., Stoltz, N., Meyer, F., Friedrich, B., 2015. Extraction of Rare Earth Elements from non-Chinese Ion Adsorption Clays, Proceedings of EMC 2015.

Wagner, N., & Matiane, A. (2018). Rare Earth Elements in Select Main Karoo Basin (South Africa) Coal and Coal Ash Samples. *International Journal of Coal Geology*, 82-92.

Wang, L., Huang, X., Yu, Y., Zhao, L., Wang, C., Feng, Z., Long., Z. (2017). Towards Cleaner Production of Rare Earth Elements from Bastnaesite in China. Journal of Cleaner Production, 231-242.

Wang, D., Zhao, Z., Yu, Y., Dai, J., Deng, M., Zhao, T., & Liu, L. (2018). Exploration and Research Progress on Ion-Adsorption Type REE Deposit in South China. China Geology, 415-424.

Wang, Y. H., Huang, C. B., Hu, Y. H., Hu, Y. M., & Lan, Y. (2008). Beneficiation of diasporic-bauxite ore by selective flocculation with a polyacrylate flocculant. *Minerals Engineering*, *21*(9), 664-672.

Wills BA, Finch JA. Wills' mineral processing technology (8th edn). Butterworth-Heinemann, Boston. 2016:409-16.

Wu, C.Y., Huang, D.H., Guo, Z.X., 1989. REE geochemistry in the weathering process of granites in Longnan County, Jiangxi Province. Acta Geologica Sinica 63, 349–362 (in Chinese with English abstract).

Xiao, Y. F., Feng, Z. Y., Hu, G. H., Huang, L., Huang, X. W., Chen, Y. Y., & Li, M. L. (2015). Leaching and mass transfer characteristics of elements from ion-adsorption type rare earth ore. *Rare Metals*, *34*(5), 357-365.

Xiao, Y.F., Feng, Z.Y., Hu, G.H., Huang, L., Huang, X.W., Chen, Y.Y., Long, Z.Q., 2016. Reduction leaching of rare earth from ion-adsorption type rare earths ore with ferrous sulfate. Journal of Rare Earths 423 34, 917-923.

Xiao, Y.F., Lai, F.G., Huang, L., Feng, Z.Y., Long, Z.Q., 2017. Reduction leaching of rare earth from ion-adsorption type rare earths ore: II. Compound leaching. Hydrometallurgy 173, 1-8.

Yanfei, X. I. A. O., Zongyu, F. E. N. G., Guhua, H. U., Huang, L., Huang, X., Yingying, C. H. E. N., & Zhiqi, L. O. N. G. (2016). Reduction leaching of rare earth from ion-adsorption type rare earths ore with ferrous sulfate. *Journal of Rare Earths*, *34*(9), 917-923.

Yanfei, X., Guohua, G., Li, H., Zongyu, F., Fuguo, L., & Zhiqi, L. (2018). A discussion on the leaching process of the ion-adsorption type rare earth ore with the electrical double layer model. *Minerals Engineering*, *120*, 35-43.

Yang, X., Honaker, R., 2020. Leaching kinetics of rare earth elements from fire clay seam coal. Minerals 10.

Yang XJ, Lin A, Li XL, Wu Y, Zhou W (2013) China's ion-adsorption rare earth resources, mining consequences and preservation, Environmental Development 8: 131-136.

Yang, M., Liang, X., Ma, L., Huang, J., He, H., & Zhu, J. (2019). Adsorption of REEs on kaolinite and halloysite: A link to the REE distribution on clays in the weathering crust of granite. *Chemical Geology*, *525*, 210-217.

Yang, Z.M., 1987. A study on clay minerals from the REE-rich weathering crust developed in the Longnan granite in Jiangxi.

Yoon, H., Kim, C., Chung, K., Kim, S., Lee, J., & Kumar, J. (2016). Solvent Extraction, Separation and Recovery of Dysprosium (Dy) and Neodymium (Nd) from Aqueous Solutions: Waste Recycling Strategies for Permanent Magnet Processing. *Hydrometallurgy*, 27-43.

Zhang, J., Zhao, B., Schreiner, B., 2016. Rare Earth Beneficiation and Hydrometallurgical Processing, Separation Hydrometallurgy of Rare Earth Elements. Springer International Publishing, Cham, Switzerland, pp. 19-54.

Zhang, W., Honaker, R. (2018). Rare Earth Elements Recovery Using Stages Precipitation from A Leachate Generated from Coarse Coal Refuse. *International Journal of Coal Geology*, 189-199.

Zhang, W., Rezaee, M., Bhagavatula, A., Li, Y., Groppo, J., & Honaker, R. (2015). A Review of the Occurrence and Promising Recovery Methods of Rare Earth Elements from Coal and Coal By-Products. *International Journal of Coal Preparation and Utilization*, 295-330.

Zhang W, Honaker R, Groppo, J. Concentration of rare earth minerals from coal by froth flotation. Minerals & Metallurgical Processing. 2017 Feb 28, 34(3):132-137.

Zhang, W., Honaker, R., 2019a. Enhanced leachability of rare earth elements from calcined products of bituminous coals. Miner. Eng. 142, 105935.

Zhang, W., Honaker, R., 2019. Calcination pretreatment effects on acid leaching characteristics of rare earth elements from middlings and coarse refuse material associated with a bituminous coal source. Fuel 249, 130-145.

Zhou, H., Wang, Y., Guo, X., Dong, Y., Su, X., & Sun, X. (2018). The Recovery of Rare Earth by A Novel Extraction and Precipitation Strategy using Functional Ionic Liquids. *Journal of Molecular Liquids*, 414-420.

Zhou, B., Li, Z., & Chen, C. (2017). Global potential of rare earth resources and rare earth demand from clean technologies. *Minerals*, *7*(11), 203.

Chapter 2. A study of rare earth ion-adsorption clays: The speciation of rare earth elements on kaolinite at various pH

2.1 Abstract

Synthesized rare earth ion-adsorption clays (La, Ce, Nd, Dy, and Y, ~ 400 ppm each) were prepared from kaolinite at various pHs in open-air conditions. X-ray diffraction (XRD), X-ray photoelectron spectroscopy (XPS), Time-of-Fight Secondary Ion Mass Spectroscopy (TOF-SIMS) and inductively coupled plasma mass spectrometry (ICP-MS) were used to characterize the effect of pH on the adsorption mechanism of rare earth elements (REEs) on kaolinite. The crystal structure of kaolinite by XRD analysis is not altered after REE adsorption, suggesting that REEs are bound to the surface of kaolinite. Elemental analysis by XPS and ICP-MS show that the surface concentration of REEs on kaolinite is pH dependent, and a local maximum of the surface concentration is achieved at pH 10. Three characteristics of the La 3d5/2 XPS photoemission feature were measured and compared to those of standard La compounds to probe the speciation of REEs, and electrostatically bound hydroxides such as $REE(OH)_2^+$ are identified as the primary species on the surface of kaolinite. Compared to the typical ion-adsorption clays with intrinsic acidic pH, clays synthesized at basic pH exhibit similarly high rare earth ion-exchange efficiency with ammonium sulfate (AS), suggesting that rare earth ion-adsorption clays can exist in both acidic and basic environments.

2.2 Introduction

Rare earth elements (REEs) consist of 17 metallic elements, including 15 lanthanides from lanthanum through lutetium (La–Lu), as well as scandium and yttrium due to their similar chemical properties. REEs are best known as “the vitamins of modern industry”, and play critical roles in many industries, such as aerospace and defense, healthcare, clean energy, electronic, transportation and vehicles, oil refining and chemical manufacturing. Contrary to its name, rare earth elements are not truly rare on Earth - the abundance of REEs on Earth’s upper continental crust is on par with some common industrial metals such as chromium, nickel, copper, zinc and tin, and is more than two orders of magnitude higher than the crust concentration of many noble metals including gold and platinum (Haxel et al., 2002). However, REEs are rarely found as concentrated ore deposits, resulting in extravagant mining and recovery costs. Currently, the rare earth industry relies on two major types of deposits for REE production, *i.e.* rare earth minerals (REMs) and ion-

adsorption clays (IACs). REM sources with higher REE content such as bastnaesite, monazite, and xenotime are distributed across the world but require aggressive and/or expensive hydrometallurgical processes (*e.g.* acid roasting) to facilitate REE recovery. The IACs on the other hand have lower REE content (0.05–0.3% rare earth oxides), but the cost of extracting REE from IACs is relatively low due to the simplicity of the overall process (Moldoveanu and Papangelakis, 2012; Zhang et al., 2016). In addition, IACs usually contain a wide variety of REEs and are particularly rich in heavy rare earth elements (HREE >40%) (Zhang et al., 2016), making them an economical and desirable REE source. For the typical ion-adsorption clays, REE^{3+} ions are adsorbed onto the negatively charged clay surface *via* electrostatic attraction (Xiao et al., 2016b).

The physisorbed REE^{3+} ions can be readily displaced from the clay surface by monovalent cations (*e.g.* Na^+ and NH_4^+) following the reaction mechanism, $Clay - REE^{3+} + 3NH_4^+ \rightarrow Clay - (NH_4^+)_3 + REE^{3+}$. An ammonium sulfate solution is typically employed in the ion-exchange leaching and the solution pH is maintained at 4 to prevent the hydrolysis of REE^{3+} ions and minimize the dissolution of impurities such as aluminum- and iron-bearing minerals (Zhang et al., 2016). The REE^{3+} ions extracted into the solution are selectively precipitated as oxalates or carbonates and subsequently converted to rare earth oxides (REO) by calcination (Chi and Xu, 1999).

Contrary to the worldwide spread of REM ores, IAC deposits have only been found in a few regions, with the majority of them in South China (Bao and Zhao, 2008; Huang et al., 1989; Ishihara et al., 2008; Moldoveanu and Papangelakis, 2016; Sanematsu et al., 2013; Voßenkaul et al., 2015; Wu et al., 1990). At present, China supplies over 60% of global REE demands, and the IACs in southern China alone account for ~80% of the world's HREE production (Voßenkaul et al., 2015). Riding on the uncertainty of trade policies and global markets, many other countries, including the United States, are seeking to diversify their REE supply chains. In light of the Critical Materials Strategy report (Bauer et al., 2010) that was first issued in 2010 by the U.S. Department of Energy, the U.S. Geological Survey (USGS) and private companies have identified significant amounts of REEs in coals throughout the basins of the United States (Bryan et al., 2015; Stuckman et al., 2018). These REEs could have been introduced into the coal basin at the late stage of the magmatic process by volcanic tephra and chemical/mechanical weathering of REE-rich igneous sources, and mobilized by hydrothermal fluids during diapiric emplacement until they find a suitable receptor material (Bryan et al., 2015). However, the nature of the REE-bearing materials

in U.S. coal basins is still unknown. Statistical analysis of the concentration of REEs and other elements in the USGS Coal Qual Database reveals a correlation between total REE content and aluminum (Al) content in coals, suggesting that REEs favor partitioning to coal byproducts such as clays and ashes. Assuming that all REEs are associated with the kaolinite clay content in coals, the REE grade is up to 1500 ppm in clays and over 1 × 107 metric tons of REEs are estimated to be associated with major eastern and western coal basins (Bryan et al., 2015). Since clay minerals such as kaolinite, illite and smectite are also the major host materials for ion-adsorbed REEs in known IAC deposits, we hypothesize that waste products from U.S. coal preparation plants can serve as viable sources of IACs, from which one can extract REEs at low costs with minimal environmental impacts. Unlike the typical IACs in China with intrinsic acidic pH, the REEs in many U.S. coal basins exist in a basic environment as the eastern U.S. coals are commonly found in the basal part of limestone, thus are presumably subjected to hydrolysis and/or REE carbonate formation either before or after adsorption on clays. However, fundamental studies are required to acquire a more comprehensive understanding of the REE adsorption mechanism on U.S. coal and coal byproducts, so that appropriate and targeted extraction processes can be developed.

A few studies of IACs that are synthesized at acidic pH have been conducted to investigate the ion-exchange mechanism of REEs on clays at a wide range of leaching solution pH (Alshameri et al., 2019; Bradbury and Baeyens, 2002; Coppin et al., 2002; Xiao et al., 2016b). Alshameri et al. (2019) synthesized La- and Y-IACs at pH 4.5 and performed a systematic study to understand the influence of several operative parameters on the ion-exchange leaching efficiency of REEs on clays. It was found that a lixiviant (ammonium sulfate) concentration of 0.5 M and a contact time of 30 min are sufficient to achieve the maximum REE recovery under acidic leaching solution (pH 4–6). The REE recovery drops drastically to zero when the leaching solution is raised above pH 7, which is attributed to the formation and precipitation of REE hydroxide complexes at basic pH. This observation has been validated by simulation of lanthanide speciation and solubility dependence on pH in the sulfate system (Moldoveanu and Papangelakis, 2013). These REE hydroxides are proposed to be strongly bound to the surface *via* clay-O-REE^{2+} covalent bonds and such species, known as the *colloidal phase*, cannot be extracted by an ion-exchange mechanism (Bradbury and Baeyens, 2002). However, studies into REE adsorption/ desorption behavior on IACs formed at basic pH, such as the environment experienced by U.S. coal and coal byproducts, have yet to be reported.

The work presented here serves as a fundamental study into REE adsorption and speciation on model clay surfaces under various pH conditions without the introduction of other ligands and metals that are commonly found on the clay minerals in U.S. coal basins. Kaolinite was used as the model clay for REE adsorption because it is the most common clay minerals found in the U.S. coal basins (Bryan et al., 2015; Zhang and Honaker, 2019) and one of the primary REE-bearing materials in global IAC deposits (Moldoveanu and Papangelakis, 2016; Voßenkaul et al., 2015; Wang et al., 2016). Kaolinite is a layered aluminosilicate mineral with repeated unit layers consisting of one octahedral alumina sheet and one tetrahedral silica sheet (Zhang et al., 2017). Substitution of surface Si^{4+} or Al^{3+} by cations of lower valency leads to negative charges on the surface of kaolinite, facilitating REEs binding by electrostatic attraction (Coppin et al., 2002). In this work, REEs were adsorbed on kaolinite at various basic pH in open air conditions. A number of analytical techniques including X-ray powder diffraction (XRD), inductively coupled plasma mass spectrometry (ICP-MS), and X-ray photoelectron spectroscopy (XPS) were used to characterize the effect of pH on REE adsorption behavior on kaolinite. Furthermore, XPS was used to probe the speciation of REEs on the REE-kaolinite. Lastly, ion-exchange leaching tests were performed on the REE-kaolinite, and the results were compared and discussed.

2.3 Experimental

2.3.1 Materials and chemicals

The Kaolinite sample and five different rare earth chlorides (La, Ce, Nd, Dy, Y, 99.9%) were purchased from Sigma-Aldrich. Upon arrival, all chemicals were stored in a desiccator and used as received. Deionized water with a resistivity of 18.2 MΩ·cm at 298.15 K was used in all solution preparation and leaching tests. Reagent grade NaOH and HCl from Fisher Scientific were used for pH adjustment. American Chemical Society (A.C.S.) reagent grade $(NH_4)_2SO_4$ was used as a lixiviant for ion-exchange leaching tests (Fisher Scientific, 99.3% purity).

2.3.2 Sample characterization

2.3.2.1 XRD

Powder XRD measurements were performed on a Rigaku Miniflex 600 instrument with Cu-Kα radiation (λ = 1.54 Å). XRD Spectra were acquired over a 2θ range from 3◦ to 80◦ with a step size of 0.04◦ and a dwell time of 2 s.

2.3.2.2 XPS

XPS measurements were performed on a PHI VersaProbe III scanning XPS microscope equipped with a monochromatic Al K-alpha X-ray source (1486.6 eV) with a base pressure of 3×10^{-8} Pa. XPS Spectra were acquired with 100 μm/100 W/20 kV settings over a 1400 μm × 100 μm sample area using 55 eV pass energy, which gives an Ag $3d_{5/2}$ full width at half maximum of 0.65 eV. All binding energies were referenced to adventitious carbon peak at 284.8 eV. A Shirley background and Gaussian-Lorentzian peak shape were used for curve fitting. Quantification was accomplished using PHI MultiPak 9.9.0.8, using the appropriate corrected sensitivity factors.

2.3.3 Methods and Procedure

2.3.3.1 Synthesis of REE-kaolinite

In order to synthesize an ion-adsorption clay, the Kaolinite sample was mixed with known concentrations of rare earth chlorides including 0.58 mM $LaCl_3$, 0.506 mM $NdCl_3$, 0.57 mM $CeCl_3$, 0.49 mM $DyCl_3$, and 0.91 mM YCl_3. To perform the experiments, 15 g of clay samples were placed in a 125 mL Erlenmeyer flask at a 1:5 solid-to-liquid ratio, and the mixtures were agitated for 24 h at 25°C at pH 3, 5, 7, and 10.5. After the agitation, the clay samples were filtered, washed with deionized water, and dried overnight at 60 ˚C. The composition of the adsorbed rare earth elements (REEs) was also determined by fusion digestion using borate flux, following Inductively-Coupled Plasma (ICP, Agilent 7900 ICP- MS) analysis.

2.3.3.2 Ion- Exchange leaching tests

The clay samples synthesized at various pH values were subjected to a series of leaching experiments at 25°C using the 0.5M conventional lixiviant $(NH_4)_2SO_4$ at a 1:2 solid-to-liquid ratio, and the mixture was agitated in Lab-Line Orbit Environ-Shaker for 1 h at pH 5. After the agitation, the clay sample was washed with 250 ml of deionized water, filtered through 413 ashless filter paper, dried overnight at 60 ˚C, and assayed by ICP-MS. During leaching, HCl and NaOH solutions both of 0.5 M were added to maintain the pH at 5.0 ±0.1. The efficiency of extraction was determined by comparing the amount of rare earth elements (REEs) remaining in the residue after leaching to the initial amount of REEs present in the feed material. The recovery (R) of an REE species was determined using the following relationship in Eq. (3.1),

$$\text{Recovery}(\%) = 100 - [\frac{\text{T.t}}{\text{F.f}} \text{x}100] \quad (3.1)$$

in which T and t are the weight (%) and REE concentration (ppm) of the residue, respectively; and F and f are the weight (%) and REE concentration (ppm) of the feed, respectively. Each test was repeated at least twice with the results averaged.

2.3.4 Chemical analysis and ICP-MS

2.3.4.1 Chemical Analysis

The fusion analysis method was applied to prepare the samples for ICP/MS analysis. In the 95% Pt - 5% Au crucibles, clay samples were mixed with a borate flux (lithium tetraborate), heated to 1000 °C until the flux melted, and then dissolved homogeneously in the flux at 70 ^{o}C with 5% Nitric Acid (HNO_3), ACS, 68-70%, Spectrum Chemical Fisher Scientific. To conduct the ICP-MS analysis, the dissolved samples were diluted appropriately. Elemental analyses of the REEs were conducted using an Agilent 7900 ICP-MS. Calibration curves were made with known concentrations of the analytes using the same dilute acid solution as samples.

2.3.4.2 ICP-MS

Elemental analysis for REEs was performed on an Agilent 7900 ICP-MS. A stock solution mixture of the lanthanides, scandium, yttrium, thorium, and uranium made up in 5% *v*/v nitric acid (HNO_3) was purchased from Inorganic Ventures (Christiansburg, VA; Catalog # CMS-1- 125ML). Further dilutions of the stock were made up in 2% *w*/*v* HNO_3. Individual REE content was quantified using a seven-point calibration curve made with known concentrations of the analytes of interest in the same dilute acid solution as the samples. Linear calibration curves ranging from 10 parts per trillion (ppt) to 100 parts per billion (ppb) with coefficient of determination (R^2) values of >0.999 were observed for each element of interest. Clay samples were prepared for ICP-MS analysis by adding 6 mL of 50% (*w*/*v*) sodium hydroxide (NaOH) to 50 mg of the samples for microwave digestion at 180 ˚C (Cai et al., 2008). The NaOH treated samples were acidified by HNO_3 (70% w/v) and the dissolved samples were diluted appropriately before being subjected to ICP-MS analysis.

2.4 Results and Discussion

2.4.1 The effect of pH on REE adsorption on synthetic ion adsorption clay

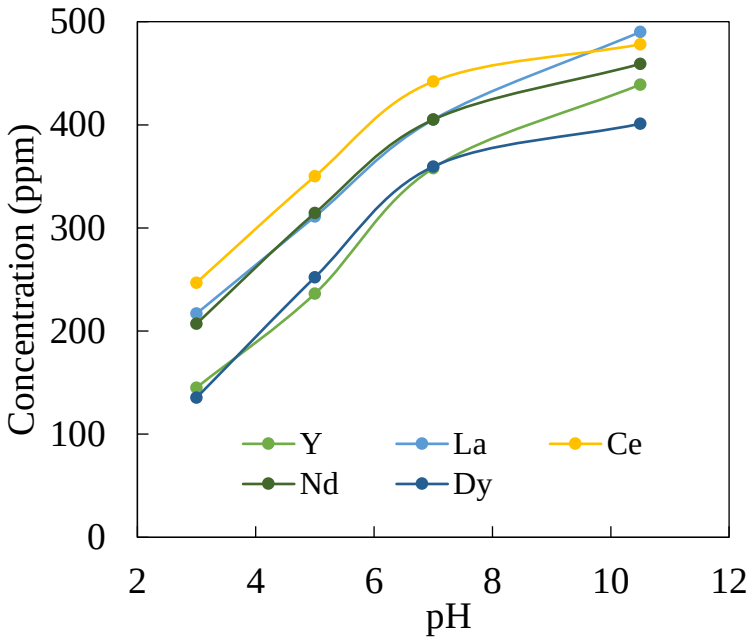

Figure 2.1 REE concentration in the synthetic IACs.

Figure 2.1 shows the results obtained with a series of synthetic clay preparation tests conducted at 24 h and various pH values from 3 to 10.5 at 25 ^{o}C. REE concentration of Ce is 247 ppm while Y, La, Nd, and Dy are in the range of 140 to 200 ppm synthetic ion adsorption clay synthesized at pH 3. When the pH value was increased by 2 points from 3 to 5, the REE concentrations increased as shown in Figure 2.1. The Ce concentration on the Kaolinite surface increases by 70 % with a value of 350 ppm while the other LREEs La and Nd are 311 and 314 ppm, respectively. Figures 2.1 show that the REEs concentrations do not change significantly after pH 7. The findings indicate that at pH 10.5, rare earth elements tended to adsorb more on the clay mineral`s surface. The concentration of the REEs is around 400 ppm, the same concentration used in synthesizing the clay sample for all pH values. It can be caused by the different molecular bonds like Ln-hydroxide that can take place at pH 10.5.

As shown in Figure 2.1, the surface concentrations of Y to Dy all increase with increasing pH from 3 to 10, with maximum concentrations observed at pH 10. The results indicate that pH 10 is a favorable condition for REE adsorption on kaolinite.

2.4.2 The effect of pH on REE adsorption on kaolinite

XRD was used to examine the crystal structures of kaolinite before and after REE adsorption. Figure 2.2 shows the XRD patterns of kaolinite and REE-kaolinite synthesized at various pH from 7 to 13. The XRD peaks of the blank kaolinite sample (Figure 2.2a) match those of kaolinite with a trace impurity of quartz and illite. The composition of the clay is consistent with previously published data for naturally occurring kaolinite (Alshameri et al., 2019). Illite has

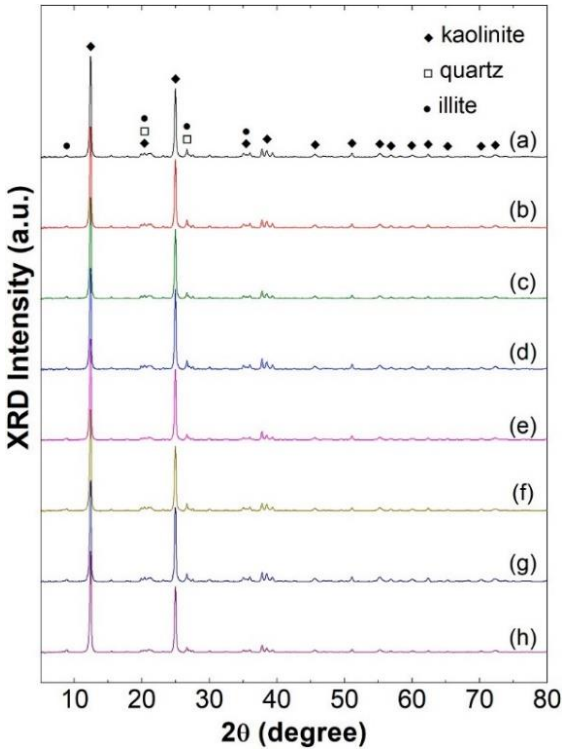

Figure 2.2 XRD patterns of (a) kaolinite and REE-kaolinite synthesized at pH (b) 7; (c) 8; (d) 9; (e) 10; (f) 11; (g) 12; (h) 13.

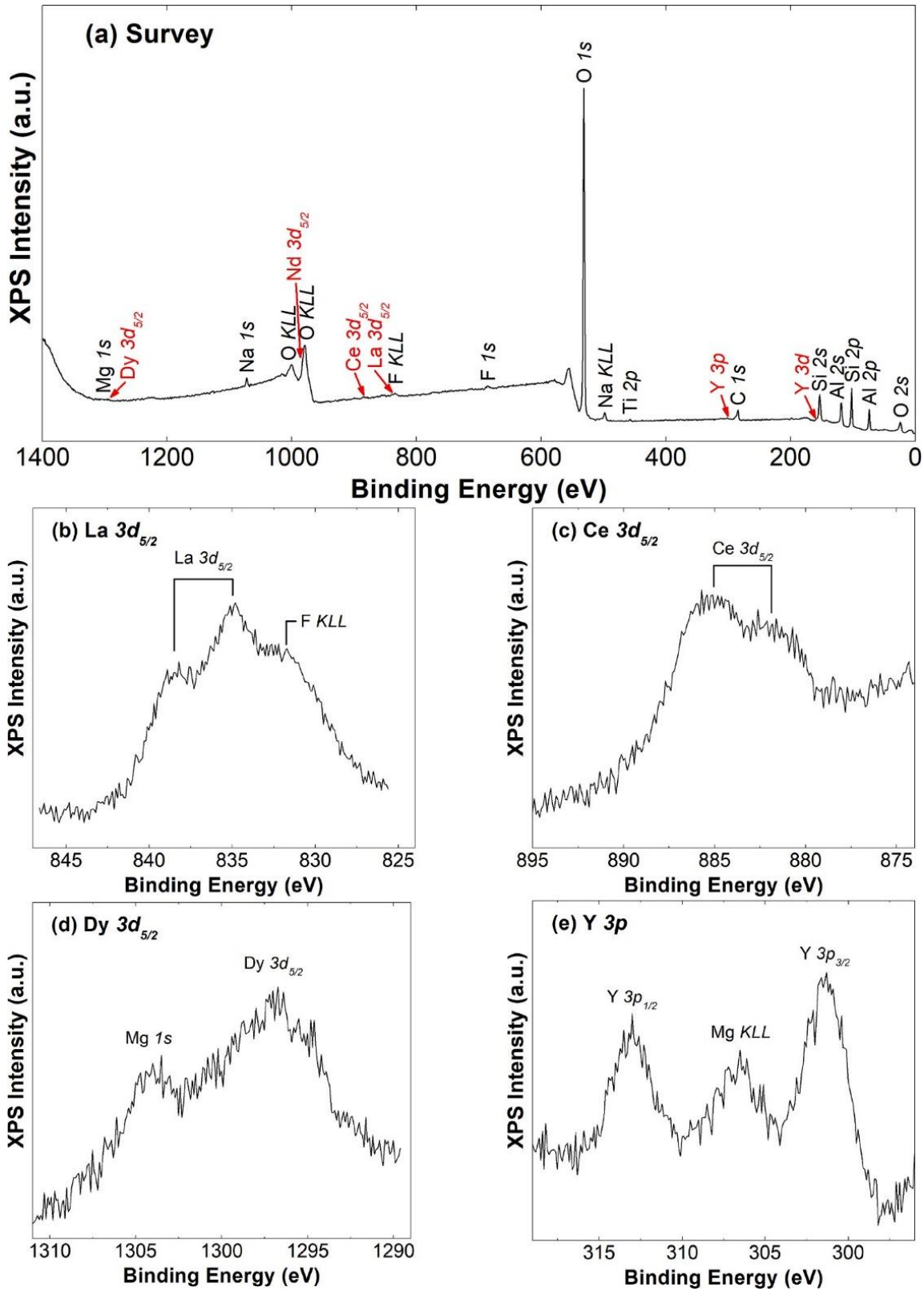

Figure 2.3 XPS spectra of REE-kaolinite synthesized at pH 10. (a) survey; (b) La 3d5/2; (c) Ce 3d5/2; (d) Dy 3d5/2; (e) Y 3p.

higher adsorption efficiency (Alshameri et al., 2019), thus the small amount of illite in the kaolinite sample is anticipated to have a negligible effect on the REE adsorption in this work. For the REE-kaolinite prepared at pH 7–13, no substantial differences are observed in the XRD pattern (Figure 2.2b–h), indicating that the synthesis conditions do not impact the bulk crystal structure of the kaolinite. Since kaolinite is known to have negligible isomorphic substitution (Schulze, 2005; Sparks, 2003) and the intercalation of kaolinite would increase the basal spacing of the 1:1 alumina/silicate layers which results in the shift of the (001) diffraction peak to a smaller angle (Cheng et al., 2010; Liu et al., 2016; Valaskova et al., 2007; Zhang et al., 2017), this result suggests that the adsorbed REE species bind to the surface of kaolinite. Potential surface-bound REE phases are not detected, which is expected since the concentrations of adsorbed REE (~ 400 ppm) are below the nominal XRD detection limit of 1% by volume.

XPS was used to provide chemical information on rare earth elements (REEs) on the surface of synthesized REE-kaolinite. Figure 2.3 shows the XPS spectra of a REE-kaolinite sample prepared at pH 10. The survey scan of this sample (Figure 2.3a) indicates major elements: O (68.0 at. %), Al (10.4 at. %), and Si (12.4 at. %), which closely resemble the composition of kaolinite $Al_2Si_2O_5(OH)_4$. Small amounts of C, Mg, Na, Ti, and F are also present, presumably from impurities in the clay. Signals from the adsorbed REEs are small (approaching the surface detection limit in concentration) but clearly apparent in the survey spectra. High-resolution scans of the primary photoemission region for individual REEs are also included in Figure 2.3. The 3d5/2 region was measured for La, Ce, and Dy. The La 3d5/2 feature (Figure 2.3b) exhibits multiplet splitting (Berthou et al., 1976) with a photoemission peak at 834.9 eV and a satellite peak at 838.6 eV. An F KLL feature is also present in this region and partially overlaps with the La 3d5/2 photoemission peak.

The Ce 3d5/2 feature (Figure 2.3c) shows a similar multiplet splitting (Berthou et al., 1976; Kim et al., 2017), with the photoemission and satellite peaks at 881.8 and 885.2 eV respectively. The Dy 3d5/2 feature (Figure 2.3d) appears as a single peak (Barreca et al., 2007; Kang et al., 2015) at 1296.8 eV and partially overlaps with the Mg 1s peak at 1304.2 eV. To characterize the presence of Y, the alternative 3p region (Figure 2.3e) was used because the primary Y 3d signals overlap with those of Si 2s. The adsorbed Y yields a Y 3p3/2 peak at 303.5 eV and a Y 3p1/2 peak at 313.0 eV, along with an Mg KLL peak at 306.6 eV in this region. The Nd 3d5/2 signals are completely embedded in the strong O KLL features (Mullica et al., 1995) and are thus not shown

here. C *1s* spectra of kaolinite and REE-kaolinite (Figure 2.2a) show a similar carbonate peak at 289.4 eV, suggesting that the formation of REE carbonates *via* contact with ambient CO_2 during the open-air synthesis is negligible. To our knowledge, this is the first report of high-resolution XPS spectra of multiple REEs on clay materials. It demonstrates the capability of contemporary XPS instrumentation to detect REEs at extremely low concentrations (ppm), and highlights the potential for XPS to probe the chemical state information of REE on IACs.

2.4.2.1 Speciation of La

In order to explain the relationship between pH and RE concentration on the synthetic IAC surface, thermodynamic calculations were performed. Tables 2.1 and 2.2 show the reactions and thermodynamic constants that were obtained from the literature to create speciation and solubility diagrams for La- and La-hydroxide systems.

Table 2.1 Thermodynamic Data Used for the Specious Diagram for La^{3+} in Solution

Reaction	log K
$La^{3+} + H_2O \leftrightarrow La(OH)^{2+} + H^+$	-8.8
$La^{3+} + 2H_2O \leftrightarrow La(OH)_2^{+} + 2H^+$	-17.2
$La^{3+} + 3H_2O \leftrightarrow La(OH)_{3(aq)} + 3H^+$	-25.9
$La^{3+} + 4H_2O \leftrightarrow La(OH)_4^{-} + 4H^+$	-36.9
$La^{3+} + 3H_2O \leftrightarrow La(OH)_{3(s)} + 3H^+$	-20.9

(Data sources: Visual MINTEQ 3.1, Kragten and Decnop-Weever, 1978, Zhang, 2017).

Table 2.2 Thermodynamic Data Used for the Solubility Diagram for $La(OH)_3(s)$

Reaction	log K
$H_2O \leftrightarrow H^+ + OH^-$	-14
$La(OH)_{3(s)} \leftrightarrow La^{3+} + 3OH^-$	-21.22
$La(OH)^{2+} \leftrightarrow La^{3+} + OH^-$	-5.34
$La(OH)_2^{+} \leftrightarrow La^{3+} + 2OH^-$	-9.86
$La(OH)_{3(aq)}^{+} \leftrightarrow La^{3+} + 3OH^-$	-14.09
$La_2(OH)_2^{4+} \leftrightarrow 2La^{3+} + 2OH^-$	-9.59
$La(OH)^-_4 \leftrightarrow La^{3+} + 4OH^-$	-15.14

(Data sources: Shkolnikov, 2009; Hass et al., 1995; Lee and Byrne, 1992).

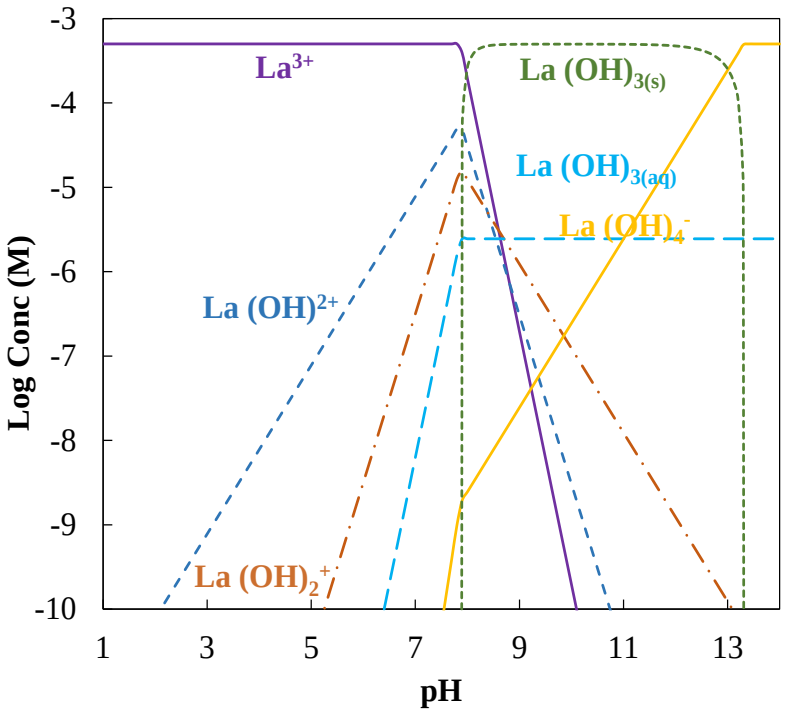

Figure 2.4 Speciation diagram of La as a function of pH.

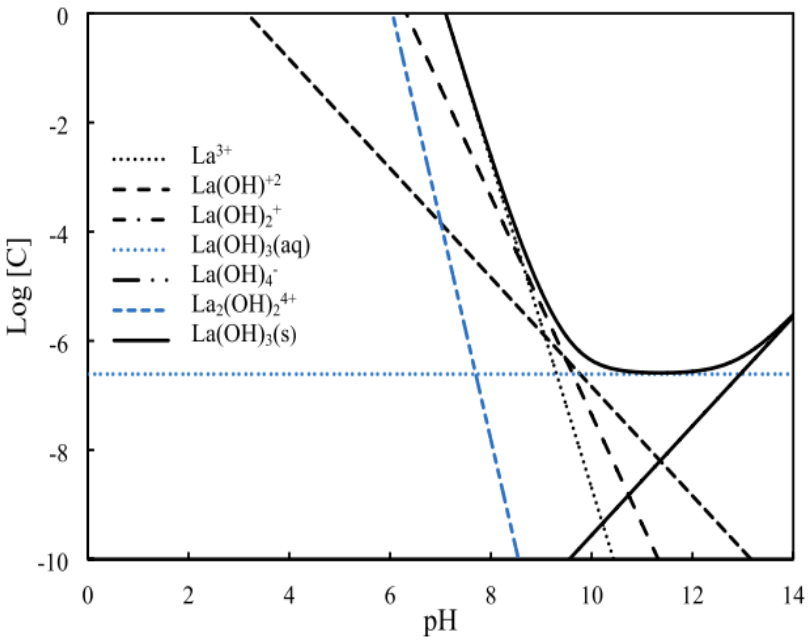

Figure 2.5 The solubility diagram La $(OH)_{3(s)}$ in water at 25 ^{o}C (Liu, et al. 2022).

The results of the thermodynamic calculations are given in Figures 2.4 and 2.5. For $La(OH)_3(s)$, various La-bearing species, e.g., La^{3+}, $La(OH)^{2+}$, $La_2(OH)_2^{4+}$, shown in Figure 2.5, would adsorb on the negatively charged clay surface. As shown in Figure 2.4, hydrolysis is not observed in an acidic medium and the La^{3+} ion is the predominant species in the solution at pH 7 or lower. At pH 10, the concentration of La^{3+} ion drops rapidly and is negligible, whereas La hydroxides, such as $La(OH)_2^+$, $La(OH)^{2+}$, $La(OH)_3$, and $La(OH)_4^-$, rise and then reach maximum values over pH ranges 7 to 11. Consequently, La hydroxides were considered the cause of the local maximum in REE concentrations at pH 10. We thus hypothesize that the local maximum in the concentration of adsorbed REEs at pH 10 is associated with REE hydroxides. These results suggest that REE hydroxides, *e. g.* $La(OH)_3$, are the primary species to be adsorbed on kaolinite in a basic environment.

As shown in Figures 2.4 and 2.5, the La^{3+} ion concentration increases with decreasing pH, which should favor the ion-exchange leaching in accordance to Reaction (2.1).

$$Clay\text{-}Ln^{3+} + 3NH_4^+ \rightarrow Clay\text{-}(NH_4^+) + Ln^{3+} \quad (2.1)$$

In the present study, the $(NH_4)_2SO_4$ leaching tests were conducted at pH 5, in which La^{3+} ions are the most prevalent La-bearing species. Further, the speciation diagrams indicate that the rare earth colloids are readily soluble under slightly acidic conditions in solution.

From the above discussion of the speciation diagram of La (Figure. 2.4), REE hydroxides are the favorable species in solution at basic pH. To explore the chemical nature of the REEs on the surface of the clay, XPS was used to characterize the chemical state of La. It is well known that the photoelectrons generated from the La *3d* level, the primary La XPS transition, has two features ($3d_{5/2}$ and $3d_{3/2}$) resulting from spin-orbit splitting, either of which conveys the same chemical information of the La compound. Furthermore, each spin-orbit peak is split into two components by multiplet splitting, where the lower binding energy component is the primary La $3d_{5/2}$ peak and the higher binding energy component is due to a satellite peak. In addition to the peak position of the two multiplet split components, the magnitude of the multiplet splitting and the intensity ratio of each multiplet split component are also characteristic of different La compounds (Berthou et al., 1976; Iannicelli-Zubiani et al., 2015; Siegmann et al., 1978; Suzuki et al., 1998).

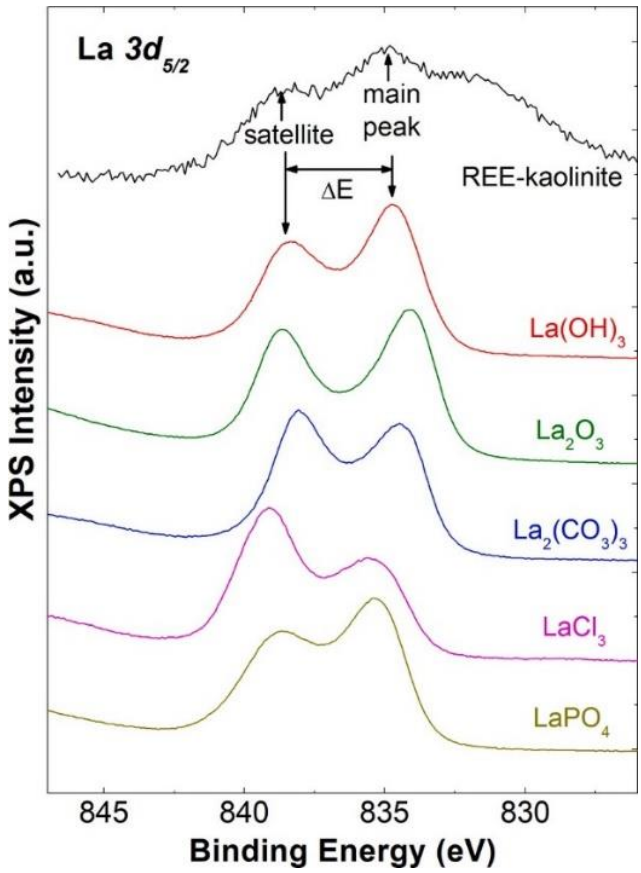

Figure 2.6 La 3d5/2 XPS spectra of REE-kaolinite synthesized at pH 10 and several standard La compounds.

Figure 2.6 shows the La $3d_{5/2}$ XPS spectra of the REE-kaolinite synthesized at pH 10 and several standard La compounds including $La(OH)_3$, La_2O_3, $La_2(CO_3)_3$, $LaCl_3$ and $LaPO_4$. Characteristic values of their La $3d_{5/2}$ features including the peak position of the two multiplet-split components, the magnitude of the multiplet splitting (ΔE) and the intensity ratio of each multiplet split component are summarized in Table 2.3. $La(OH)_3$ shows a La $3d_{5/2}$ peak position of 834.7 eV and a multiplet splitting of 3.7 eV, which agree with previously reported values (Sunding et al., 2011). The peak intensity ratio of the satellite peak (838.4 eV) with respect to the La $3d_{5/2}$ peak is 0.71. Compared to $La(OH)_3$, $La_2(CO_3)_3$ has a similar main peak position of 834.5 eV and multiplet splitting of 3.6 eV, however its satellite: peak ratio of 1.01 is much larger that of $La(OH)_3$, which can be used to distinguish these two La compounds. $LaPO_4$ shows an identical value of satellite:peak ratio as $La(OH)_3$, but its higher main peak position of 835.3 eV and narrower multiplet splitting of 3.3 eV sufficiently distinguishes itself from $La(OH)_3$. It is apparent that each standard La compound demonstrates a different value in at least one of the three peak

characteristics, which provides the fingerprint to identify its speciation by XPS. The synthesized REE-kaolinite sample exhibits a La $3d_{5/2}$ peak at 834.9 eV, a multiplet splitting of 3.7 eV, and a satellite: peak intensity ratio of 0.68.

Table 2.3 La 3d5/2 characteristic values for REE-kaolinite synthesized at pH 10 and several standard La compounds.

Sample	**La $3d_{5/2}$ BE (eV)**		**ΔE (eV)**	**Satellite: Peak Ratio**
	Peak	**Satellite**		
REE-kaolinite	834.9	838.6	3.7	0.68
$La(OH)_3$	834.7	838.4	3.7	0.71
La_2O_3	834.1	838.6	4.5	0.77
$La_2(CO_3)_3$	834.5	838.1	3.6	1.01
$LaCl_3$	835.6	839.1	3.5	1.43
$LaPO_4$	835.3	838.6	3.3	0.71

All three values closely match those of La $(OH)_3$, indicating that the primary La species on the surface of the REE-kaolinite sample is La $(OH)_3$. Unfortunately, XPS could not further distinguish the exact type of hydroxide among La $(OH)^{2+}$, La $(OH)_2^+$ and La $(OH)_3$ due to the subtle changes that may accompany differences in the chemical environments. However, the overall result is consistent with the hypothesis, stated above, that REE hydroxides are favored to adsorb on kaolinite at basic pH. Most importantly, we have demonstrated that spectroscopic approaches, particularly XPS in this work, has the capability to probe the speciation of low-concentrations of REEs on clay materials.

2.4.3 Speciation of LREE (La) on Synthetic Clay Sample by TOF-SIMS Analysis

XPS studies showed that La exists as La $(OH)_3$ at basic pH. To complement the XPS results, another surface analysis technique was utilized, *i.e.*, Time-of-Fight Secondary Ion Mass Spectroscopy (TOF-SIMS), to obtain chemical and molecular information of the REEs present on the surface of synthetic clay samples. Fragment patterns of the synthetic La clay samples were compared to those of the La standards to provide further insights into the identification of La speciation on the synthetic sample.

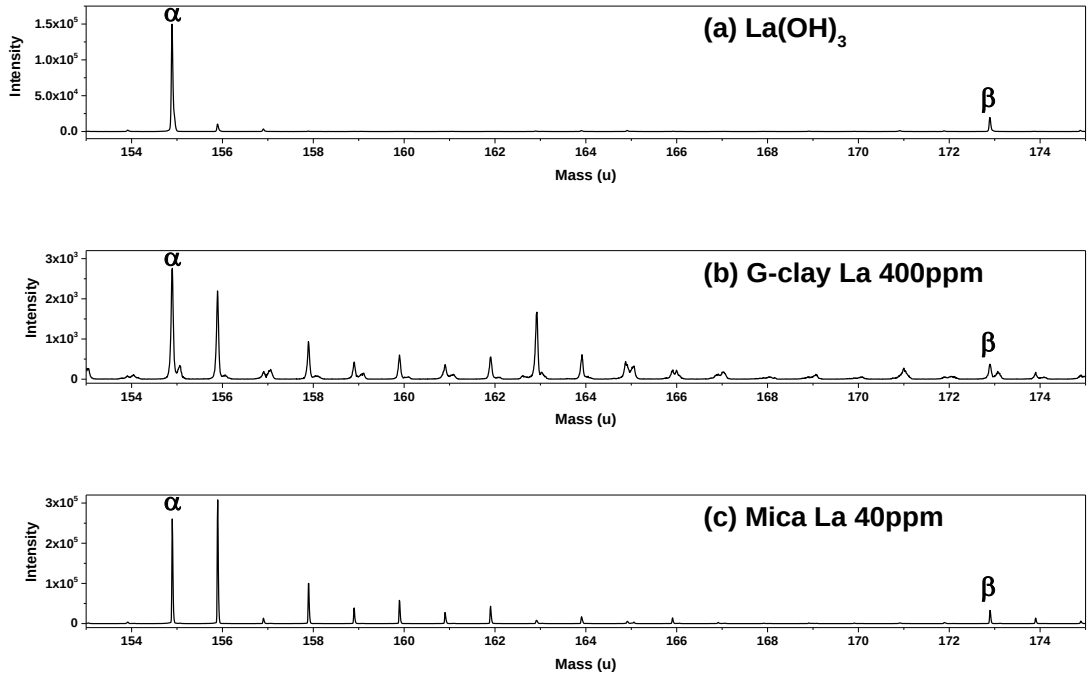

Figure 2.7 Positive ion mass spectra of various La compounds. (a) La $(OH)_3$; (b) synthetic La G-clay sample prepared at pH 10.5, 25°C, 24h; (c) synthetic La Mica sample prepared at pH 10.5, 25°C, 24h. α - LaO^+; β - $LaO_2H_2^+$.

La $(OH)_3$ (Sigma-Aldrich, 99.99%) was stored in a desiccator upon arrival and used as received. A Synthetic La-kaolinite sample was prepared with 5 REEs (La, Ce, Nd, Dy, and Y) on Georgia clay with 400 ppm each at pH 10.5, 25°C, and 24 h contact time. A synthetic La-mica sample was prepared with 5 REEs (La, Ce, Nd, Dy, and Y) adsorbed to a ~2 cm×2 cm mica sheet with 40 ppm each at pH 10.5, 25 °C, 24h contact time. TOF-SIMS characterization was performed on an ION-TOF SIMS 5 Mass Spectrometer in Analytical Instrumentation Facility (AIF) at North Carolina State University.

Figure 2.7 shows the positive ion mass spectra of the La $(OH)_3$ standard and the synthetic La clay sample. In addition, a synthetic La mica sample was also prepared and measured as a model supplement of the clay sample, presumably with better signal resolution due to its flat surface. Mica was chosen because its basal surface consists of a layer of silica octahedra, which is also found in kaolinite. Two primary fragments of La $(OH)_3$ were detected in the m/z region of 150 to 180 at m/z=154.9 and m/z=172.9, which are attributed to LaO^+ (α) and $LaO_2H_2^+$ (β) respectively, with the peak intensity ratio $\beta/\alpha = 0.13$. For the synthetic clay and mica samples,

LaO^+ (α) and $LaO_2H_2^+$ (β) fragments were also present, with similar peak intensity ratio β/α of 0.15 and 0.14 respectively. These results suggest that the primary La species on synthetic clay samples was La $(OH)_3$, which was consistent with the XPS analysis results.

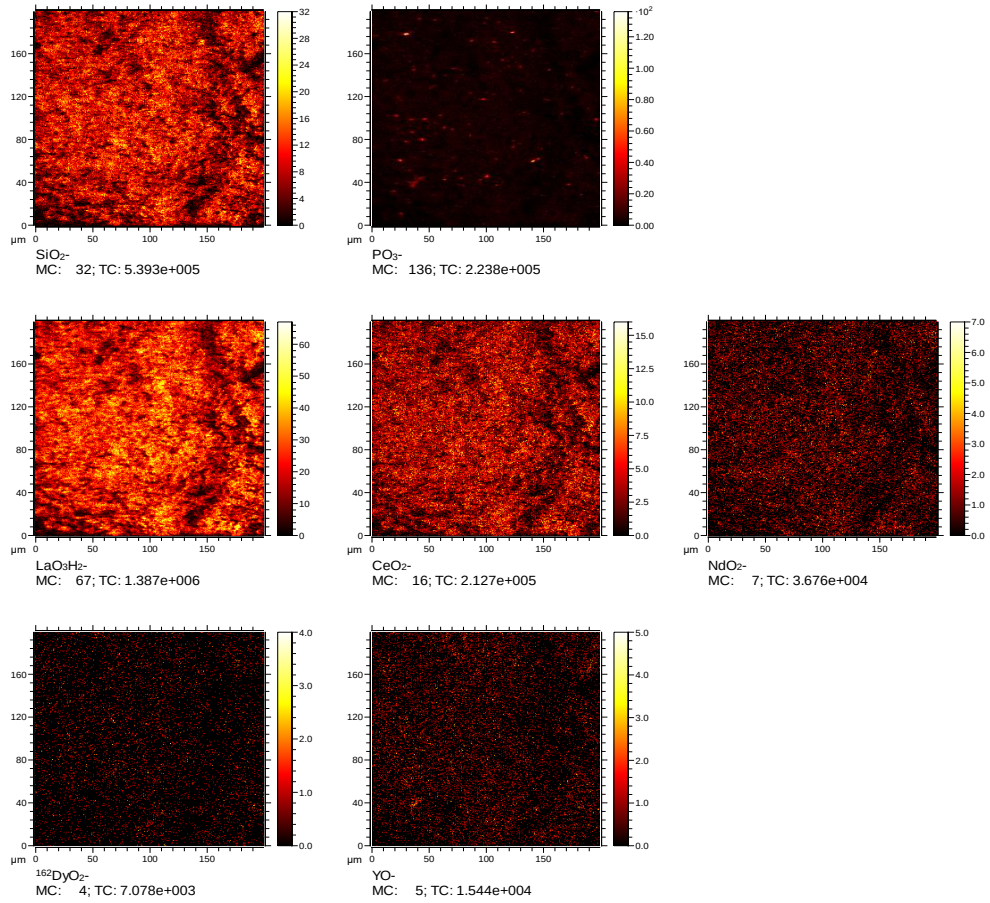

Figure 2.8 Negative ion mass spectra mapping of the synthetic La clay sample in a 200 μm × 200 μm area.

Figure 2.8 shows the negative ion mapping of the synthetic La G-clay sample in a 200 μm × 200 μm area by measuring the primary fragments of clay (SiO_2^-), phosphates (PO_3^-), and those of the five rare earth elements added: $LaO_3H_2^-$, CeO_2^-, NdO_2^-, DyO_2^- and YO^-. All five rare earth elements demonstrate the same distribution pattern on the clay surface, suggesting that there are no preferred binding sites on the clay surface for individual rare earth species. PO_3^- was not detected, which further confirms that $LaPO_4$/Monazite is not present on the synthetic sample surface. Similar but more distinct results were obtained from the negative ion mapping of the synthetic La mica sample shown in Figure 2.9. All five rare earth elements form aggregates on the mica surface, excluding the formation of phosphates. The combination of XPS and TOF-SIMS

characterizations conclude that rare earth hydroxides in alkaline pH conditions were the primary rare earth species on the surface of the synthetic clay sample.

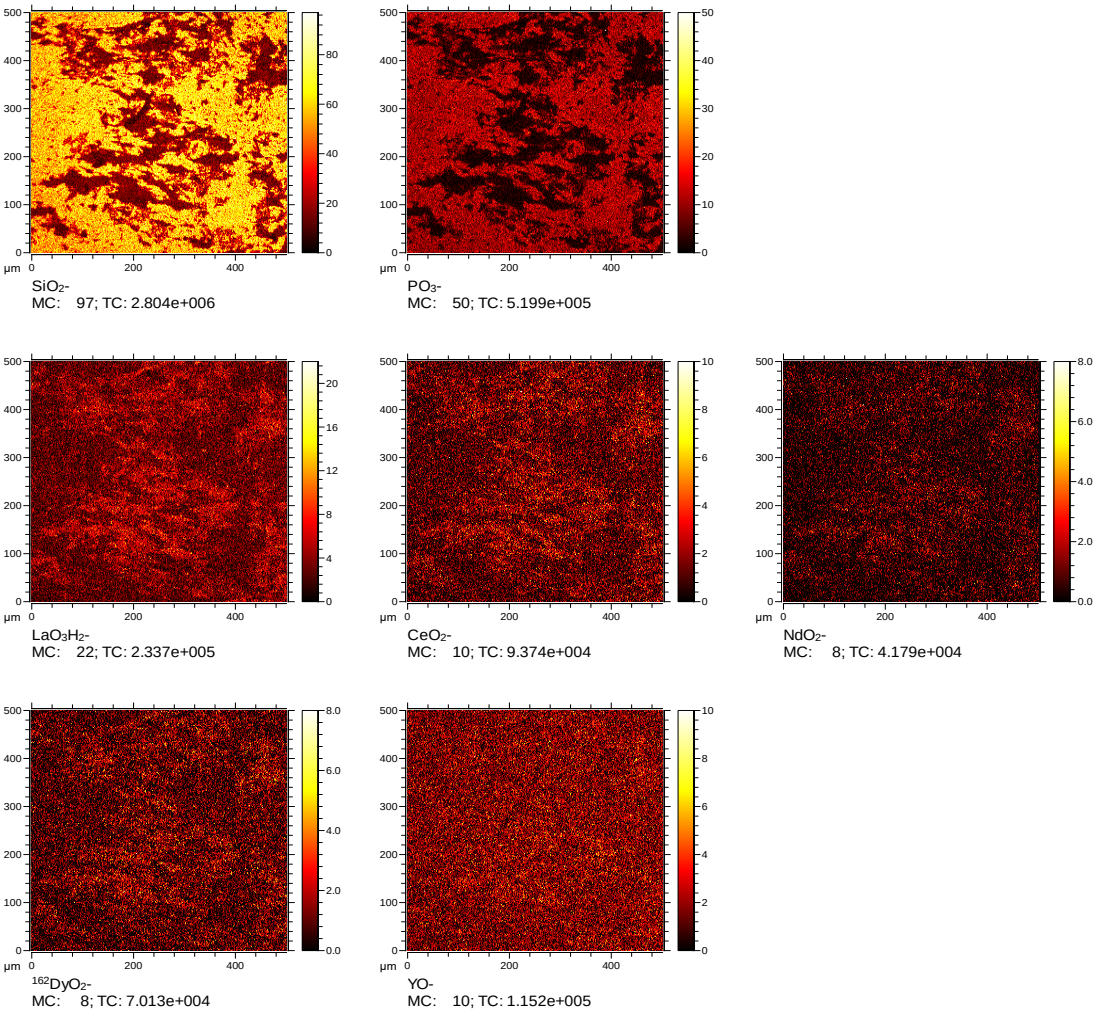

Figure 2.9 Negative ion mass spectra mapping of the synthetic La Mica sample in a 200 µm × 200 µm area.

2.4.4 Ion-Exchange Leaching Mechanism

In theory, the ion exchange mechanism is thoroughly explained by the hydration enthalpies of the ions involved. The enthalpy data published by Marcus in 1985 shows that all Ln^{3+} ions have more negative enthalpies of hydration (ΔH_{hyd}) than the Na^+ and NH_4^+ ions. The literature data summarized that the hydration enthalpy for trivalent Ln^{3+} ions is in the range of -3,285 to -3,668 kJ/mol, with values generally becoming more negative with increasing atomic number. Alternatively, the cations in traditional ion exchange lixiviants, such as Na^+ and NH_4^+, are much

less negative, varying from -406 to -322 kJ/mol (Smith, 1977). This result indicates that the Ln^{3+} ions have a greater tendency to stay in bulk water than Na^+ and NH_4^+ ions, which explains why the NH_4^+ ions used as lixiviants for leaching RE^{3+} ions from ion-adsorption clays (Marcus, 1985). Besides, Papangelakis and Moldoveanu published a model of an ion exchange mechanism in 2012 based on the significant difference in hydration enthalpies between the $NH_4^+$and Ln^{3+} ions. Furthermore, the studies published by Spedding et al. between 1979-80 investigated the hydration numbers of rare earth elements which indicate the number of water molecules in the first hydration sphere of the hydrated ions across the rare earth series. According to a study published by Jia in 1987 states that the hydration numbers are varying between 8 to 9 for rare earth elements. Additionally, the hydration number of the NH_4^+ ion is 4 (Liu et all, 2022). Consequently, the ammonium ions become readily liberated from the hydration water and form stronger bonds with the negatively charged basal surfaces of the clay.

2.4.5 Ion-exchange Leaching Results of REE-kaolinite

Figure 2.10 illustrates the ICP/MS results after 0.5M $(NH_4)_2SO_4$ leaching at pH 5 on four different synthesized IAC samples at pH 3, 5, 7, and 10.5 respectively. The test results obtained using the ammonium sulfate provided above 80% recovery values. In general, 60 - 90% of the REEs in IACs are in the form of free hydrated ions, i.e., REE $(H_2O)_n^{3+}$, which can readily be ion-exchanged by a lixiviant such as NH_4^+ ions. Above pH 7, however, they are hydrolyzed to become 'clay-O-REE^{2+}' species that are chemically bound to the surface. In previous studies, it has been shown that these species cannot be extracted by a simple ion exchange mechanism (Chi and Tian, 2008). As explained by using thermodynamic data given in Figures 2.4 and 2.5, in the range of pH 3 to 7 free Ln^{3+} ions are the dominant phase and they readily adsorb on negatively charged clay surfaces via electrostatic attraction however the bonding energy is not strong as pH 10 because of hydroxides. Hence, the concentration of REEs increases with increasing pH values.

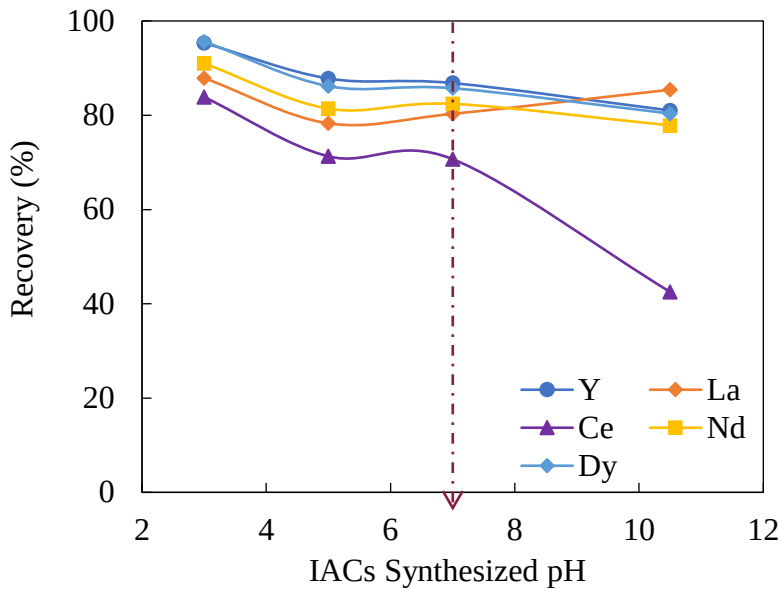

Figure 2.10 Ion exchange leaching test results of synthesized IACs at various pH values from 3 to10.5 by using 0.5 M $(NH_4)_2SO_4$ at pH 5.

Figure 2.10 shows no significant differences between the four synthesized IAC samples in terms of recovery values. However, as shown in Figure 2.10, the reagent (Ammonium sulfate, $(NH_4)_2SO_4$) was particularly efficient for the extraction of La and Nd from clay which was synthesized at pH 10. Ammonium sulfate was also efficient for the extraction of Y and Dy (~90% recovery) but not for Ce. The results presented in Figure 2.10 show that $(NH_4)_2SO_4$ can be used as a lixiviant for Ln-Hydroxides species at pH 5.

Contrary to other lanthanide elements, which are usually physically adsorbed as trivalent cations, Ce^{3+} ions can be easily oxidized by atmospheric oxygen (O_2) to Ce^{4+} in alkaline pH range, and precipitates as cerianite, CeO_2, which makes it difficult to be recovered by ion-exchange leaching (Papangelakis and Moldoveanu, 2012; Kim and Osseo-Asare, 2012; Bao and Zhao, 2008). It has been reported that CeO_2 or $Ce(OH)_4$ are sparingly soluble in weakly acidic solutions and hence dissolve only under aggressive conditions (Kumari et al., 2019; Li et al., 2017). The low solubility of CeO_2 may account for the low extraction efficiencies of cerium observed in the present work.

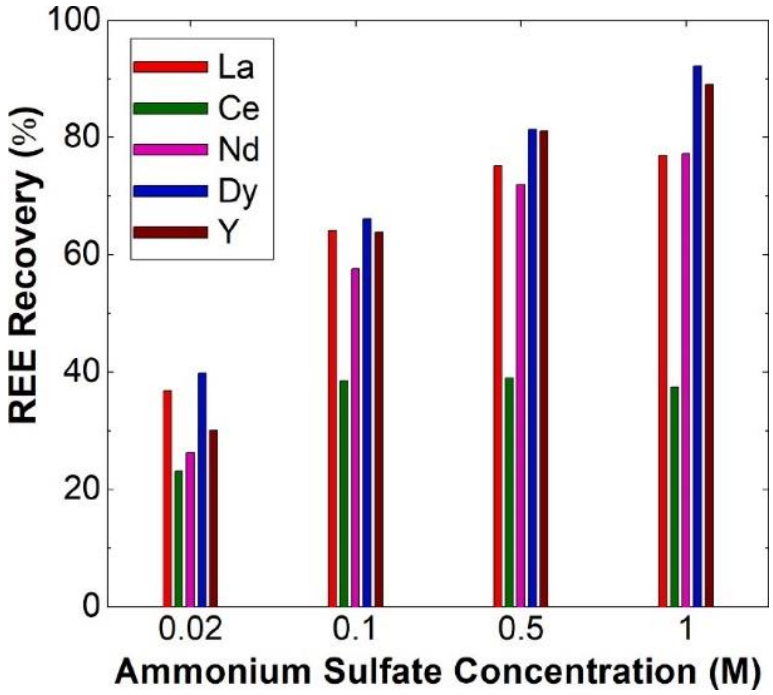

Figure 2.11 REE recoveries of REE-kaolinite at various ammonium sulfate concentrations at pH 5.

A set of leaching tests were performed to determine the REE ion-exchange efficiency of the synthesized REE-kaolinite materials. Figure 2.11 shows the REE recovery from the REE-kaolinite (pH 10) using ammonium sulfate (AS) as a lixiviant at different concentrations. The data clearly shows that recoveries of REEs increase with the increasing AS concentration. The recovery of La is 37% at 0.02 M of AS, and rises sharply to 64% when the AS concentration increases to 0.1 M. With further increases in AS concentration, the recovery of La reaches 75% and 77% at 0.5 M and 1.0 M of AS respectively. A similar trend is observed for Ce, Nd, Dy, and Y. It is worth noting that the recovery of Ce is considerably lower than that of other REEs using the same AS leaching solution. Ce is known to favor the formation of more stable Ce (IV) compounds in naturally occurring IACs which exhibit poor ion-exchange efficiency (Lai et al., 2018; Xiao et al., 2016a; Xiao et al., 2017). However, the characteristics of Ce *3d* XPS features (Figure 2.3c) for our model system match those of Ce (III) compounds such as $CeCl_3$ and Ce $(OH)_2Cl$ (Kim et al., 2017), indicating that the major Ce species on the REE-kaolinite is in the chemical state of Ce (III). A weak satellite peak at 916 eV is also observed, which indicates the presence of minor Ce (IV) (Beche et al., 2008; Kim et al., 2017). Similar to La, the primary Ce (III) species on kaolinite at basic pH is attributed to Ce (III) hydroxides such as Ce $(OH)_2^+$. Therefore, the lower Ce recovery does not appear to be due to the formation of Ce (IV) species on the model REE-kaolinite materials.

We postulate that Ce (III) is oxidized to Ce (IV) during the AS leaching process in the presence of sulfate at pH 5, which results in a subsequent lower Ce recovery by ion-exchange leaching.

Ion exchange leaching tests repeated three times to obtain rebuts results. Figure 2.12 shows the ion-exchange test results obtained at pH 5 by using 0.5M ammonium sulfate on the synthetic ion adsorption clay sample. As shown Figure 2.12, the ion exchange test results give accurate data with the ± 5% for La and Nd elements.

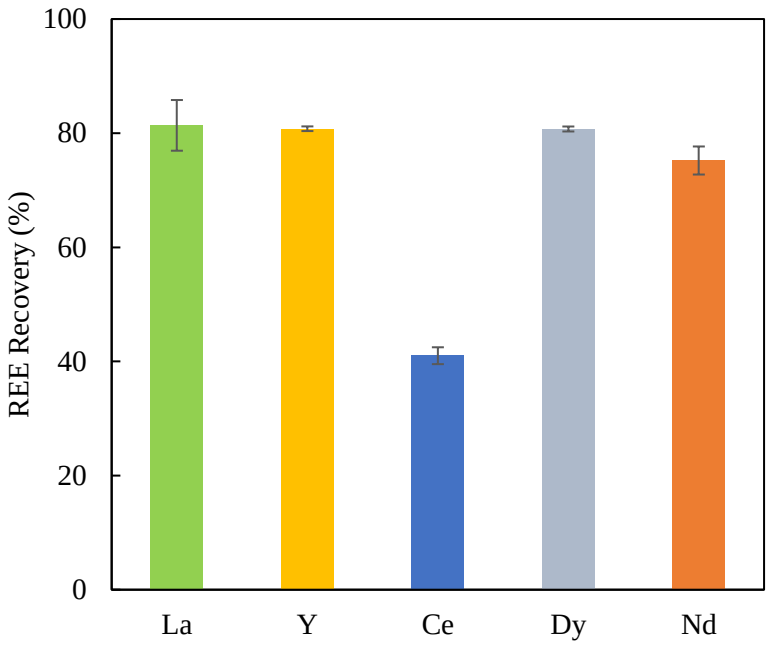

Figure 2.12 REE recoveries of REE-kaolinite at 0.5 M ammonium sulfate concentration at pH 5.

It is well acknowledged that typical ion-adsorption clays, like those found in south China, have hydrated REE ions physisorbed on the negatively charged surface of clays *via* electrostatic attraction at acidic pH. For these systems, a straightforward ion-exchange mechanism can displace REE ions from the clay surface by monovalent cations such as NH_4^+. In a basic environment, previous studies show that REE ions are hydrolyzed and chemisorbed on the clay surface *via* proposed clay-O-REE^{2+} covalent bonds, and ion-exchange mechanism does not liberate the REEs into solution (Bradbury and Baeyens, 2002). However, in this study we have observed that the synthesized REE-kaolinite clays prepared at basic pH in open air conditions without the introduction of other ligands and metals that are commonly found on the clay minerals in U.S. coal basins respond well to ion-exchange leaching using a common lixiviant comprised of 0.5 M

ammonium sulfate with recoveries over 70% of all REEs with the exception of Ce. The primary REE species on these clays are REE hydroxides as identified by XPS, but unlike the hypothesized clay-O-REE^{2+} covalent bonds (Bradbury and Baeyens, 2002), they are physisorbed on the clays *via* electrostatic attraction and available for ion-exchange. Therefore, we conclude that rare earth ion-adsorption clays can be found in both acidic and basic environments, with hydrated REE ions at acidic pH and hydroxylated REEs, such as La $(OH)_2^+$, at basic pH.

Despite our evidence for the existence of ion-exchangeable REE hydroxides on the surface of clay under basic pH conditions, the initial chemical environment likely plays a major role in determining the precise chemical state of the surface REE adsorbates in U.S. coal and coal byproducts. Electrostatic adsorption of REE hydroxides may occur when the REE ions undergo hydrolysis in basic conditions prior to adsorption, resulting in the IACs, as our model studies suggest. Alternatively, if REEs adsorb on clays as hydrated ions (REE^{3+}) at acidic pH, predominant clay-O-REE^{2+} covalent bonds (Bradbury and Baeyens, 2002) may form on the clay surface, which cannot be extracted by simple ion-exchange. Either scenario could govern REE binding in actual U.S. eastern coal and coal byproducts – each requiring distinctly different extraction strategies. Furthermore, co-existing elements such as Fe, Ca and Mn that are commonly found in coal byproducts may also affect the REE adsorption mechanism on the clay minerals, resulting in varying REE speciation and responses to ion-exchange leaching. This work provides a foundation for our studies on model systems upon which additional fundamental studies will be performed under more complex conditions and subsequently on natural samples derived directly from U.S. coal and coal byproducts.

2.5 Conclusion

Ion-adsorption clays were synthesized at different pHs in open-air conditions and examined by XRD, XPS, ICP-MS, and subjected to ion-exchange leaching tests. Results showed that REE ions physiosorbed on the surface of kaolinite *via* an electrostatic attraction mechanism at pH < 7. Therefore, they can be readily desorbed (extracted) into solution using $(NH_4)_2SO_4$ as lixiviant. At pH > 7, the REE ions adsorb on the clay mineral surfaces in colloidal form as hydroxo-complexes or hydroxides, which made it difficult to extract them using the same lixiviant. It was possible, however, to extract the REEs into solution using $(NH_4)_2SO_4$ as lixiviant by simply reducing the pH below 7.

Acknowledgments

XPS was performed in part at the Surface Analysis Laboratory in Department of Chemistry at Virginia Tech, which is supported by the National Science Foundation under Grant No. CHE-1531834. This material is based upon work supported by the Department of Energy under Award Number DE-FE0029900. Disclaimer: This report was prepared as an account of work sponsored by an agency of the United States Government. Neither the United States Government nor any agency thereof, nor any of their employees, makes any warranty, express or implied, or assumes any legal liability or responsibility for the accuracy, completeness, or usefulness of any information, apparatus, product, or process disclosed, or represents that its use would not infringe privately owned rights. Reference herein to any specific commercial product, process, or service by trade name, trademark, manufacturer, or otherwise does not necessarily constitute or imply its endorsement, recommendation, or favoring by the United States Government or any agency thereof. The views and opinions of authors expressed herein do not necessarily state or reflect those of the United States Government or any agency thereof.

Bibliography

Alshameri, A., He, H., Xin, C., Zhu, J., Xinghu, W., Zhu, R., Wang, H., 2019. Understanding the role of natural clay minerals as effective adsorbents and alternative source of rare earth elements: Adsorption operative parameters. Hydrometallurgy 185, 149–161.

Bao, Z., Zhao, Z., 2008. Geochemistry of mineralization with exchangeable REY in the weathering crusts of granitic rocks in South China. Ore Geol. Rev. 33, 519–535.

Barreca, D., Gasparotto, A., Milanov, A., Tondello, E., Devi, A., Fischer, R.A., 2007. Nanostructured Dy2O3 films: an XPS Investigation. Surf. Sci. Spectra 14, 52–59.

Bauer, D., Diamond, D., Li, J., Sandalow, D., Telleen, P., Wanner, B., 2010. U.S. Department of Energy Critical Materials Strategy. U.S. Department of Energy.

Beche, E., Charvin, P., Perarnau, D., Abanades, S., Flamant, G., 2008. Ce 3d XPS investigation of cerium oxides and mixed cerium oxide (CexTiyOz). Surf. Interface Anal. 40, 264–267.

Berthou, H., Jørgensen, C.K., Bonnelle, C., 1976. Influence of the ligands on 3d photoelectron spectra of the first four lanthanides. Chem. Phys. Lett. 38, 199–206.

Bradbury, M.H., Baeyens, B., 2002. Sorption of Eu on Na- and Ca-montmorillonites: experimental investigations and modelling with cation exchange and surface complexation. Geochim. Cosmochim. Acta 66, 2325–2334.

Bryan, R.C., Richers, D., Andersen, H.T., Gray, T., 2015. Assessment of Rare Earth Elemental Contents in Select United States Coal Basins. Tetra Tech, Inc.

Cai, H.-W., Jiang, P., Jin, L., Hu, J.-M., 2008. Microwave enhanced alkaline digestion of silicate samples for determination of Fe2O3. Talanta 77, 800–803.

Chanaud, P., Julbe, A., Vaija, P., Persin, M., & Cot, L. (1994). "Study of lanthanum-based colloidal sols formation." *Journal of materials science*, *29*(16), 4244-4251.

Cheng, H., Liu, Q., Zhang, J., Yang, J., Frost, R.L., 2010. Delamination of kaolinite–potassium acetate intercalates by ball-milling. J. Colloid Interface Sci. 348, 355–359.

Chi, R., Xu, Z., 1999. A solution chemistry approach to the study of rare earth element precipitation by oxalic acid. Metall. Mater. Trans. B Process Metall. Mater. Process. Sci. 30, 189–195.

Chi, R., & Tian, J. (2008). Weathered crust elution-deposited rare earth ores. Nova Science Publishers.

Coppin, F., Berger, G., Bauer, A., Castet, S., Loubet, M., 2002. Sorption of lanthanides on smectite and kaolinite. Chem. Geol. 182, 57–68.

Haxel, G.B., Hedrick, J.B., Orris, G.J., 2002. Rare Earth Elements—Critical Resources for High Technology. U.S. Geological Survey.

Huang, D., Wu, C., Han, J., 1989. REE Geochemistry and Mineralization Characteristics of the Zudong and Guanxi Granites, Jiangxi Province. Acta Geol. Sin. 2, 139–157.

Iannicelli-Zubiani, E.M., Cristiani, C., Dotelli, G., Gallo Stampino, P., Pelosato, R., Mesto, E., Schingaro, E., Lacalamita, M., 2015. Use of natural clays as sorbent materials for rare earth ions: Materials characterization and set up of the operative parameters. Waste Manag. 46, 546–556.

Ishihara, S., Hua, R., Hoshino, M., Murakami, H., 2008. REE Abundance and REE Minerals in Granitic Rocks in the Nanling Range, Jiangxi Province, Southern China, and Generation of the REE-rich Weathered Crust Deposits. Resour. Geol. 58, 355–372.

Jia, Y.Q., 1987. Quantum chemical studies on the hydrated lons of the rare earths. Inorganica chimica acta 133 (2), 331–336.

Kang, J.G., Gwag, J.S., Sohn, Y., 2015. Synthesis and characterization of $Dy(OH)_3$ and Dy2O3 nanorods and nanosheets. Ceram. Int. 41, 3999–4006.

Kim, H., Kim, M., Byeon, S.-H., 2017. Ce^{4+}/Ce^{3+} redox-controlled luminescence 'off/on' switching of highly oriented $Ce(OH)_2Cl$ and Tb-doped Ce(OH)2Cl films. J. Mater. Chem. C 5, 444–451.

Kim, E., Osseo-Asare, K., 2012. Aqueous stability of thorium and rare earth metals in monazite hydrometallurgy: Eh–pH diagrams for the systems Th–, Ce–, La–, Nd– (PO4)–(SO4)–H2O at 25 C. Hydrometallurgy 113, 67–78.

Kumari, A., Jha, M.K., Yoo, K., Panda, R., Lee, J.Y., Kumar, J.R., Pathak, D.D., 2019. Advanced process to dephosphorize monazite for effective leaching of rare earth metals (REMs). Hydrometallurgy 187, 203–211.

Kragten, J., & Decnop-Weever, L. G. (1987). "Hydroxide complexes of lanthanides—VIII: Lanthanum (III) in perchlorate medium." *Talanta*, *34*(10), 861-864.

Lai, F.G., Huang, L., Gao, G.H., Yang, R., Xiao, Y.F., 2018. Recovery of rare earths from ion-absorbed rare earths ore with MgSO4-ascorbic acid compound leaching agent. J. Rare Earths 36, 521–527.

Li, M., Zhang, D., Yan, Y., Gao, K., Liu, X., Li, J., 2017. Effect of oxidation behavior of cerium during the roasting process on the leaching of mixed rare earth concentrate. Hydrometallurgy 174, 156–166.

Liu, Q., Li, X., Cheng, H., 2016. Insight into the self-adaptive deformation of kaolinite layers into nanoscrolls. Appl. Clay Sci. 124–125, 175–182.

Liu, W., Feng, X., Noble, A., & Yoon, R. H. (2022). Ammonium sulfate leaching of NaOH-treated monazite. Minerals Engineering, 188, 107817.

Marcus, Y., 1985. Ion Solvation. John Wiley & Sons Ltd., New York, NY, USA.

Moldoveanu, G.A., Papangelakis, V.G., 2012. Recovery of rare earth elements adsorbed on clay minerals: I. Desorption mechanism. Hydrometallurgy 117-118, 71–78.

Moldoveanu, G.A., Papangelakis, V.G., 2013. Recovery of rare earth elements adsorbed on clay minerals: II. Leaching with ammonium sulfate. Hydrometallurgy 131–132, 158–166.

Moldoveanu, G.A., Papangelakis, V.G., 2016. An overview of rare-earth recovery by ionexchange leaching from ion-adsorption clays of various origins. Mineral. Mag. 80, 63–76.

Mullica, D.F., Lok, C.K.C., Perkins, H.O., Benesh, G.A., Young, V., 1995. The X-ray photoemission spectra of Nd $(OH)_3$, $Sm(OH)_3$, $Eu(OH)_3$ and $Gd(OH)_3$. J. Electron Spectrosc. Relat. Phenom. 71, 1–20.

Ran, X., Ren, Z., Gao, H., Zheng, R., Jin, J., 2017. Kinetics of Rare Earth and Aluminum Leaching from Kaolin. Minerals 7 (9), 152.

Sanematsu, K., Kon, Y., Imai, A., Watanabe, K., Watanabe, Y., 2013. Geochemical and mineralogical characteristics of ion-adsorption type REE mineralization in Phuket, Thailand. Mineral. Deposita 48, 437–451.

Schulze, D.G., 2005. Clay minerals. In: Hillel, D. (Ed.), Encyclopedia of Soils in the Environment. Elsevier, Oxford, pp. 246–254.

Siegmann, H.C., Schlapbach, L., Brundle, C.R., 1978. Self-restoring of the active surface in the hydrogen sponge LaNi5. Phys. Rev. Lett. 40, 972–975.

Smith, D.W., 1977. Ionic hydration enthalpies. Journal of Chemical Education 54 (9), 540.

Sparks, D.L., 2003. 2 - inorganic soil components. In: Sparks, D.L. (Ed.), Environmental Soil Chemistry, Second edition. Academic Press, Burlington, pp. 43–73.

Stuckman, M.Y., Lopano, C.L., Granite, E.J., 2018. Distribution and speciation of rare earth elements in coal combustion by-products via synchrotron microscopy and spectroscopy. Int. J. Coal Geol. 195, 125–138.

Sunding, M.F., Hadidi, K., Diplas, S., Lovvik, O.M., Norby, T.E., Gunnaes, A.E., 2011. XPS characterisation of in situ treated lanthanum oxide and hydroxide using tailored charge referencing and peak fitting procedures. J. Electron Spectrosc. Relat. Phenom. 184, 399–409.

Suzuki, C., Mukoyama, T., Kawai, J., Adachi, H., 1998. Calculation for the charge transfer effect of La compounds in the 3d core-hole state. Phys. Rev. B 57, 9507–9514.

Valaskova, M., Rieder, M., Matejka, V., Capkova, P., Slíva, A., 2007. Exfoliation/ delamination of kaolinite by low-temperature washing of kaolinite–urea intercalates. Appl. Clay Sci. 35, 108 118.

Voßenkaul, D., Stoltz, N., Meyer, F., Friedrich, B., 2015. Extraction of Rare Earth Elements from non-Chinese Ion Adsorption Clays, Proceedings of EMC, p. 2015.

Wang, Y.Q., Liang, H.Y., Chang, Q.B., Zhang, X.Z., Zhou, J.E., 2016. Separation of kaolinite from ion-adsorption rare earth tailings in southern China and iron removal treatment. J. Miner. Mater. Charact. Eng. 4, 40–47.

Wu, C., Huang, D., Guo, Z., 1990. REE geochemistry in the weathered crust of granites, Longnan area, Jiangxi province. Acta Geol. Sin. 3, 193–209.

Xiao, Y.F., Feng, Z.Y., Hu, G.H., Huang, L., Huang, X.W., Chen, Y.Y., Long, Z.Q., 2016a. Reduction leaching of rare earth from ion-adsorption type rare earths ore with ferrous sulfate. J. Rare Earths 34, 917–923.

Xiao, Y.F., Huang, L., Long, Z.Q., Feng, Z.Y., Wang, L.S., 2016b. Adsorption ability of rare earth elements on clay minerals and its practical performance. J. Rare Earths 34, 543–548.

Xiao, Y.F., Lai, F.G., Huang, L., Feng, Z.Y., Long, Z.Q., 2017. Reduction leaching of rare earth from ion-adsorption type rare earths ore: II. Compound leaching. Hydrometallurgy 173, 1–8.

Zhang, W., Honaker, R., 2019. Calcination pretreatment effects on acid leaching characteristics of rare earth elements from middlings and coarse refuse material associated with a bituminous coal source. Fuel 249, 130–145.

Zhang, J., Zhao, B., Schreiner, B., 2016. Rare Earth Beneficiation and Hydrometallurgical Processing, Separation Hydrometallurgy of Rare Earth Elements. Springer International Publishing, Cham, Switzerland, pp. 19–54.

Zhang, S., Liu, Q., Gao, F., Li, X., Liu, C., Li, H., Boyd, S.A., Johnston, C.T., Teppen, B.J., 2017. Mechanism associated with kaolinite intercalation with urea: combination of infrared spectroscopy and molecular dynamics simulation studies. J. Phys. Chem. C 121, 402–409.

Chapter 3. Rare earth ion-adsorption clays in the presence of iron at various pH: Adsorption mechanism and extraction method

3.1 Abstract

The uptake mechanism and influence of iron (Fe) co-adsorption on the binding of rare-earth elements (REEs) on kaolinite have been investigated. REEs and varying concentrations of Fe were co-adsorbed onto kaolinite at various pH. Inductively coupled plasma mass spectrometry (ICP-MS), powder X-ray diffraction (PXRD), and X-ray photoelectron spectroscopy (XPS) were used to characterize how Fe co-adsorption influenced the uptake mechanism of REEs on kaolinite at pH 10.5. Elemental analysis by ICP-MS revealed that the REE concentrations on kaolinite were unaffected by the presence of Fe. The crystal structure of kaolinite, determined by PXRD, was not altered after REE and Fe co-adsorption. XPS suggests that the adsorbed Fe is in the form of FeOOH, while the greatly attenuated REE XPS signals upon Fe co-adsorption implies that REEs are encapsulated by Fe species. Based on these results, we conclude that FeOOH layers were formed on top of REEs on the surface of kaolinite. Synthesized REE-Fe-kaolinite samples respond poorly to ion-exchange leaching, indicating that Fe is detrimental to the REE ion-exchange efficiency. The inhibition of ion-exchange REE extraction appears to be due to the passivating FeOOH layers. In contrast to ion-exchange methods, reductive leaching was found to dissolve the FeOOH passivating layers and liberate REEs such that they became available for ion-exchange leaching.

3.2 Introduction

From permanent magnets to LED lighting, from wind turbines to electric vehicles, from refining catalysts to laser guidance systems, the global demand for rare earth elements (REEs) has been increasing constantly and rapidly in the 21st century. Many US and international agencies have denoted several REEs as critical materials given their strategic importance and restricted supply. With respect to crustal concentrations, REEs are not truly rare but instead are rarely found as concentrated ore deposits, which often results in prohibitively high mining and recovery costs (Haxel et al., 2002). At present, REEs are produced from two major resources, *i.e.* rare earth minerals (REMs) and ion-adsorption clays (IACs). IACs are highly demanded in global rare earth production due to low environmental impact and enhanced partition of critical heavy rare earth elements (HREEs) (Moldoveanu and Papangelakis, 2012; Zhang et al., 2016). REE in IACs consist

of three major phases (Chi et al., 2005; Huang et al., 2021; Voßenkaul et al., 2015): (1) ion-exchange phase in which REE ions adsorb on the negatively charged clay surface *via* electrostatic attraction; (2) colloidal phase as REE oxides, hydroxides, carbonates, or part of polymeric organometallic compounds; (3) mineral phase such as monazite. REEs in the ion-exchange phase account for 60–90% of the total REEs in IACs and can be exchanged on the clay surface by monovalent cations such as NH_4^+ following the reaction, $Clay - REE^{3+} + 3NH_4^+ \rightarrow Clay - (NH_4^+)_3 + REE^{3+}$. Two main types of colloidal phase have been found on IACs, *i.e.* REEs bound to iron (Fe)/manganese (Mn) oxides or hydroxides by coordination, and REE oxides or hydroxides that are bonded with or deposited on cerium (IV) oxide (CeO_2) (Chi et al., 2005; Chi et al., 2000; Lai et al., 2018; Xiao et al., 2016; Xiao et al., 2017). The REE-Fe/Mn colloid can be effectively dissolved by direct acid leaching or reductive leaching using sulfur dioxide (SO_2) or sodium sulfite (Na_2SO_3) (Chi et al., 2000), while REE-CeO_2 only responds to reducing agents such as ferric sulfate ($FeSO_4$) and ascorbic acid (Lai et al., 2018; Xiao et al., 2016; Xiao et al., 2017). The mineral phase requires more aggressive treatments such as NaOH roasting to liberate REEs into leaching solution (Chi et al., 2005).

To date, China possesses the majority of IAC deposits and produces ~80% of the world's HREE supply (Bao and Zhao, 2008; Huang et al., 1989; Ishihara et al., 2008; Moldoveanu and Papangelakis, 2016; Sanematsu et al., 2013; Voßenkaul et al., 2015; Wu et al., 1990). In many ways, the limited nature of the current supply chain threatens long-term viability. Upon a nationwide survey of feasible domestic REE sources in the U.S., REEs with grade up to 1500 ppm have been found in several major coal basins, and are evidenced to be associated with coal byproducts such as kaolinite clays – one of the major host materials of IACs (Bryan et al., 2015). Therefore, we hypothesize that waste products from U.S. coal preparation plants can serve as viable sources of IACs. However, limited reports concerning REE extraction from U.S. coal byproducts show that < 10% of total REE content are ion exchangeable (Montross et al., 2020; Zhang and Honaker, 2019). Therefore, we aim to understand the nature and variation of REE-bearing clays in U.S. coal basins by means of well-controlled experimental conditions, which is crucial for the development of targeted extraction processes.

The intrinsic acidic pH of IAC deposits in China favors the hydrated REE ion-adsorption mechanism where the majority of REEs exist within the ion-exchange phase. On the contrary, since eastern U.S. coals are commonly found in the basal part of limestone (Greb et al., 1992),

clay-adsorbed REEs in these U.S. coal basins have subjected to hydrolysis and/or REE carbonate formation either before or after adsorption on clays. Therefore, the REE adsorption mechanism on U.S. coal byproducts could be substantially different from that of known IACs. With such motivation, we have initiated a fundamental study of REE adsorption and speciation on model clay surfaces under basic pH conditions to acquire a more comprehensive understanding of the REE adsorption mechanism on U.S. coal and coal byproducts (Feng et al., 2021). Specifically, REEs were adsorbed on kaolinite at various basic pH conditions without the presence of ligands or metals commonly found on clay minerals in U.S. coal basins. It has been found that REEs are electrostatically attached to clay surfaces at basic pH in the form of hydroxides such as $REE(OH)_2^+$. These synthesized clays exhibit excellent ion-exchange efficiency using ammonium sulfate, indicating that the formed REE hydroxides on the clay surface are in the ion-exchange phase. These results demonstrate that IACs can occur under both acidic and basic environments. However, the presence of common co-existing elements in U.S. eastern coal and coal byproducts, such as iron (Fe), calcium (Ca), manganese (Mn), phosphorus (P) and sulfur (S), could greatly impact the uptake mechanism and speciation of REEs on clays. The influence of such co-adsorbates on the nature of REEs within clays has yet to be elucidated.

Among those elements that co-exist with REEs in U.S. eastern coal and coal byproducts, Fe draws the most interest as it accounts for 1.7–9.0 wt % (17,000–90,000 ppm) of the eastern coal waste materials on a dry ash basis (Montross et al., 2020; Zhang and Honaker, 2019). In this work, co-adsorption of Fe with REEs on kaolinite at various pH conditions was studied. Powder X-ray diffraction (PXRD), inductively coupled plasma mass spectrometry (ICP-MS), and X-ray photoelectron spectroscopy (XPS) were used to characterize the influence of Fe on the REE adsorption behavior on kaolinite and provide insights into the speciation of co-adsorption products on the synthesized REE-Fe-kaolinite at basic pH. Ion-exchange and reductive leaching tests were performed on the REE-Fe-kaolinite, and the REE and Fe recoveries were compared to those of REE-kaolinite. Overall, the work shows that Fe inhibits the REE ion-exchange efficiency on kaolinite resulting from the formation of FeOOH passivating layers upon Fe and REE co-adsorption at basic pH conditions.

3.3 Experimental

3.3.1 Materials and chemicals

The Kaolinite sample from Georgia Thiele Kaolin Company was used for the synthesis of ion adsorption clay. $REECl_3$ (La, Ce, Nd, Dy, Y, 99.9%) and $FeCl_3$ (99.9%) were purchased from Sigma-Aldrich Inc. All chemicals were stored in a desiccator upon arrival, and all were used as received. Deionized water with a resistivity of 18.2 MΩ·cm at 298.15 K was used in all solution preparation and leaching tests. Reagent grade NaOH and HCl from Fisher Scientific were used for pH adjustment and $(NH_4)_2SO_4$ was used as a lixiviant for ion-exchange leaching tests (Fisher Scientific, 99.3% purity). $Na_2O_4S_2$ (Sodium dithionite, Sigma-Aldrich Inc., 90% purity) was used as a reducing agent to control the Eh of the leaching solution.

3.3.2 Methods and procedure

3.3.2.1 Synthesis of REE-Fe-kaolinite

The Georgia Clay sample was contacted with solutions of known $REECl_3$ and $FeCl_3$ concentrations including, $LaCl_3$, $NdCl_3$, $CeCl_3$, $DyCl_3$, and YCl_3. The concentrations of the REE chloride solutions were determined in such a way that the resulting ion-adsorption clay would contain 400-500 ppm for each REE and 2,000 ppm TREEs while increasing the $FeCl_3$ concentrations from 0.4 to 1.6 % gradually. Thus, the REE^{3+} (or Ln^{3+}) ions and Fe could co-adsorb on the negatively charged clay surface. The cation exchange capacity (CEC) of kaolinite typically ranges from about 3 to 15 milliequivalents per 100 grams (meq/100g) of clay (Grim,1953). The adsorb REEs represent the 45% of the CEC limit of Kaolinite. In each experiment, a 15 g clay sample was placed in a 125 ml Erlenmeyer flask at a 1:5 solid-to-liquid ratio. The mixture was agitated by a magnetic stirrer at pH 3–10.5 at room temperature for 24h. After the agitation, the clay samples were filtered, washed 3 times with 250 ml deionized water, dried overnight at 60 ˚C, and used for leaching tests. The synthetic ion adsorption clays prepared in this manner were analyzed for REE contents by means of ICP/MS. Blank tests showed that the run-of-mine (ROM) Georgia kaolinite sample contained 65 ppm La, 100 ppm Ce, 15 ppm Y, and 45 ppm Nd, while the Dy content was only 3 ppm.

3.3.3 Sample characterization

3.3.3.1 Powder X-ray diffraction (PXRD)

PXRD measurements were performed on a Rigaku Miniflex 600 instrument with Cu-Kα radiation (λ = 1.54 Å). PXRD trace were acquired over a 2θ range from 3° to 80° with a step size of 0.04° and a dwell time of 2 s.

3.3.3.2 X-ray photoelectron spectroscopy (XPS)

XPS measurements were performed on a PHI VersaProbe III scanning XPS microscope equipped with a monochromatic Al K-alpha X-ray source (1486.6 eV) with a base pressure of 3×10^{-8} Pa. XPS Spectra were acquired with 100 μm/100 W/20 kV settings over a 1400 μm × 100 μm sample area using 55 eV pass energy, which gives an Ag $3d_{5/2}$ full width at half maximum of 0.65 eV. All binding energies were referenced to adventitious carbon peak at 284.8 eV. A Shirley background and Gaussian-Lorentzian peak shape were used for curve fitting. Quantification was accomplished using PHI MultiPak 9.9.0.8, using the appropriate corrected sensitivity factors.

3.3.3.3 Inductively coupled plasma mass spectrometry (ICP-MS)

Elemental analysis for REEs was performed on an Agilent 7900 ICP-MS. A stock solution mixture of the lanthanides, scandium, yttrium, thorium, and uranium made up in 5% *v*/v nitric acid (HNO3) was purchased from Inorganic Ventures (Christiansburg, VA; Catalog # CMS-1-125ML). Another custom mix stock solution comprised of magnesium, aluminum, silicon, calcium, iron, manganese, and cobalt was also purchased from Inorganic Ventures. Both stocks were combined and further diluted in 2% *w*/*v* HNO_3 + 0.5% w/v hydrochloric acid (HCl). Individual elemental concentrations were quantified using a seven-point calibration curve made with known concentrations of the analytes of interest in the same dilute acid solution as the samples. Linear calibration curves ranging from 10 parts per trillion (ppt) to 100 parts per billion (ppb) for the REEs, and 20 to 2000 ppb for the non-REE elements, with coefficient of determination (R^2) values of >0.999 were observed for each element of interest.

Both the leaching solutions and the solids were analyzed in this experiment for mass balance and comparison purposes. Leaching solutions that were centrifuged from their original pellet were quickly and easily prepared for ICP-MS analysis by direct dilution into the 2% *w*/*v* HNO_3 + 0.5% w/v HCl diluent.

Clay samples were prepared for ICP-MS analysis by adding 6 mL of 50% (*w*/*v*) sodium hydroxide (NaOH) to 50 mg of the samples for microwave digestion at 180 ˚C (Cai et al., 2008). The NaOH-treated samples were acidified by HNO_3 (70% w/v) and the dissolved samples were diluted appropriately with the 2% w/v HNO_3 + 0.5% w/v HCl solution before being subjected to ICP-MS analysis.

3.3.3.4 Ion-Exchange leaching (IXL) tests

Synthesized ion-adsorption clays prepared with 5 $REECl_3$ at various pH values with and without $FeCl_3$ were subjected to a series of leaching tests at room temperature using the 0.5M conventional lixiviant $(NH_4)_2SO_4$ at a 1:2 solid-to-liquid ratio, and the mixture was agitated in Lab-Line Orbit Environ-Shaker for 1 h at pH 5. The pH was adjusted to 5 ±0.1 by using HCl and NaOH solutions. After the agitation, the clay sample was washed with 250ml of deionized water, filtered through 413 ashless filter paper, dried overnight at 60 ˚C, and assayed by ICP-MS.

3.3.3.5 Reductive leaching tests

Synthesized ion-adsorption clay samples were prepared with 5 $REECl_3$ (~2000 ppm TREE) at various pH values in the presence of $FeCl_3$ (~8000 ppm Fe) and subjected to reductive leaching tests. All leaching tests were conducted at pH 5 and 25˚C using a 4 g clay sample at a 1:10 solid/liquid ratio. Sodium dithionite and sodium sulfite were used as reducing agents to keep Eh around -300 mV as measured using the EG&G Potentiostat/Galvanostat, model 273A. The leaching vessel was flushed with N_2 gas to maintain a constant potential. After achieving the desired pH and potential, the slurry was initially conditioned for one hour. Following that period, ammonium sulfate was added to the solution (0.5 M), and the leaching reaction was conducted for a second hour. Following the two-hour sequence, the samples were centrifuged for 10 minutes at 5000 rpm, washed 3 times with 150 ml deionized water, dried in an oven overnight at 60˚C, and analyzed for REEs to determine the recoveries. Afterward, extraction efficiency was calculated by comparing the leaching residue`s REEs content to the initial feed material`s REEs content.

The recovery (R) of an REE species was determined using the following relationship in Eq. (1),

$$\text{Recovery}(\%) = 100 - [\frac{\text{T.t}}{\text{F.f}} \text{ x}100] \quad (1)$$

in which T and t are the weight (%) and REE concentration (ppm) of the residue, respectively; and F and f are the weight (%) and REE concentration (ppm) of the feed, respectively.

3.4 Results and Discussion

REEs and varying concentrations of Fe were co-adsorbed onto kaolinite at pH 10.5. The influence of Fe on the uptake mechanism and speciation of REEs on kaolinite were probed by ICP-MS, PXRD, and XPS, followed by ion exchange and reductive leaching tests.

3.4.1 Speciation of Fe on REE-Fe-kaolinite

Elemental analysis was performed by inductively coupled plasma mass spectrometry (ICP-MS) on the synthesized REE-kaolinite and REE-Fe-kaolinite samples. Concentrations (ppm) of REEs and Fe are listed in Table 3.1. The REEs and Fe in the blank kaolinite sample were found to have negligible effects on the REE and Fe adsorption and leaching (not shown), thus the amounts of REEs and Fe in the blank kaolinite sample can be deducted from the total values to obtain the amount of adsorption. For the REE-kaolinite prepared at pH 10.5, the concentrations of adsorbed REEs (La, Ce, Nd, Dy, and Y) are close to 400 ppm, which are consistent with those of similarly prepared REE-kaolinite samples discussed in previous Chapter 2. The REE-Fe-kaolinite samples synthesized with various Fe concentrations (3000, 7000 and 13,000 ppm) were found to have similar surface-bound REE concentrations as those of REE-kaolinite. This result indicates that co-adsorbed Fe does not inhibit the adsorption of REEs, suggesting that the co-adsorption of REEs and Fe on kaolinite at basic pH is not a competitive process.

Table 3.1 Concentrations of REE and Fe (ppm) in REE-kaolinite and REE-Fe-kaolinite

Sample	La	Ce	Nd	Dy	Y	Fe
kaolinite	65	100	45	3	15	6,089
REE-kaolinite	490	478	459	401	439	6,038
REE-Fe-kaolinite-1	480	477	462	395	422	9,106
REE-Fe-kaolinite-2	504	502	469	400	425	13,040
REE-Fe-kaolinite-3	486	487	477	400	424	18,905

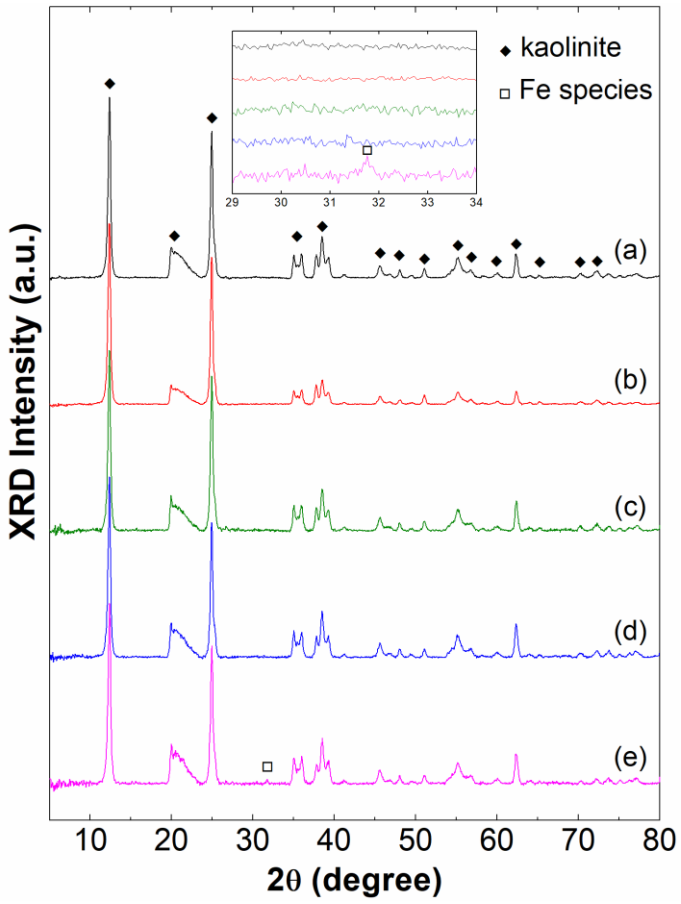

Figure 3.1 PXRD patterns of (a) kaolinite; (b) REE-kaolinite; (c) REE-Fe-kaolinite-1; (d) REE-Fe-kaolinite-2; (e) REE-Fe-kaolinite-3.

Insight into the overall crystal structures of kaolinite before and after REE and Fe co-adsorption was provided by powder X-ray diffraction (PXRD) measurements. Figure 3.1 shows the PXRD reflections of REE-kaolinite and REE-Fe-kaolinite with various Fe concentrations. The PXRD peaks of the blank kaolinite sample (Figure 3.1a) match those of kaolinite, while the broad, non-resolved feature from 0.467 to 0.371 nm (2θ from 19° to 24°) can be attributed to minor disorder of kaolinite due to non-regular displacements of the Al vacancy in the octahedral sheet (Raven and Self, 2017). The REE-kaolinite prepared at pH 10.5 produces a PXRD pattern that is nearly identical to that of the kaolinite (Figure 3.1b), indicating that the REE adsorption does not alter the bulk crystal structure of the kaolinite, suggesting that REEs bind to the surface of kaolinite. Furthermore, REEs and Fe co-adsorption on kaolinite at pH 10.5 does not appear to affect the PXRD pattern (Figure 3.1c and 3.1d), suggesting that Fe does not disrupt the bulk

crystallographic presentation of the clay. Notwithstanding, a small peak at 0.282 nm ($2\theta = 31.7^{\circ}$) was detected in the REE-Fe-kaolinite-3 sample with the highest Fe concentration (Figure 3.1e and insert), however, this peak position does not match any major phase of iron oxyhydroxides including goethite (α-FeOOH), lepidocrocite (γ-FeOOH) and feroxyhyte (δ-FeOOH), or iron oxides including hematite (α-Fe_2O_3), maghemite (γ-Fe_2O_3) and magnetite (Fe_3O_4).

Details regarding the chemical state of surface-adsorbed Fe and REEs on kaolinite were provided *via* XPS. Figure 3.2 shows the XPS spectra of REE-kaolinite and REE-Fe-kaolinite-1 synthesized at pH 10.5. The survey scan of REE-kaolinite (Figure 3.2a) shows major elements of O (67.9 at. %), Al (10.5 at. %) and Si (12.6 at. %) that closely resemble the composition of native kaolinite $Al_2Si_2O_5(OH)_4$. Small amounts of C, Mg, Na, Ti and F on the surface are well-known impurities in the clay. Importantly, no surface Fe was detected for the kaolinite sample, indicating that native Fe in kaolinite resides in the bulk of the clay particles and are not accessible for surface chemistry. In contrast, the sample prepared in the presence of Fe (REE-Fe-kaolinite-1) shows the same surface composition as the native kaolinite with the addition of surface-bound Fe. The overall surface composition was found to be: O 69.2 at. %, Al 10.7 at. %, Si 12.9 at. %, Fe 0.5%. The surface Fe/Al atomic ratio of 0.047 is much higher than the bulk ratio of 0.018 from the ICP-MS analysis, indicating that the adsorbed Fe is concentrated on the surface of kaolinite.

Comparisons of Fe $2p_{3/2}$ and O *1 s* high-resolution spectra of REE- kaolinite and REE-Fe-kaolinite-1 (Figure 3.2b and 3.2c respectively) provide information about the nature of Fe-REE interactions on the surface. As expected, no surface Fe is detected on REE-kaolinite (Figure 3.2b), while a broad Fe feature is present on REE-Fe-kaolinite-1 (Figure 3.2c). The Fe $2p_{3/2}$ photoemission peak at 710.7 eV on the REE-Fe-kaolinite-1 sample falls in the range of Fe(III), while the Fe $2p_{3/2}$ curve can be fitted by a five-peak set similar to those of FeOOH (Grosvenor et al., 2004). Both samples show a predominant O *1 s* peak at 532.3 eV from Al–O and Si–O on the clay surface (Figure 3.2c), while a small shoulder feature centered at 529.6 eV on REE-Fe-kaolinite-1 can be attributed to Fe–O bonds (Moulder et al., 1995) of the REE-Fe complexes.

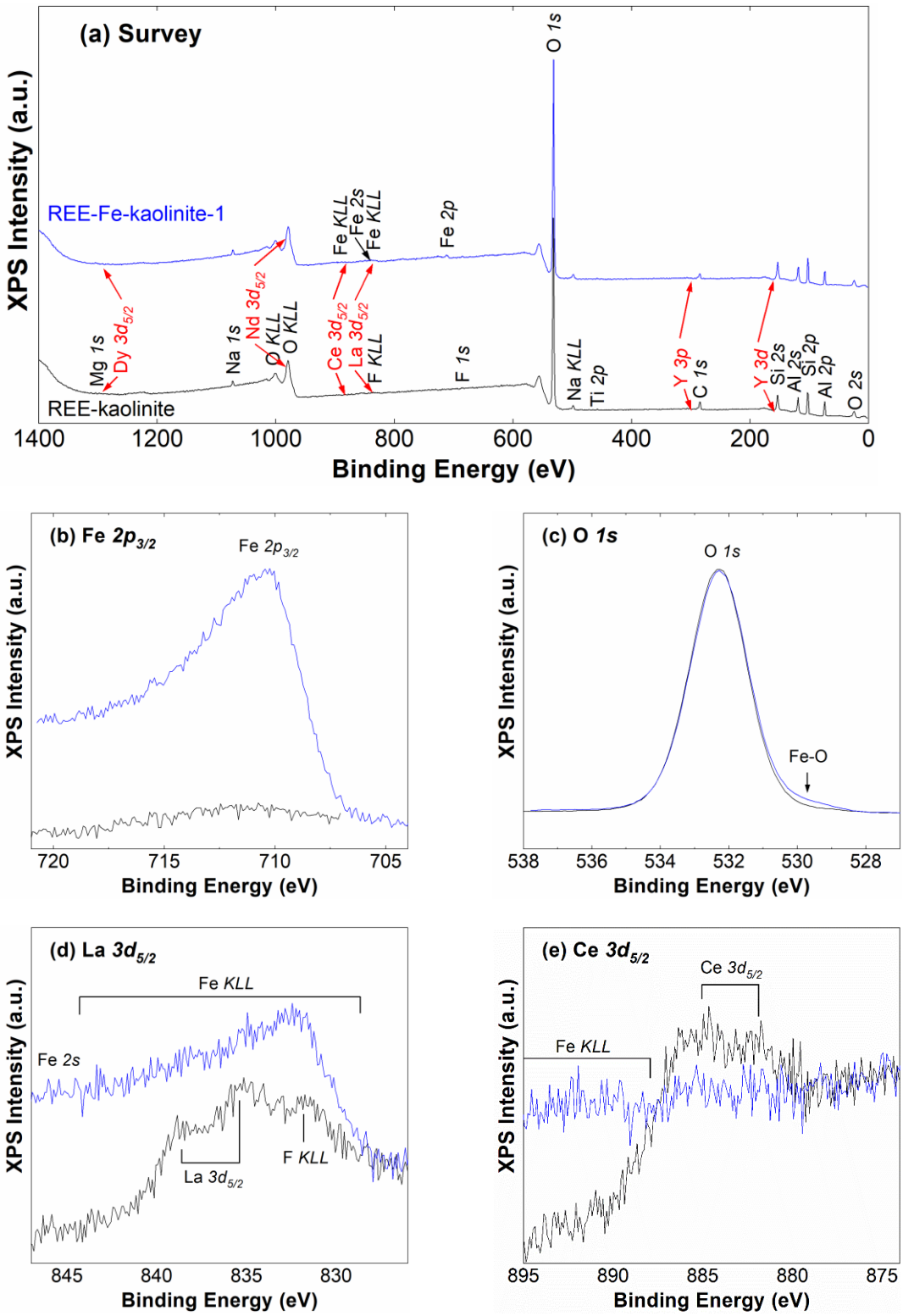

Figure 3.2 XPS spectra of REE-kaolinite (black lines) and REE-Fe-kaolinite-1 (blue lines) synthesized at pH 10.5. (a) survey; (b) Fe 2p3/2; (c) O 1s; (d) La 3d5/2; (e) Ce 3d5/2; (f) Dy 3d5/2; (g) Y 3p.

High-resolution scans of La $3d_{5/2}$, Ce $3d_{5/2}$, Dy $3d_{5/2}$ and Y $3p$ on both samples are also included in Figure 3.2. The spectra of individual REEs on the REE-kaolinite have been discussed elsewhere (Feng et al., 2021). Briefly, REE hydroxides have been identified to be the primary REE species on the surface of kaolinite at basic pH by matching peak characteristics to standard REE materials. For the REE-Fe-kaolinite-1 sample, the La $3d_{5/2}$ feature (Figure 3.2d) is overwhelmed by the broad, overlapping Fe *KLL* feature, thus no useful information can be found concerning the chemical state of La. The Ce $3d_{5/2}$, Dy $3d_{5/2}$ and Y $3p$ signals (Figure 3.2e – 3.2g) are all greatly attenuated upon Fe co-adsorption in sharp contrast to their unchanged bulk concentrations (Table 3.1), suggesting that the adsorbed REEs are encapsulated or reside beneath the co-adsorbed Fe. Based on the XPS results, we postulate that the adsorbed Fe form FeOOH layers on top of REEs on the surface of kaolinite. The binding mechanism between FeOOH and REEs is subject to further studies. It is possible that Fe hydroxides adsorb REE ions through inner-sphere complexation. Overall, the study shows that the FeOOH top layers significantly influences the extractability of REEs on kaolinite.

3.4.2 Ion-exchange leaching of REE-Fe-kaolinite

Figure 3.3 shows the REE recovery % of REE-kaolinite and REE-Fe-kaolinite with various Fe concentrations using 0.5 M ammonium sulfate (AS) as a lixiviant at pH 5. The REE-kaolinite in the absence of Fe co-adsorption responds well to ion exchange leaching with the recoveries of La, Nd, Dy, and Y at around 80% and Ce at 43%. In contrast, the ion exchangeability of all five REEs is continuously suppressed by increasing the concentration of co-adsorbed Fe. With the co-adsorption of 13,000 ppm Fe (REE-Fe-kaolinite-3), <20% of the surface-bound REEs can be extracted by ion exchange leaching. This Fe concentration (13,000 ppm) is approaching the Fe contents that are partitioned to U.S. eastern coal waste materials (17,000–90,000 ppm) (Montross et al., 2020; Zhang and Honaker, 2019), suggesting that the co-existing Fe could also inhibit the ion-exchangeability of REEs in U.S. eastern coal wastes. In addition, the recovery of Fe throughout all Fe concentrations stays below 20% with no substantial variation.

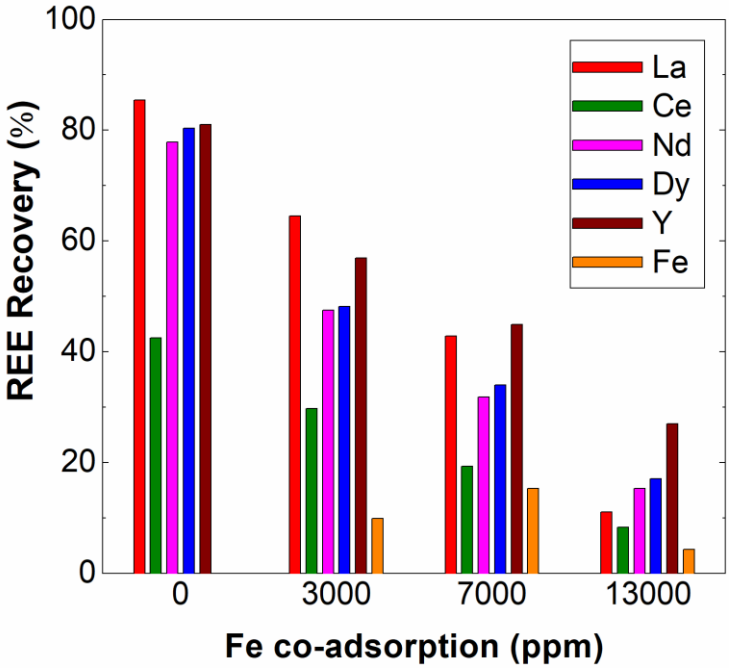

Figure 3.3 REE recoveries of REE-kaolinite and REE-Fe-kaolinite synthesized at pH 10 with various Fe concentrations and applied ion exchange leaching using 0.5 M ammonium sulfate at pH 5.

The results indicate that the FeOOH top layers formed upon REE and Fe co-adsorption inhibit typical $REE^{3+} \leftrightarrow 3NH_4^+$ ion exchange for REE liberation. REEs are passivated by FeOOH and no longer available for ion exchange. More aggressive methods such as direct acid leaching or reductive leaching are required to liberate the REEs under these conditions.

3.4.3 Reductive leaching of REE-Fe-kaolinite

An alternative strategy to direct acid leaching is to dissolve the FeOOH passivating layers under reducing conditions by decreasing the electrochemical potential (Eh) of the leaching solution. According to the published Eh-pH diagram of Fe-H_2O (Lai et al., 2018), one can dissolve Fe_2O_3/$Fe(OH)_3$ at pH 5 provided that Eh is less than ~260 mV, a mild reducing condition that can be readily obtained. If a stronger reducing agent is used, one can dissolve the complexes at pH 7. In fact, this process, known as reductive leaching, is actively employed by the kaolin-processing industry to remove Fe (III)-bearing impurities from kaolin clay (Thurlow, 2005; Zegeye et al., 2013).

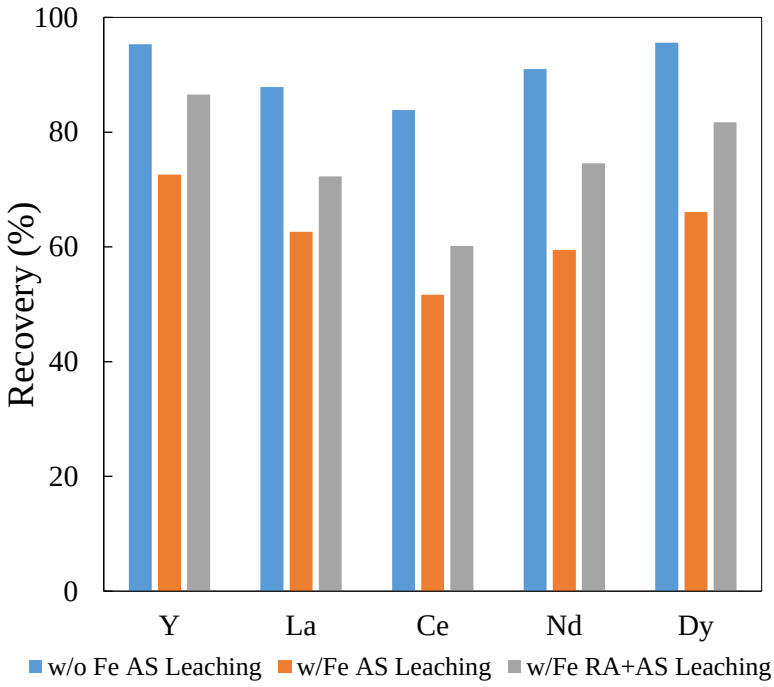

Figure 3.4 Ion exchange leaching test results of synthesized IACs at pH 3.

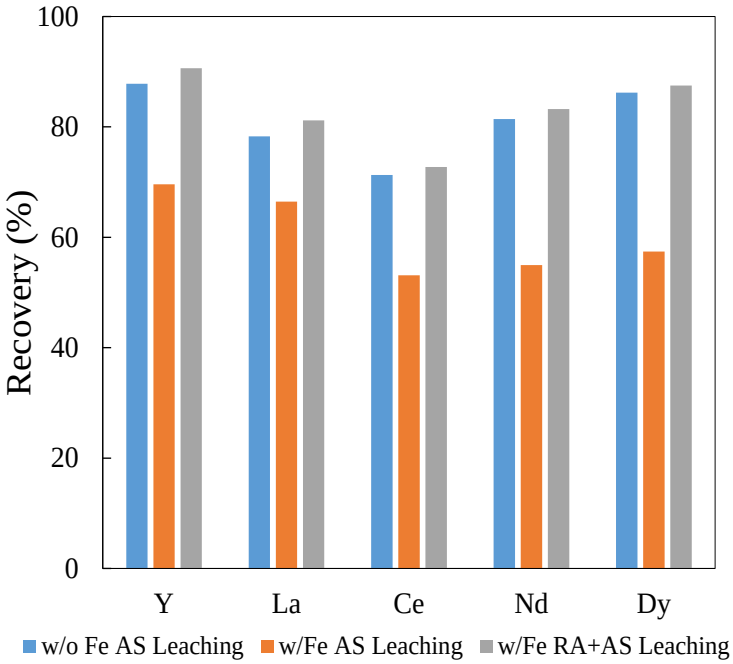

Figure 3.5 Ion exchange leaching test results of synthesized IACs at pH 5.

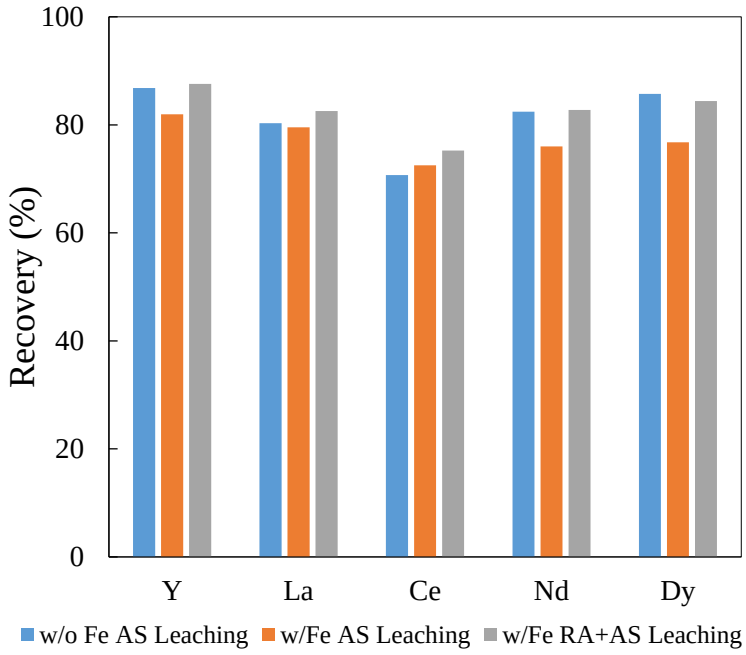

Figure 3.6 Ion exchange leaching test results of synthesized IACs at pH 7.

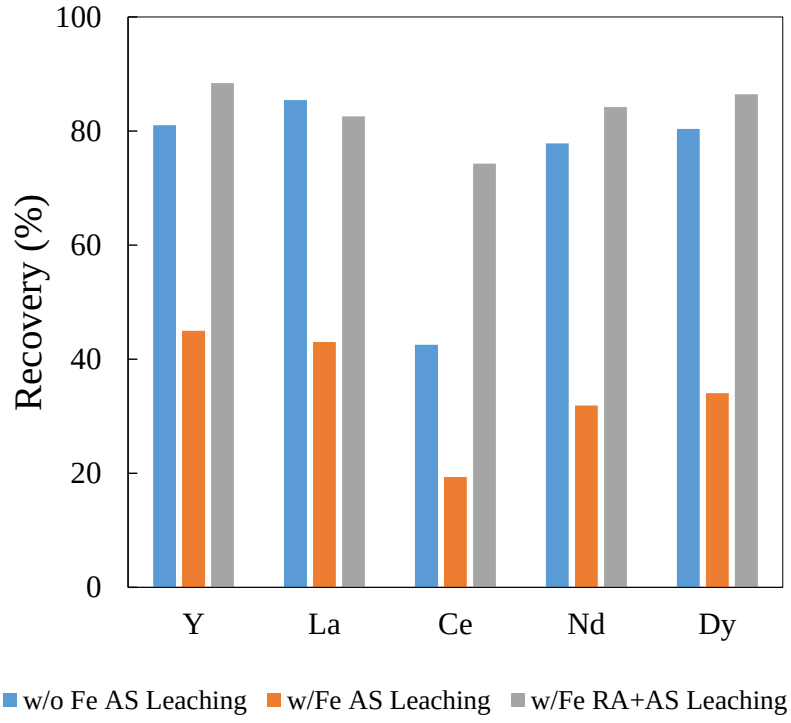

Figure 3.7 Ion exchange leaching test results of synthesized IACs at pH 10.

The previous study, submitted in Chapter 2, demonstrated that REE-kaolinite, synthesized at basic pH and in the absence of Fe, exhibits excellent REE ion exchange efficiency. Specifically, we demonstrate that REE hydroxides are electrostatically attracted to the surface of kaolinite and serve as the ion exchange phase under these conditions. However, one anticipates that the FeOOH top layers that are formed upon REE and Fe co-adsorption may affect the accessibility of the surface-bound REEs. Therefore, a set of leaching experiments were performed on the REE-Fe-kaolinite samples described above to test the effect of iron co-adsorption on the REE ion exchange efficiency.

Figures 3.4 to 3.5 show that ammonium sulfate leaching is effective for all the pH values when the kaolinite sample is synthesized without Fe addition. However, in the presence of Fe, ammonium sulfate is not effective at higher pH values (above 7). Below pH 7, 60-80% recovery values were obtained after the ion exchange leaching test by using 0.5M ammonium sulfate. Besides, the application of reductive leaching in addition to ion-exchange leaching and usage of the Na-dithionite at these low pH values increases the recovery values by around 10 %.

On the other hand, as shown in Figure 3.7 when the ion exchange leaching tests were applied by using ammonium sulfate at pH 5 to the synthesized REE-kaolinite sample without Fe, the recovery values were around 80%. In the presence of Fe, recovery values drop drastically from 80 to 30%, showing the recovery of REEs from clay samples is not possible by the ion exchange leaching test method. The reason is two colloidal forms of REEs identified on the surface of kaolinite include hydroxides Ln $(OH)_3$ and lanthanide-iron oxyhydroxide ((Ln, Fe) OOH). At pH 5, the samples synthesized at pH < 7 can be readily extracted with $(NH_4)_2SO_4$, whereas the samples prepared at basic pH > 7 can be extracted under reducing conditions. To overcome the harmful effect of Fe, reductive leaching tests were performed to examine the dissolution of FeOOH on REE-Fe-kaolinite. In the reductive leaching process, reducing the Eh value below -300 mV by adding Na-Dithionite and keeping the pH value around 5 is an alternative method of acid leaching. As an alternative to sodium dithionite (SDT), sodium sulfide (SS) was also evaluated in this study.

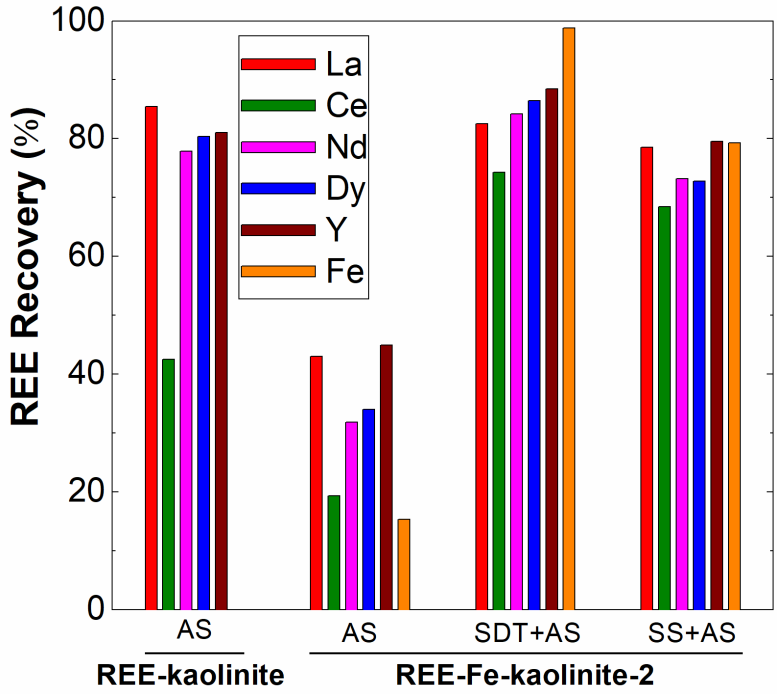

Figure 3.8 REE recoveries of REE-Fe-kaolinite-2 using various reducing agents and ammonium sulfate at pH 5. AS – ammonium sulfate; SDT – sodium dithionite; SS – sodium sulfide.

Figure 3.8 shows the REE recovery % from REE-Fe-kaolinite-2 (7000 ppm of co-adsorbed Fe) that is treated in sodium dithionite and sodium sulfide solutions respectively and leached by ammonium sulfate (AS) at pH 5. The previously shown REE recoveries of REE-kaolinite and REE-Fe-kaolinite-2 using ammonium sulfate only are also included in this figure for comparison. After sodium dithionite was added to reduce the Eh of the leaching solution, the recoveries of all REEs were found to rise sharply to ~80%. This REE extraction efficiency is comparable to that of REE-kaolinite in the absence of Fe, indicating that under this reducing condition the FeOOH passivating layers have been completely dissolved and REEs initially confined by the co-adsorbed Fe become available again. In addition, 99% of the co-adsorbed Fe was found to leach into the solution, which further demonstrates the complete dissolution of FeOOH. It is also worth noting that 74% of Ce is extracted from the REE-Fe-kaolinite-2 sample, which is close to the extraction efficiency of other REEs on REE-Fe-kaolinite-2. Remarkably, the Ce extraction efficiency under reductive conditions is almost twice of that of Ce recovery from REE-kaolinite (43%), which indicates that the reductive leaching significantly improves the ion exchange capability of Ce on kaolinite. The lower Ce recovery from REE-kaolinite is a possibility due to the oxidation of Ce

(III) to Ce(IV) during the AS leaching process, which is suppressed by the maintained reducing potential in the leaching solution and results in a much higher Ce recovery by ion-exchange leaching. Finally, we note that the REE-Fe-kaolinite-2 sample also responds well to the reductive leaching using sodium sulfide with slightly lower recoveries of REE and Fe than those using sodium dithionite, presumably from the difference in the strength of these two reducing agents.

3.5 Conclusion

Co-adsorption of REEs and Fe onto kaolinite at basic pH conditions was examined. It was found that the adsorbed Fe form passivating FeOOH layers on top of REEs on the surface of kaolinite. The FeOOH layers block the access of ion-exchange lixiviants to surface-bound REEs, resulting in poor ion-exchange efficiencies. To overcome that a reductive leaching approach effectively dissolves the passivating FeOOH layers, which activates high REE ion-exchange efficiencies.

3.6 Implications for U.S. REE Extraction

Fe is commonly found in the same locations as REEs in U.S. coal and coal byproducts (Montross et al., 2020; Zhang and Honaker, 2019). Since Fe is detrimental to the ion-exchange efficiency of REEs on clays, the concentration of Fe in the feed could be associated with the primary type of REEs in different U.S. coal waste sites. Low Fe:REE concentration ratios in the feed may signal the major presence of ion-exchangeable REEs, while high Fe:REE concentration ratios may result in predominant formation of FeOOH passivating layers, which requires distinctly different extraction process such as direct acid leaching or reductive leaching. Furthermore, REEs may also interact with other co-existing elements including Ca, Mn, P and S, and their co-adsorption mechanism are subject to future studies. Therefore, a careful selection and clear understanding of the major REE phases in individual U.S. coal waste sites is critical to the development of feasible REE extraction strategies from U.S. coal and coal byproducts.

Bibliography

Bao, Z., Zhao, Z., 2008. Geochemistry of mineralization with exchangeable REY in the weathering crusts of granitic rocks in South China. Ore Geol. Rev. 33 (3), 519–535.

Bryan, R.C., Richers, D., Andersen, H.T., Gray, T., 2015. Assessment of Rare Earth Elemental Contents in Select United States Coal Basins. Tetra Tech, Inc.

Cai, H.-W., Jiang, P., Jin, L., Hu, J.-M., 2008. Microwave enhanced alkaline digestion of silicate samples for determination of Fe2O3. Talanta 77 (2), 800–803.

Chi, R., Zhu, G., Zhou, Z., Xu, Z., 2000. A novel process for recovering rare earth from weathered black earth. Metall. Mater. Trans. B Process Metall. Mater. Process. Sci. 31 (1), 191–196.

Chi, R., et al., 2005. Existing state and partitioning of rare earth on weathered ores. J. Rare Earths 23 (6), 756–759.

Feng, X., Onel, O., Council-Troche, M., Noble, A., Yoon, R. H., & Morris, J. R. (2021). A study of rare earth ion-adsorption clays: The speciation of rare earth elements on kaolinite at basic pH. Applied Clay Science, 201, 105920.

Fuerstenau, M. C., & Palmer, B. R. (1976). Anionic flotation of oxides and silicates. *Flotation--A. M. Gaudin Memorial*.

Greb, S.F., Williams, D.A., Williamson, A.D., 1992. Geology and stratigraphy of the western Kentucky coal field. Kentucky Geological Survey Bulletin 3.

Grim, R. E. (1953). *Clay mineralogy* (Vol. 76, No. 4, p. 317). LWW.

Grosvenor, A.P., Kobe, B.A., Biesinger, M.C., McIntyre, N.S., 2004. Investigation of multiplet splitting of Fe 2p XPS spectra and bonding in iron compounds. Surf. Interface Anal. 36 (12), 1564–1574.

Haxel, G.B., Hedrick, J.B., Orris, G.J., 2002. Rare Earth Elements—Critical Resources for High Technology. U.S. Geological Survey.

Huang, D., Wu, C., Han, J., 1989. REE Geochemistry and Mineralization Characteristics

of the Zudong and Guanxi Granites, Jiangxi Province. Acta Geologica Sinica – English Edition 2 (2), 139–157.

Huang, J., et al., 2021. REE fractionation controlled by REE speciation during formation of the Renju regolith-hosted REE deposits in Guangdong Province, South China. Ore Geology Reviews 134, 104172.

Ishihara, S., Hua, R., Hoshino, M., Murakami, H., 2008. REE Abundance and REE Minerals in Granitic Rocks in the Nanling Range, Jiangxi Province, Southern China, and Generation of the REE-rich Weathered Crust Deposits. Resour. Geol. 58 (4), 355–372.

Lai, F.G., Huang, L., Gao, G.H., Yang, R., Xiao, Y.F., 2018. Recovery of rare earths from ion-absorbed rare earths ore with MgSO4-ascorbic acid compound leaching agent. J. Rare Earths 36 (5), 521–527.

Moldoveanu, G.A., Papangelakis, V.G., 2012. Recovery of rare earth elements adsorbed on clay minerals: I. Desorption mechanism. Hydrometallurgy 117-118, 71–78.

Moldoveanu, G.A., Papangelakis, V.G., 2016. An overview of rare-earth recovery by ion exchange leaching from ion-adsorption clays of various origins. Mineral. Mag. 80 (1), 63–76.

Montross, S., Yang, J., Britton, J., McKoy, M., Verba, C., 2020. Leaching of rare Earth elements from central Appalachian coal seam underclays. Minerals 10, 577.

Moulder, J.F., Stickle, W.F., Sobol, P.E., Bomben, K.D., 1995. Handbook of X-Ray Photoelectron Spectroscopy. Physical Electronics USA, Inc.

Noble, Aaron, & Yoon, Roe-Hoan. 2020. *Development of a Cost-Effective Extraction Process for the Recovery of Heavy and Critical Rare Earth Elements from the Clays and Shales Associated with Coal*. United States.

Raven, M., Self, P., 2017. Identification and Quantification of Clays. In: McFarlane, A.J., Klauber, C., Robinson, D.J., Gr¨afe, M. (Eds.), Clays in the Minerals Processing Value Chain. Cambridge University Press, Cambridge, pp. 142–204.

Sanematsu, K., Kon, Y., Imai, A., Watanabe, K., Watanabe, Y., 2013. Geochemical and mineralogical characteristics of ion-adsorption type REE mineralization in Phuket, Thailand. Mineralium Deposita 48 (4), 437–451.

Thurlow, C., 2005. China Clay from Cornwall and Devon: The Modern China Clay Industry. Cornish Hillside Publications.

Voßenkaul, D., Stoltz, N., Meyer, F., Friedrich, B., 2015. Extraction of rare earth elements from non-chinese ion adsorption clays. Proceedings of EMC 2015.

Wu, C., Huang, D., Guo, Z., 1990. REE Geochemistry in the Weathered Crust of Granites, Longnan Area, Jiangxi Province. Acta Geologica Sinica - English Edition 3 (2), 193–209.

Xiao, Y.F., et al., 2016. Reduction leaching of rare earth from ion-adsorption type rare earths ore with ferrous sulfate. J. Rare Earths 34 (9), 917–923.

Xiao, Y.F., Lai, F.G., Huang, L., Feng, Z.Y., Long, Z.Q., 2017. Reduction leaching of rare earth from ion-adsorption type rare earths ore: II. Compound leaching. Hydrometallurgy 173, 1–8.

Zhang, W., Honaker, R., 2019. Calcination pretreatment effects on acid leaching characteristics of rare earth elements from middlings and coarse refuse material associated with a bituminous coal source. Fuel 249, 130–145.

Chapter 4. Effect of Novel Lixiviants on the Leaching Process of Ion Adsorption Type Rare Earth Ore

4.1 Abstract

In modern industry, rare earth metals play an increasingly important role in the development of high-tech products. Ion-adsorption clays (IACs) are the major source of heavy rare earth elements (HREEs) found in weathered clay (e.g., kaolinite). Ion-exchange leaching is one of the most common ways to obtain HREEs from IACs by using $(NH_4)_2SO_4$. In the present work, the synthetic ion-adsorption clays were subjected to ion-exchange leaching tests using a series of novel lixiviants. While $(NH_4)_2SO_4$ is a favored lixiviant due to differing hydration enthalpies between Ln^{3+} and NH_4^+ ions (around 3,000 kJ/mol), this study explored alkylammonium ions with varying chain lengths. Novel reagents showed improved results as compared with those obtained using the conventional lixiviant, *i.e.*, NH_4^+ ions. The best results were obtained using hexadecyltrimethylammonium chloride (HTAC) and dodecylamine hydrochloride (DAH).

4.2 Introduction

Rare earth metals play an essential role in advancing modern industry and designing high-technology products that have become integral to our daily lives. The primary sources of these essential elements are Monazite, Bastnaesite, Xenotime, and Ion-adsorption clays, which serve as the main mineral resources for rare earth extraction. These minerals possess unique characteristics that enable the extraction and utilization of rare earth metals, contributing significantly to technological innovation and social progress.

Ion adsorption clay ore in southern China represents a unique and strategically significant resource for rare earth elements. It is formed through a geological process involving the weathering and transformation of granodioritic and volcanic rocks under warm and humid climatic conditions. This intricate process results in the emergence of clay minerals, including kaolinite, halloysite, and illite. Concurrently, rare earth elements are released from the original rocks during the same geological conditions, subsequently giving rise to REE-hydroxyl aqueous ions that become adsorbed onto the clay minerals (Chi et al, 2005, Qiu et al, 2014, Tian et al 2013).

Rare earth distribution within ores can be classified into four distinct phases (Chi and Tian, 2006). In the first phase, rare earth elements are present in a water-soluble form, accounting for a

negligible fraction, less than one in ten thousand of the total rare earth contents. Moving to the second phase, the majority of rare earth elements exist in an ion-exchangeable state, where they are adsorbed onto clay minerals through electrostatic interactions. This phase constitutes over 80% of the total rare earth content and can be easily released into leaching solutions upon encountering specific cations, such as NH_4^+, and Mg^{2+}. The smaller the ionic radii, the higher the charge density, which is why ion adsorption clays are the major source of HREEs. The third phase involves the colloidal sediment, encompassing two components: rare earth elements adsorbed onto iron and manganese colloids through coordination, and rare earth oxide or hydroxide compounds bonded with minerals, such as CeO_2/Ce $(OH)_4$. Understanding the distribution of rare earth elements across these distinct phases provides crucial insights into their behavior and potential extraction methods (Chi and Tian, 2006; Yanfei et al, 2016).

Rare earth mining in southern China primarily involves in-situ leaching of ion adsorption clay ore and ion exchange using $(NH_4)_2SO_4$ solution in the industry (Huang et al, 2015; Xiao et al, 2015). The process of cation exchange occurring at the surfaces of charged clay minerals has been the subject of extensive research. Despite the considerable efforts devoted to this field, a comprehensive explanation that fully elucidates the controlling forces of selectivity in this process is still lacking. According to the hypothesis put forth by Jia (1987) and McBride (1980), the selectivity observed during cation exchange in clay minerals can be attributed to the ionic radius of the cations involved. The theory posits that smaller cations exhibit a more pronounced electrostatic interaction with the charged clay surface, resulting in enhanced adsorption capabilities. Moreover, this hypothesis suggests that cations that have comparable radii to lanthanides are more effective in displacing them from the clays since they fulfill similar steric demands on the surface. Besides Marcus (1985) proposed that the radii of RE^{3+} ions decrease with increasing atomic number, leading to an increase in the charge densities of the lanthanide ions as their atomic weight increases. The tendency described above implies that the surfaces of layer-structured clay minerals are more likely to attract heavier rare earth ions compared to lighter ones. This, in turn, accounts for why ion-adsorption clays serve as the primary source of heavy rare earth elements. Over geological time frames, the clay minerals acted as a discerning filter for heavy rare earth elements.

Marcus (1985) emphasized the importance of considering the hydration enthalpies, ionic radii, and charge densities of lanthanide ions and cations in understanding the ion exchange

process, with the study's findings indicating that the more negative hydration enthalpies (ΔH_{hyd}) of RE^{3+} ions, relative to Na^+ and NH_4^+ ions, result in their preferential retention in bulk water and enable effective extraction by Na^+ and NH_4^+ ions from ion-adsorption clays.

Teppen and Miller (2005) provided an effective explanation for the selective adsorption of alkali ions on clay minerals by examining hydration energies instead of unhydrated ionic radii. They proposed that the ion with stronger hydration energy (i.e., more negative ΔH_{hyd}) is preferred in the solution phase since it requires a greater amount of energy to dehydrate and attach to the surface. This is because partial dehydration is necessary to overcome steric hindrance. According to their definition, cation exchange is a partitioning reaction between the clay surface and aqueous solution. When two cations are present, the one that is less hydrated (i.e., with a less negative ΔH_{hyd}) tends to partition into the surface clay layer, while the more highly hydrated ion is more likely to remain in the solution (Moldoveanu & Papangelakis, 2012).

The research conducted by Spedding et al. (1977) established a clear and consistent increase in the hydration levels of lanthanide ions across the lanthanide series from La to Lu, which can be attributed to the contraction of their respective ionic radii. Similarly, Jia (1987) and Ikeda et al. (2005) found significantly higher hydration numbers for lanthanides (ranging between 8 and 9) compared to monovalent cations such as Cs^+, NH_4^+, Na^+, and Li^+. These findings align with Marcus' (1985) study and provide a robust foundation for understanding the preferential order of alkali ions in selectivity sequences. Furthermore, they elucidate the mechanism behind the preference of clays to bind monovalent cations over trivalent lanthanides, thereby facilitating the extraction of rare earth elements through ion exchange processes (Moldoveanu & Papangelakis, 2012).

Kraepiel's model highlights the unique structure of clay particles, which are characterized by a layered structure and significant porosity. The presence of a permanent negative charge, which arises due to the isomorphic substitution of certain elements in the matrix, is a crucial aspect of this structure. The presence of electrostatically-adsorbed counterions, in this case, trivalent lanthanides, serves to balance out this negative charge, thereby maintaining the overall neutrality of the clay particle. Understanding the complex structure of clay particles and the role of counterions is essential in explaining the process of ion exchange and the extraction of REEs from clays (Kraepiel et al., 1999).

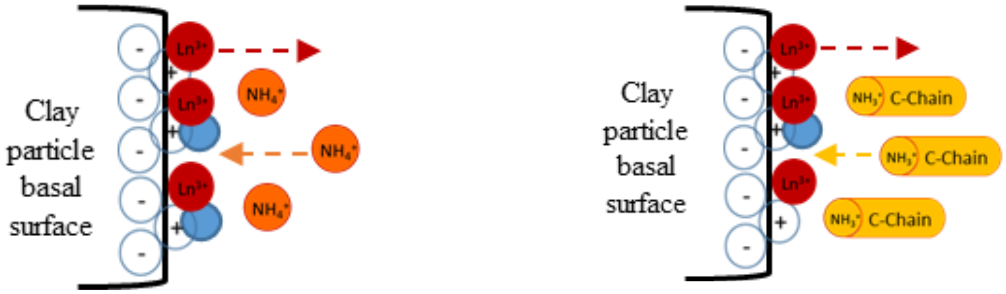

Figure 4.1 Proposed mechanism for REE desorption from clays with monovalent cations

The proposed model, for desorbing lanthanides from clays shown in Figure 4.1, involves several steps. First, monovalent ions from the surrounding electrolyte solution diffuse into the porous clay particle and reach the sites where the Ln^{3+} ions are adsorbed. Second, the monovalent cations undergo partial or total dehydration depending on their hydration enthalpy, with cations having low$-\Delta H_{hyd}$ values dehydrating completely and establishing a strong electrostatic bond with the clay surface. Third, an ion-exchange reaction occurs, resulting in monovalent ion adsorption on clay and Ln^{3+} desorption. The selectivity of cation exchange is influenced by the relative ΔH_{hyd} of the ions and the entropic/steric factor of the trivalent cations. Finally, the desorbed lanthanide ions hydrate and migrate into the bulk electrolyte solution (Miller et al., 1982; Kraepiel et al., 1999; Moldoveanu & Papangelakis, 2012).

As previously mentioned, China's annual leaching and exploitation of tens of millions of tons of ionic rare earth ore contribute to ammonium pollution. It is expected that pollution from mining sites and nearby soils will continue to worsen, posing a threat to both surface and underground water sources (Jing et al, 2017). NH_4^+ -N exists in two distinct forms within the mined soil. The first form is associated with the leakage of ammonium sulfate solution, while the second form relates to the adsorption of clay minerals (Yu et al, 2014; Wang et al, 2015). Recent laboratory investigations have focused on reducing or eliminating ammonia-nitrogen emissions associated with ammonium sulfate leaching (Luo et al, 2013; Tian et al, 2013; Wang et al, 2013). Another approach involves the use of magnesium salt compounds for ecologically friendly leaching of ion-adsorption type rare earth ores. However, the recovery of rare earths adsorbed on iron-manganese colloids, a component of the colloidal sediment phase, requires stronger adsorbing ions or acidic conditions (Xiao et al, 2015; Chi et al, 2000).

In this study, the objective was to suggest a novel approach that allows for the efficient recovery of rare earth elements (REE) while minimizing the utilization of ammonium sulfate. To do this, synthetic ion-adsorption clays were prepared by immersing a kaolinite sample in solutions of REE chlorides of known concentration and at the known pH, contact time, and temperature. The samples were subjected to ion exchange extraction tests using a series of novel lixiviants. The free energies of hydration determined to clarify the mechanism and results were compared with those obtained using the conventional lixiviant, namely NH_4^+ ions.

4.3 Experimental

4.3.1 Materials

The kaolinite sample used in this work was purchased from Sigma Aldrich. Some rare earth elements (REEs) were presented in the as-received kaolinite sample. According to the ICP/MS analysis, the as-received kaolinite contained 113 ppm La, 198 ppm Ce, 26 ppm Y, and 92 ppm Nd, and 6 ppm Dy. To prepare the ion-adsorption clay samples for leaching tests, the kaolinite was contacted with REE salt solutions so that the REE ions could adsorb on the kaolinite surface. The REE solutions were prepared from the following salts: $DyCl_3$, YCl_3, $LaCl_3$, $CeCl_3$, and $NdCl_3$ purchased from Fisher Scientific. Note that Dy and Y were heavy rare earth elements (HREE), while the others were light rare earth elements (LREE). Thus, the ion exchange leaching of both HREE and LREE was investigated in the present work. The concentrations of the REE chloride solutions were determined in such a way that the resulting synthetic ion-adsorption clay would contain 400-500 ppm for each REE and 2,000 ppm TREEs.

As an alternative to ammonium sulfate, nine different novel lixiviants were used for the ion-exchange leaching process. The chemicals purchased from Sigma-Aldrich and TCI Chemical companies were listed in Table 4.1.

Table 4.1 List of lixiviants used for ion-exchange leaching tests

Chemical Name	***Molecular Formula***	***Hydrocarbon Chain Length***
Ammonium sulfate (AS)	$(NH_4)_2SO_4$	-
Tetramethylammonium chloride (TMAC)	$(CH_3)_4N(Cl)$	1
Tetraethylammonium chloride (TEAC)	$(C_2H_5)_4N(Cl)$	4
Hexadecyltrimethylammonium chloride (HTAC)	$C_{19}H_{42}ClN$	16*
Octadecyltrimethylammonium chloride (OTAC)	$C_{21}H_{46}ClN$	18*
Aminomethyl propanol (AMP)	$C_4H_{11}NO$	3*
Ethylamine Hydrochloride (EAH)	$C_2H_7N.HCl$	2
Butylamine Hydrochloride (BAH)	$C_4H_{11}N.HCl$	4
Hexylamine Hydrochloride (HAH)	$C_6H_{15}N.HCl$	6
Dodecylamine Hydrochloride (DAH)	$C_{12}H_{28}ClN$	12*

* Response similar to AS

4.3.2 Methods and Procedure

4.3.2.1 Synthesis of REE-Doped Kaolinite

In each experiment, 15 g sample of the clay was mixed with 75 mL of deionized water in a 125 ml Erlenmeyer flask to obtain a 1:5 solid-to-liquid ratio. The mixture was agitated by a magnetic stirrer for 24 h at pH 10. REE salts is also doped right after the clay sample was weighed then added the water and arranged the pH. Throughout the synthesized clay preparation time, REE ions adsorb to the negatively-charged clay surface, thus increasing the concentration of the feed sample in a controlled manner. The concentrations of the REE chloride solutions were determined in such a way that the resulting ion-adsorption clay would contain 400-600 ppm TREEs after drying. After the agitation, the clay samples were filtered, washed with deionized water repeatedly, and dried in an oven overnight at 60 ˚C. The synthetic ion-adsorption clays prepared in this manner were analyzed for REEs contents by means of ICP/MS.

4.3.2.2 Ion-Exchange Leaching Procedure for Synthetic REE-Kaolinite Sample

The prepared synthetic clay samples were contacted with a selected lixiviant solution at a solid-to-liquid ratio of 1:2 by weight in a 125 ml Erlenmeyer flask. Table 4.1 gives the various lixiviants used in the leaching tests. Leaching tests were conducted on representative splits of synthetic clay samples using several different ionic lixiviants, including but not limited to ammonium sulfate (AS), aminomethyl propanol (AMP), ethylamine hydrochloride (EAH),

dodecylamine hydrochloride (DAH), and hexadecyltrimethylammonium chloride (HTAC). These lixiviants were used to assess the ability to leach the REE ions adsorbed on the clay surface. Ammonium sulfate, $(NH_4)_2SO_4$, was widely used for the extraction of REEs from South China clay in the related literature (Chi et al., 2013; Yang et al., 2013). Other types of lixiviants tested were straight-chain alkyl amines, with chain lengths in the range of 8 to 16, tetramethyl and ethyl ammonium chlorides, and methyl propanol. It is difficult to dissolve OTAC ($C_{21}H_{46}ClN$), DAH ($C_{12}H_{28}ClN$) and HTAC ($C_{19}H_{42}ClN$) in water due to their long chain lengths. To overcome this problem, these lixiviants were dissolved in ethanol (10 ml) and the lixiviant-in-ethanol solution was mixed with 90 mL of deionized water.

During ion exchange leaching, the suspension was agitated by means of a Lab-Line Orbit Environ-Shaker to ensure adequate mixing. The pH was adjusted to 5 to eliminate the hydrolysis effect by using a 10 % HCl solution to prevent the hydrolysis of REE ions. After a preset contact time (1 hour), the solids residue was separated from the solution by filtration, washed with deionized water repeatedly, and then dried in an oven overnight at 60 ˚C. The dried residue and the filtrate were then weighed and analyzed for REEs contents to determine the REE recoveries. The leaching reaction is shown as Eq. (4.1).

$$[Al_2SiO_5(OH)_4]_m \text{ x } nRE+3nMe^{+}= [Al_2SiO_5(OH)_4]_m \text{ x } 3nMe+nRE^{3+} \quad [4.1]$$

where Me could be NH_4^+ or novel lixiviants.

Ion exchange leaching tests were done under atmospheric pressure at 25 ^oC temperature to prevent lanthanide loss from permanent chemisorption, especially hydroxide precipitation, which is more common at higher temperatures (Moldoveanu & Papangelakis, 2012; Tertre et al., 2006). An increase in pH can result in the hydrolysis of rare earth elements (REEs), which leads to a decrease in the leaching rate. Conversely, a decrease in pH can facilitate the dissolution of impurities such as aluminum and iron during leaching (Zhang et al.,2016). Therefore, pH 5 was chosen to run ion exchange leaching tests. Despite differences in the origin of clay minerals and the content of rare earth elements (REEs), the studies consistently observed rapid attainment of maximum REE extraction levels under ambient conditions. Based on the literature review, a fixed leaching time of 1 hour was utilized for all of the ion exchange leaching tests (Papangelakis and Moldoveanu, 2014; Bonnot-Courtois and Jaffrezic-Renault, 1982; Aja, 1998; Tian et al.,2010c).

4.4 Results

4.4.1 Effect of Ammonium Sulfate

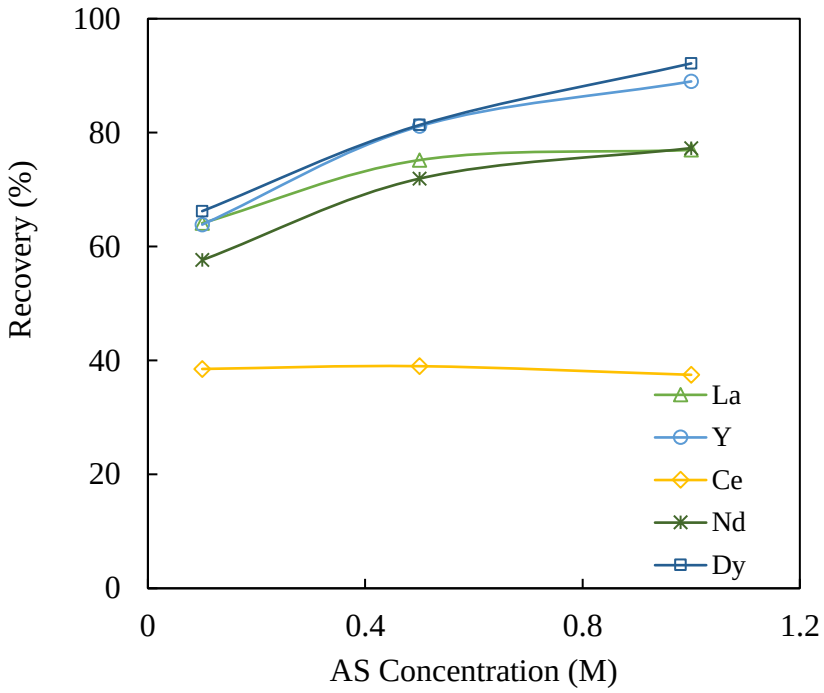

Figure 4.2 Effect of Ammonium Sulfate $(NH_4)_2SO_4$.

Figure 4.2 shows the results of the ion-exchange leaching tests using $(NH_4)_2SO_4$ as a conventional lixiviant on the synthetic REE-kaolinite sample. It clearly shows that recoveries of REEs increase with the increasing lixiviant concentration. At 0.1 M $(NH_4)_2SO_4$, the recovery is nearly 65%, but when the concentration increases five times higher, the recovery rises to 80 % and the peak point is 92% at 1 M $(NH_4)_2SO_4$. The recoveries of synthetic REE-Kaolinite samples vary between 75 and 91%. $(NH_4)_2SO_4$ does not affect Cerium and its recovery is mostly the same at different molarities with 40%.

4.4.2 Effect of Ammonium Chlorides

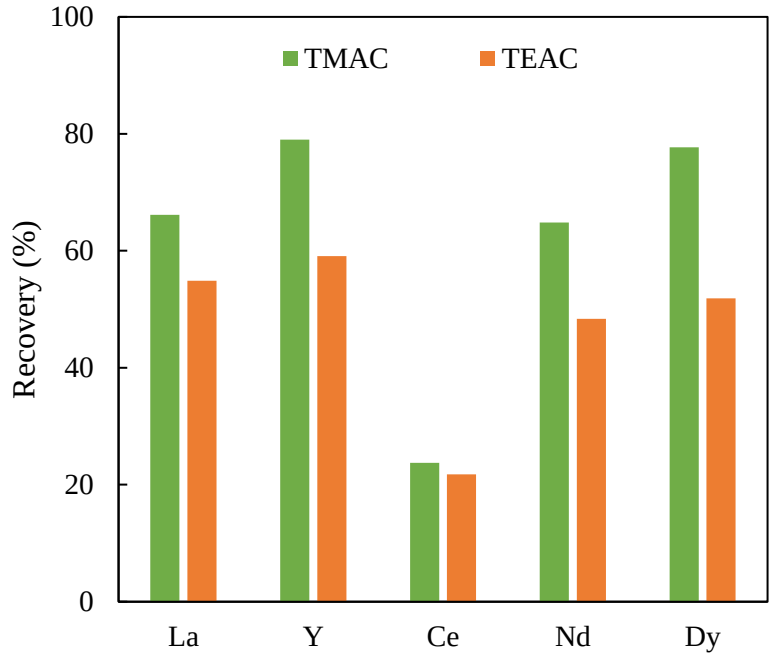

Figure 4.3 Effect of 0.5M Tetramethylammonium chloride (TMAC) and Tetraethylammonium chloride (TEAC).

Figure 4.3 shows the results of the ion-exchange leaching tests using tetramethylammonium chloride and tetraethylammonium chloride on REE-kaolinite samples. As shown in Figure 4.3, using 0.5 M TMAC which is the solubility limit, the recovery of REE on the Kaolinite sample is between 60 to 80 %. Cerium did not affect by TMAC and TEAC with a recovery range of 21 to 23 %. Using 0.5 M TEAC, the recoveries of Ln^{3+} ions on the kaolinite sample are between 50 to 60 %. Methyl ammonium chloride responds better than ethyl ammonium chloride at the same concentration value, 0.5M.

The results of the ion-exchange leaching tests using hexadecyltrimethylammonium chloride on synthetic REE-kaolinite samples are shown in Figure 4.4. According to Figure 4.4, 0.05 M HTAC resulted in an REE recovery percentage ranging from 80 to 90% for the REE-kaolinite sample. Figure 4.5 also shows the results of OTAC as a novel lixiviant. The recovery range is between 50 to 60 % when the concentration is 0.05M. The recovery of Ce was 20-40 % of other REEs.

Contrary to other lanthanide elements, which are usually physically adsorbed as trivalent cations, Ce^{3+} ions can be easily oxidized by atmospheric oxygen (O_2) to Ce^{4+}, and precipitates as cerianite, CeO_2, which makes it difficult to be recovered by ion-exchange leaching (Papangelakis and Moldoveanu,2014; Kim and Osseo-Asare,2012).

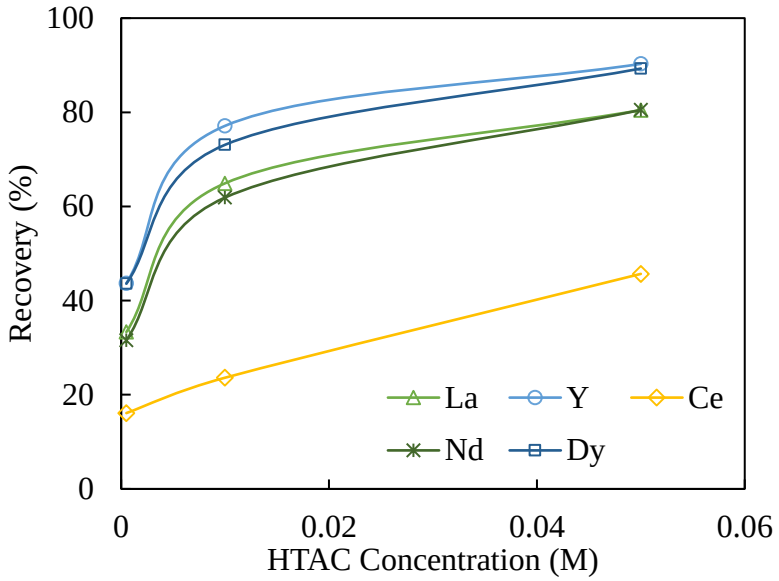

Figure 4.4 Effect of Hexadecyltrimethylammonium chloride (HTAC).

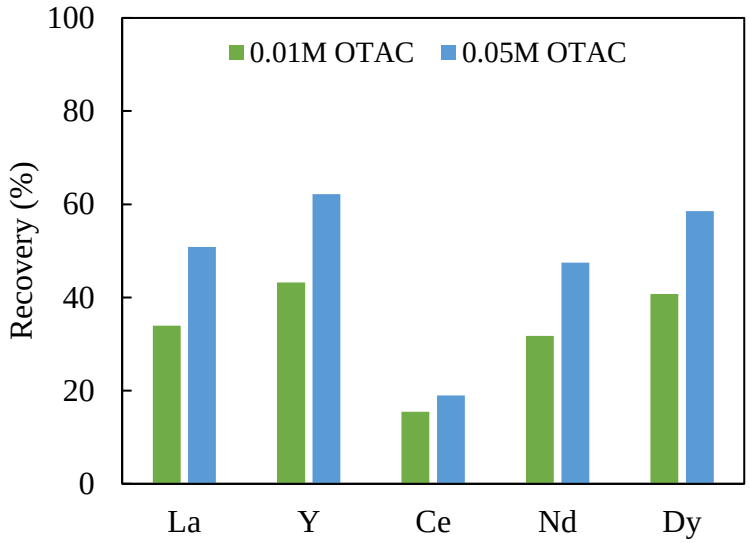

Figure 4.5 Effect of Octadecyl trimethyl ammonium chloride (OTAC).

As summarized in Figure 4.6, 0.05 M OTAC recovery is almost the same as the TEAC and TEAC which have ten times high molarity than OTAC. Besides, the results obtained by HTAC gave better recovery values than ammonium sulfate and almost the same values as TMAC. The most important takeaway of the experiments is the concentration amount of these novel lixiviants. HTAC and OTAC are ten times less than others which makes their usage extremely important for economic and environmentally friendly ways during the ion exchange process.

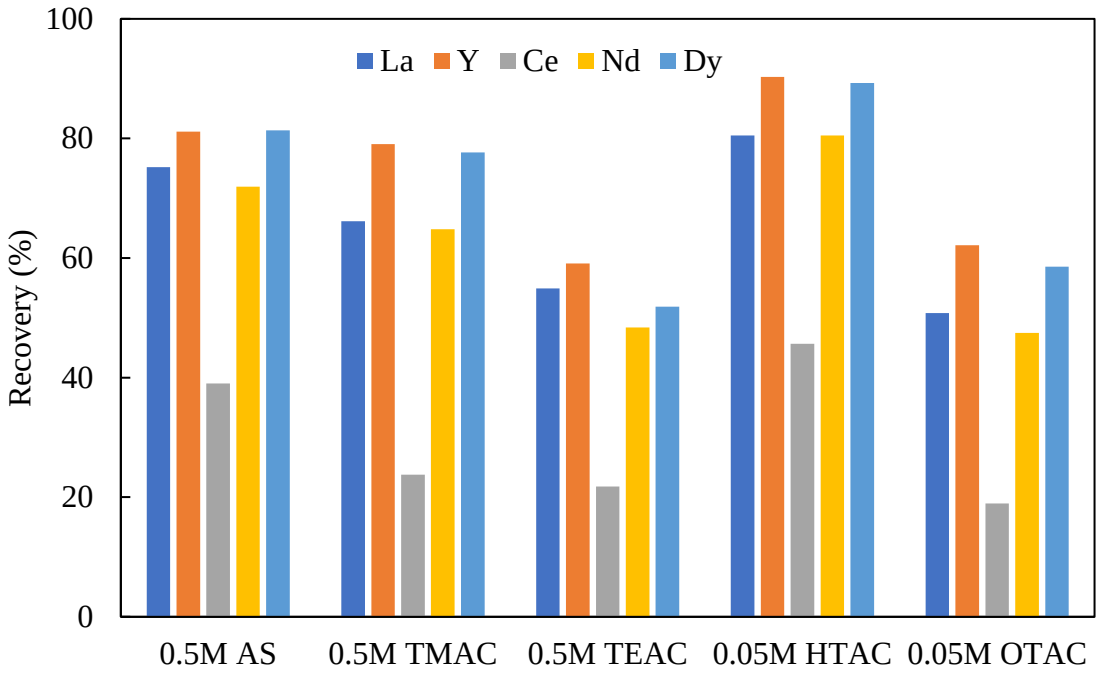

Figure 4.6 Comparisons of Ammonium Sulfate with n-Ammonium Chlorides.

4.4.3 Effect of n-Alkylamine Hydrochloride

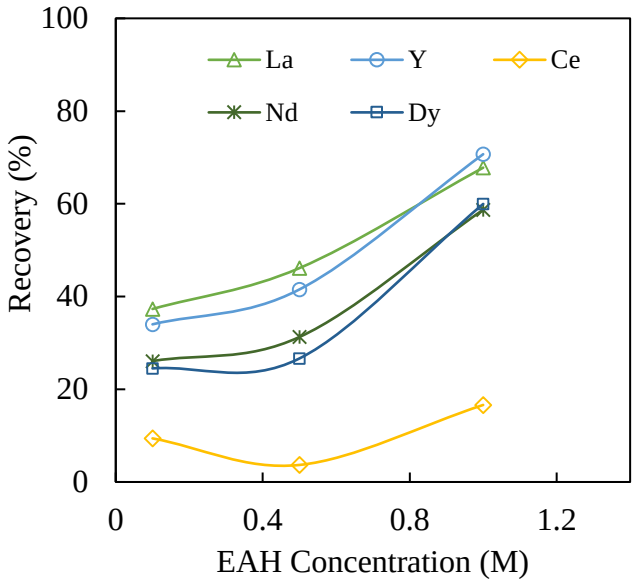

Figure 4.7 Effect of Ethylamine Hydrochloride (EAH).

Figure 4.7 show the results of the ion-exchange leaching tests using ethylamine hydrochloride on kaolinite samples. The figure shows high ethylamine hydrochloride concentration increases the recovery for REEs on Kaolinite. Lanthanum and yttrium elements give similar recovery values of around 70%. Neodymium and dysprosium elements also increase with high concentration and their recoveries are about 60%. Cerium recovery value is only 16% at high molarity on Kaolinite.

Figure 4.8 shows the results of the ion-exchange leaching tests using Butylamine Hydrochloride on REE-kaolinite samples. As Figure 4.8 indicates lanthanum and yttrium elements give similar recovery values in the range of 36 to 41%. Recoveries of neodymium and dysprosium remain at 21%, while Cerium recovery is only 6% with using BAH on kaolinite clay.

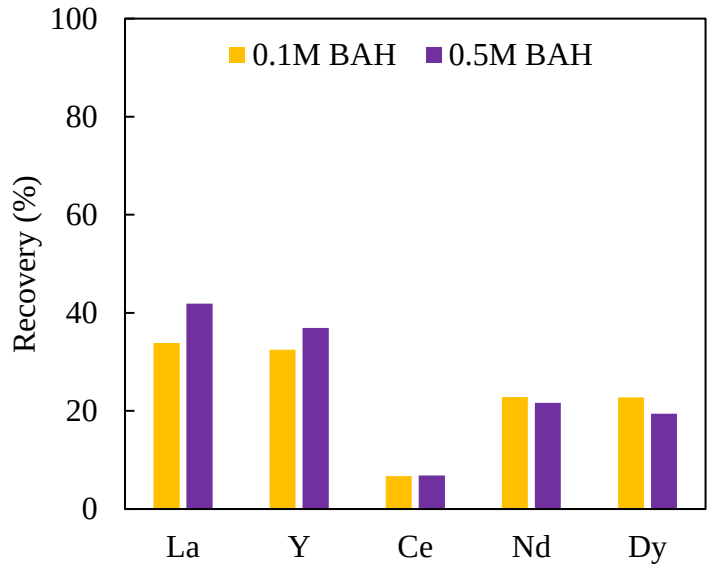

Figure 4.8 Effect of Butylamine Hydrochloride (BAH).

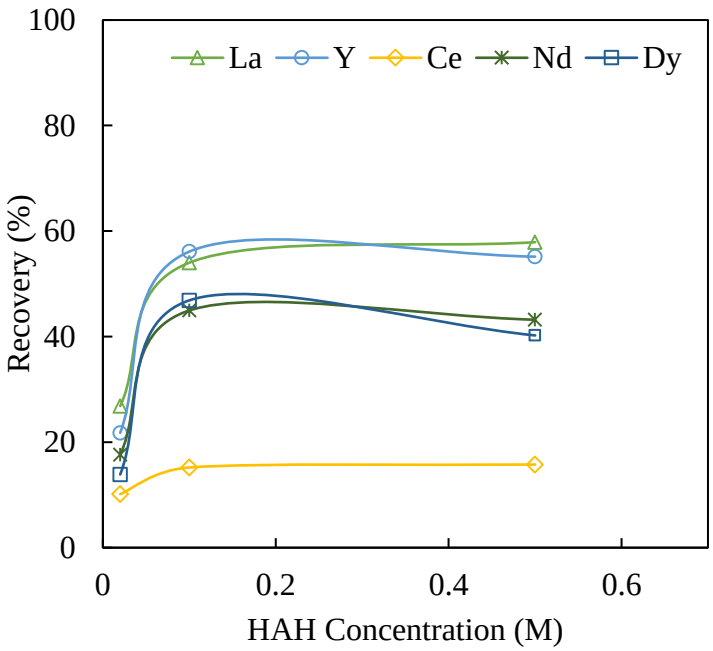

Figure 4.9 Effect of Hexylamine Hydrochloride (HAH).

Figure 4.9 shows the results of the ion-exchange leaching tests using hexylamine hydrochloride (HAH) on REE-kaolinite samples. The HAH concentration recovery reaches the maximum at 0.1 M concentration and then it reaches a steady state between 0.1 and 0.5 M on REE-kaolinite. REEs recovery is between 40 to 60 % for both RE^{3+} by using HAH as a lixiviant.

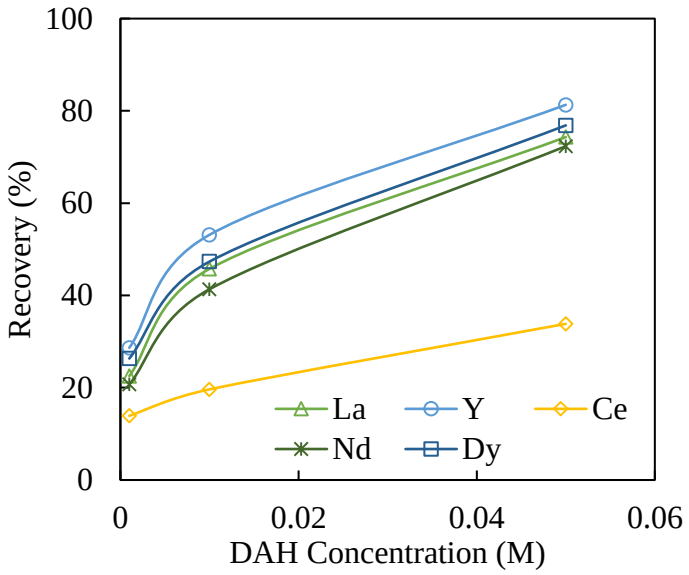

Figure 4.10 Effect of Dodeclyamine Hydrochloride (DAH).

Figure 4.10 shows the results of the ion-exchange leaching tests using dodeclyamine hydrochloride (DAH) on the kaolinite sample. The results obtained with DAH showed similar trends as those obtained using NH_4^+ ions as lixiviant. Note, however, that the DAH concentrations of 0.05 M were lower than those (0.5-1.0M) required for NH_4^+ ions.

4.4.4 Effect of Aminomethyl Propanol

Figure 4.11 shows the results of the ion-exchange leaching tests using aminomethylpropanol on the REE-kaolinite sample. Figure 4.11 indicates that at high AMP concentration, the recovery increases for the Kaolinite sample. This reagent was chosen because it has a propanol group, which makes it more water-soluble than DAH, which in turn should make it possible to increase the reagent dosage. Recovery of REEs increases ranging between 77 to 93% at the high molarity. As shown in Figure 4.11, the reagent (AMP) was particularly efficient for the extraction of La and Nd from kaolinite. It was also efficient for the extraction of Y and Dy (~90% recovery).

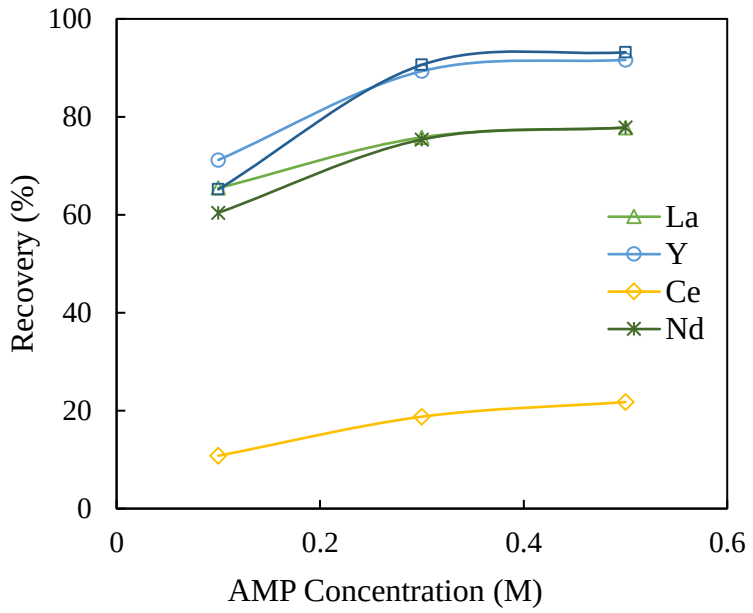

Figure 4.11 Effect of Aminomethyl Propanol (AMP).

4.5 Discussion

4.5.1 Adsorption Density

The results presented in Figure 4.12 show the effects of using various alkylamines listed in Table 4.1 as lixiviants for the ion-adsorption clays (IACs) that had been synthesized in the present work. Since the reagents were essentially surfactants with long hydrocarbon chains, their adsorption to the IAC surface may be affected by the propensity of the hydrocarbon chains to exit the aqueous phase, which may be referred to as *hydrophobic effect*. One way to study the hydrophobic effect may be to use the Stern-Grahame equation (Grahame, 1947),

$$\Gamma_\delta = 2rC\ exp\ (-\frac{\Delta G^o}{RT})(mole/cm^2) \qquad [4.2]$$

where ΔG^o is the free energy of adsorption of a surfactant at standard state. The driving force for the adsorption of a surfactant should be the sum of the electrostatic interaction ($\Delta G_{elec}^{\ o}$) and the hydrophobic interaction ($\Delta G_{hyd}^{\ o}$) as follows,

$$\Delta G^o = \Delta G^0_{elec} + \Delta G^0_{hyb} \qquad [4.3]$$

$$= -zF\Psi_\delta - n\phi$$

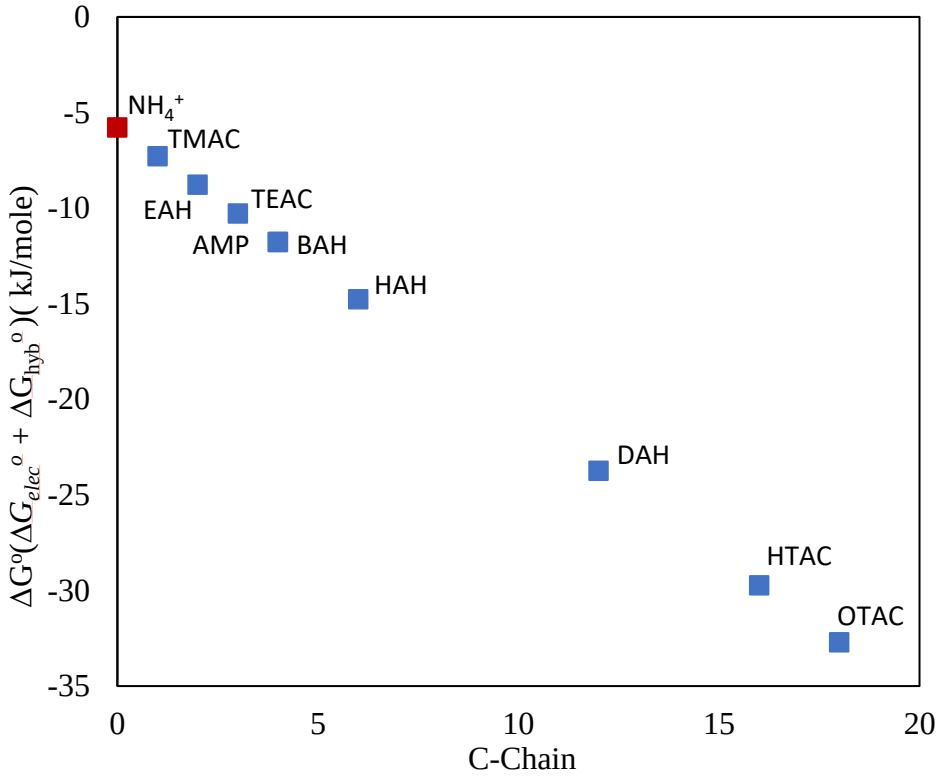

Figure 4.12 Effect of chain length on hydrophobic interaction.

The first term of Eq. [4.3] representing electrostatic contribution to the free energy of adsorption was calculated with Ψ_δ = -60 mV, which represented the ζ-potential of the clay surface at pH 10.5, z = 1 for the NH_3^+ group of the lixiviant, and F = 9.649x10^4 C/mol. The result shows that ΔG_{elec}^o = -5.79 kJ/mol for all the lixiviants used. The values of the second term representing the hydrophobic interaction were calculated using ϕ = -0.6 kT/CH_2 group (Lin and Somasundaran, 1971) by varying *n* from 2-18 the CH_2/CH_3 groups in the hydrocarbon chain of the various lixiviants used in the present work. The sum of the ΔG_{elec}^o and ΔG_{hyb}^o calculated have been plotted in Figure 4.12. As shown, the free energy change due to the hydrophobic effect increases with increasing chain lengths.

The values of ΔG^o obtained and shown in Figure 4.12 have been used to calculate the adsorption density (Γ) of the lixiviants on the IAC surface, as shown in Figure 4,13. As shown, the adsorption density begins to increase at C-12 and C-14. It is interesting to note here that the

best results were obtained using dodecyl ammonium hydrochloride (DAH) and hexadecyl trimethyl ammonium chloride (HTAC) as shown in Figure 4.4 and Figure 4.10.

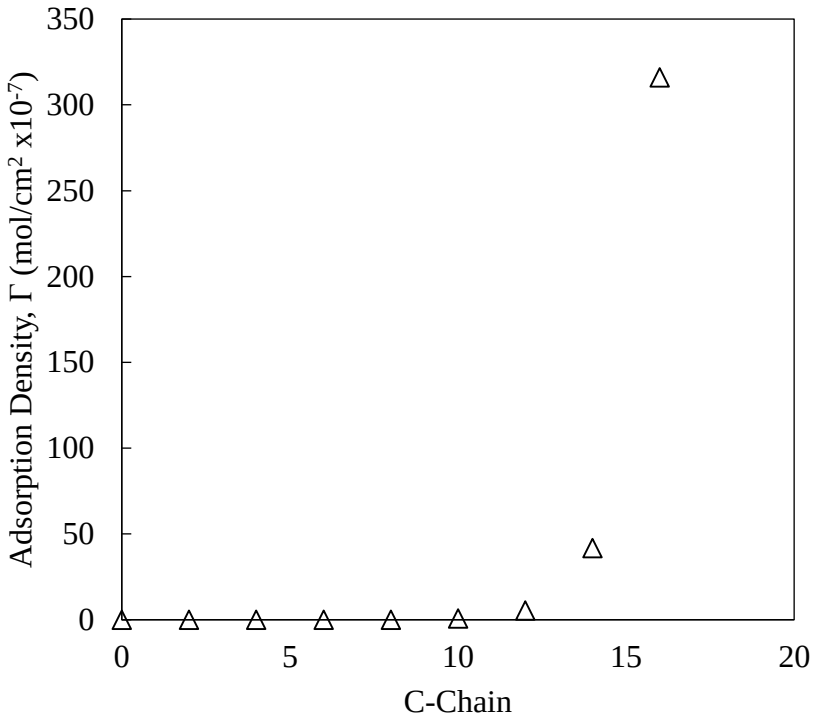

Figure 4.13 Adsorption density changes based on chain length at the same concentration.

4.5.2 Ion Concentration in Double Layer

The major advantage of using the novel lixiviants is the substantial decrease in the lixiviants required for ion-exchange leaching. In general, the amount of lixiviant required to achieve a desired recovery decreases by an order of magnitude more. One may use the Boltzmann distribution law,

$$n_i = n_i^o exp(-\frac{w_i}{kT}) \qquad [4.4]$$

to provide a thermodynamic basis for the advantage. In Eq. [4.4], n_i is the number density of ions in a potential field, *e.g.*, in an electrical double-layer, n_{io} is the same in the bulk solution, and w_i is the work done to bring ions to the position in the electrical double layer. Thus, one can substitute ΔG^o for w_i to obtain n_o as a function of the distance from the surface of a clay mineral to a large

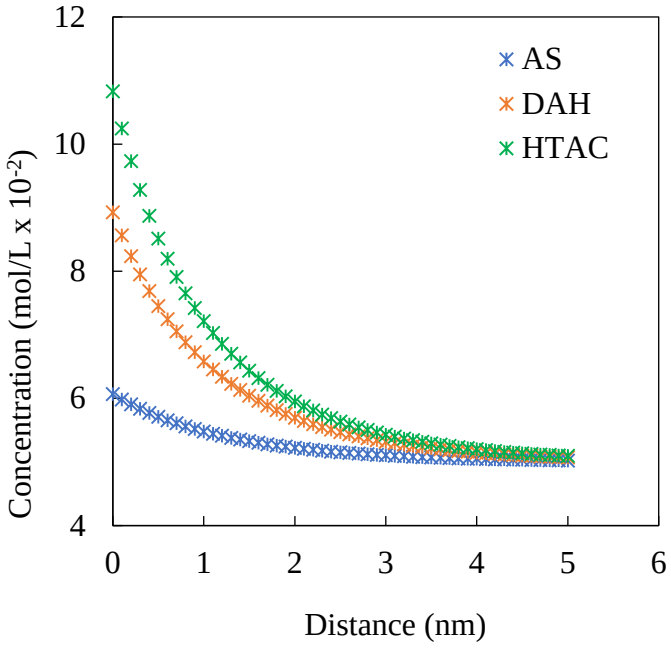

Figure 4.14 Ion concentration changes in the double layer based on chain length.

distance. The results obtained for ammonium sulfate (AS), DAH and HTAC have been plotted in Figure 4.14. As shown, the n_i increases in the order of AS, DAH and HTAC, indicating that the concentrations of the charged species increase with increasing chain lengths.

Although $(NH_4)_2SO_4$ is considered the most effective solvent for ion-adsorption clays, its ion-exchange leaching mechanism is attributed to the large differences in hydration enthalpies between Ln^{3+} and NH_4^+ ions. It has been shown in the present work that one can increase the effective concentration of the lixiviants by using the hydrophobic effect as an additional driving force. Among the alkylammonium ions tested, $C_{12}H_{25}NH_4^+$ demonstrated remarkable promise, as it provided an impressive driving force of approximately 18 kJ/mol. This finding indicates that longer the chain length of the alkylammonium ions can potentially unlock even higher driving forces for ion exchange leaching. The success of $C_{12}H_{25}NH_4^+$ prompted further exploration into other promising lixiviants. Hexadecyltrimethylammonium chloride (HTAC) has a significant impact on ion exchange leaching due to its distinct molecular configuration. Consequently, it has exhibited substantially enhanced leaching outcomes when compared to the conventional $(NH_4)_2SO_4$ lixiviant. On the other hand, OTAC with 18-C chain length has less effective and the recovery value is not high as expected. The possible reason for this situation is longer chain length

after 16-C interweaved in solution hinders the access of cations to the clay surfaces. Theoretically, TEAC should have given better recovery values than TMAC. This situation can be explained by the C bonds being stronger in TEAC. The ethyl group has two C atoms around the center of N with C_2H_5 while the methyl group is bonded only one C atom to the center of N with CH_3.

Hypothetically, higher hydration energy resulted from higher exchange efficiency on the clay surface. Although all novel lixiviants' hydration energy values are larger than ammonium sulfate, some lixiviants did not respond to the ion-exchange mechanism similar to ammonium sulfate. This difference can be caused by the ammonium ions having n-sulfate while novel lixiviants have n-chloride.

This breakthrough has significant implications for various industries that rely on ion-exchange processes to recover valuable elements from clays. The ability to optimize lixiviants by tailoring their molecular structures offers the potential to increase yields and reduce resource waste, making the entire extraction process more sustainable and economically viable.

4.6 Conclusion

While $(NH_4)_2SO_4$ is recognized as the best lixiviant for ion-adsorption clays, its driving force for ion-exchange leaching is the difference in hydration enthalpies between those of Ln^{3+} and NH_4^+ ions, which are in the range of 3,000 kJ/mole. In the present work, we used alkylammonium ions with varying chain lengths as novel lixiviants. It has been found that these reagents gave comparable results with those obtained by using $(NH_4)_2SO_4$ as lixiviant. A rationale for using these reagents was that the hydrocarbon chains would facilitate the movement of these reagents toward the clay mineral surface and improve the kinetics. In general, the longer the hydrocarbon chain lengths, the higher the kinetics of ion-exchange leaching. The best results were obtained using hexadecyltrimethylammonium chloride (HTAC) and dodecylamine hydrochloride (DAH).

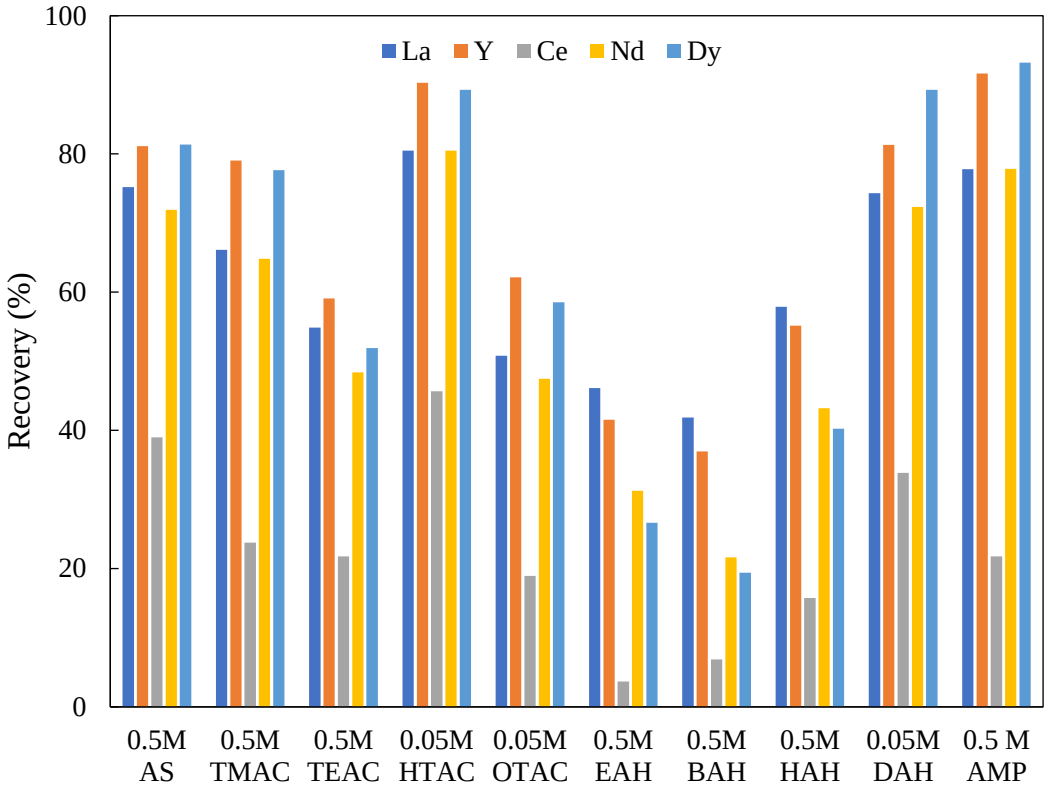

Figure 4.15 Comparisons of Ammonium Sulfate with Amine Hydrochlorides and Methyl Propanol.

As summarized in Figure 4.15, encouraging results were obtained by using ammonium sulfate (AS), tetramethylammonium chloride (TMAC), dodecyl amine hydrochloride (DAH), 2-amino-2-methyl propanol (AMP), and hexadecyltrimethylammonium chloride (HTAC). Long-chain amines offer a promising alternative to NH_4^+ at lower concentrations, owing to the inherent incompatibility between water and hydrocarbon chains.

Bibliography

Aja, S.U., 1998. The sorption of the rare earth element, Nd, onto Kaolinite at 25 °C. ClaysClay Miner. 46 (1), 103–109.

Bonnot-Courtois, C., Jaffrezic-Renault, N., 1982. Etude des echanges entre terres rares etcations interfoliares de deux argiles. Clay Miner. 17, 409–420.

Chi R A, Tian J, Li Z J, Peng C, Wu Y X, Li S R, Wang C W, Zhou Z H. Existing state and partitioning of rare earth on weathered ores [J]. Journal of Rare Earths, 2005, 23(6): 756−759.

Chi R A, Zhu G C, Tian J. Leaching kinetics of rare earth from black weathering mud with hydrochloric acid. *Trans. Nonferrous Met. Soc. China*, 2000, **10**(4): 5314.

Chi R A, Tian J. Chemical and Metallurgy Process of Weathered Crust Rare Earths Ore. Beijing: Science Press, 2006.

Chi, R., Tian, J., Luo, X., Xu, Z. and He, Z. (2013) Basic research on the weathered crust elution-deposited rare earth ores. Proceedings of the 52nd Conference of Metallurgists (COM 2013), Metallurgical Society of the Canadian Institute of Mining, Metallurgy and Petroleum (MetSoc-CIM), Montreal, Canada,189–199.

Derek W. Smith, ionic hydration enthalpies, J. Chem. Educ. 54 (9) (1977) 540–542 Grahame, D. C. (1947). The electrical double layer and the theory of electrocapillarity. *Chemical reviews*, *41*(3), 441-501.

Huang X W, Long Z Q, Wang L S, Feng Z Y. Technology development for rare earth cleaner hydrometallurgy in China [J]. Rare Metals, 2015, 34(4): 215−222.

Ikeda, T., Hirata, M., Kimura, T., 2005. Hydration structure of Y3+ and La3+ compared: an application to metadynamics. J. Chem. Phys. 122 (24), 2445071–2445075.

Jing, Q. X., Chai, L. Y., Huang, X. D., Tang, C. J., Huan, G. U. O., & Wei, W. A. N. G. (2017). Behavior of ammonium adsorption by clay mineral halloysite. *Transactions of Nonferrous Metals Society of China*, *27*(7), 1627-1635.

Jia, Y.-Q., 1987. Quantum chemical studies on the hydrated ions of the rare earths. Inorg. Chim. Acta 133, 331–336.

Kang, Y. K., Gibson, K. D., Nemethy, G., & Scheraga, H. A. (1988). Free energies of hydration of solute molecules. 4. Revised treatment of the hydration shell model. *The Journal of Physical Chemistry*, *92*(16), 4739-4742.

Kraepiel, A.M.L., Keller, K., Morel, F.M.M., 1999. A model for metal adsorption on montmorillonite. J. Colloid Interface Sci. 210, 43–54.

Kim, E., Osseo-Asare, K., 2012. Aqueous stability of thorium and rare earth metals in monazite hydrometallurgy: Eh–pH diagrams for the systems Th–, Ce–, La–, Nd– (PO4)–(SO4)–H2O at 25 C. Hydrometallurgy 113, 67–78.

Lin, I. J., & Somasundaran, P. (1971). Free-energy changes on transfer of surface-active agents between various colloidal and interfacial states. *Journal of Colloid and Interface Science*, *37*(4), 731-743.

Luo X P, Chen X M, Lian C L, Zhou H P, Zou L P, Qian Y J, Tan X K, Luo C G. A kind of leaching method for the weathered crust elution-deposited rare earths ores. China patent: CN 201310193492.6. 2013.

Marcus, Y., 1985. Ion Solvation. John Wiley & Sons Ltd., New York, NY, USA

McBride, M.B., 1980. Interpretation of the variability of selectivity coefficients for exchange between ions of unequal charge on smectites. Clays Clay Miner. 28 (4), 255–261.

Miller, S.E., Heath, G.R., Gonzalez, R.D., 1982. Effects of temperature on the sorption of lanthanides by montmorillonite. Clays Clay Miner. 30 (2), 111–122.

Moldoveanu, G. A., & Papangelakis, V. G. (2012). Recovery of rare earth elements adsorbed on clay minerals: I. Desorption mechanism. Hydrometallurgy, 117, 71-78.

Papangelakis, V. G., & Moldoveanu, G. (2014, September). Recovery of rare earth elements from clay minerals. In Proceedings of the 1st Rare Earth Resources Conference, Milos (Vol. 191, p. 202).

Qiu T S, Fang X H, Wu H Q, Zeng Q H, Zhu D M. Leaching behaviors of iron and aluminum elements of ion-absorbed-rare -earth ore with a new impurity depressant [J]. Transactions of Nonferrous Metals Society of China, 2014, 24: 2986−2990.

Spedding, F.H., Rard, J., Habenschuss, A., 1977. Standard state entropies of the aqueous rare earth ions. J. Phys. Chem. 81 (11), 1069–1074.

Tanford, C. (1980). *The hydrophobic effect: formation of micelles and biological membranes.* 2nd ed. New York (N.Y.): Wiley.

Teppen, B.J., Miller, D.M., 2005. Hydration energy determines isovalent cation exchange selectivity by clay minerals. Soil Sci. Soc. Am. J. 70, 31–40.

Tertre, E., Berger, G., Simoni, E., Castet, S., Giffaut, E., Loubet, M., Catalette, H., 2006. Europium retention onto clay minerals from 25 to 150°C: experimental measurements, spectroscopic features and sorption modeling. Geochim. Cosmochim. Acta 70, 4563–4578.

Tian J, Tang X K, Yin J Q, Chen J, Luo X P, Rao G H. Enhanced leachability of a lean weathered crust elution-deposited rare-earth ore: Effects of sesbania gum filter-aid reagent [J]. Metallurgical and Materials Transactions B, 2013, 44(5): 1070−1077.

Tian, J., Yin, J., Rao, G., Jiang, M., Chi, R., Ouyang, K., 2010c. Kinetics on leaching rare earths from the weathered crust elution-deposited rare earth ores with ammonium sulphate solution. Hydrometallurgy 101, 166–170.

Tian J, Tang X K, Yin J Q, Chen J, Luo X P, Rao G H. Enhanced leaching process of a low-grade weathered crust elution-deposited rare earth ore with carboxymethyl sesbania gum. *Hydrometallurgy*, 2013, 139: 124.

Wang T, Zhang L Y, Li C F, Yang W C, Song T T, Tang C J, Meng Y, Dai S, Wang H Y, Chai L Y, Luo J. Synthesis of core-shell magnetic Fe3O4@poly (m-Phenylenediamine) particles for chromium reduction and adsorption [J]. Environ Sci Technol, 2015, 49 (9): 5654−5662.

Wang R X, Yang Y M, Yang B, Nie H P, Ye X Y, Liao C F, Yu P, Shen W M. A kind of extraction method for ion adsorption types rare earth. China patent: CN 201310199034.3, 2013.

Xiao Y, Feng Z, Hu G, Huang L, Huang X, Chen Y, Li M. Leaching and mass transfer characteristics of elements from ion-adsorption type rare earth ore [J]. Rare Metals, 2015, 34(5): 357−365.

Xiao Y F, Feng Z Y, Huang X W, Huang L, Chen Y Y, Wang L S, Long Z Q. Recovery of rare earths from weathered crust elution-deposited rare earths ore without ammonia-nitrogen pollution: I. leaching with magnesium sulfate. *Hydrometallurgy*, 2015, (153): 58.

Yanfei, X. I. A. O., Zongyu, F. E. N. G., Guhua, H. U., Huang, L., Huang, X., Yingying, C. H. E. N., & Zhiqi, L. O. N. G. (2016). Reduction leaching of rare earth from ion-adsorption type rare earths ore with ferrous sulfate. Journal of Rare Earths, 34(9), 917-923.

Yang, J.J., Lin, A., Li, X.L., Wu, Y., Zhou, W. and Chen, Z. (2013) China's ion-adsorption rare earth resources, mining consequences and preservation. Environmental Development,8,131–136.

Yu J G, Zhao X H, Yang H, Chen X H, Yang Q, Yu L Y, Jiang J H, Chen X Q. Aqueous adsorption and removal of organic contaminants by carbon nanotubes [J]. Science of the Total Environment, 2014, 482−483(1): 241−251.

Chapter 5. Concentrate Rare Earth Elements from Coal Clay Using Blunging and Hydrophobic-Hydrophilic Separation Process

5.1 Abstract

Rare earth elements (REEs) are difficult to be concentrated using physical separation methods due to incomplete liberation and small particle size. In the present work, we have developed a novel process that can be used to concentrate REEs presented in clayey materials. The process includes two stages, dispersive liberation (blunging), followed by the hydrophobic-hydrophilic separation (HHS) process. The former aims to improve the degree of liberation of REE-bearing particles in the clay, while the latter addresses small particle size issue by using fine oil droplets to recover REE-bearing particles in the form of oil-in-water (o/w) emulsions. A series of bench-scale blunging and HHS tests have been carried out using a decarbonized clay sample obtained from a coal preparation plant. The results suggest that blunging can substantially improve the liberation of REE-bearing particles from barren gangue minerals. High pulp density and use of dispersant in blunging lead to better performance of liberation. It is also found that the driving force for liberation in blunging is the repulsive electrical double layer (EDL) force. The surface force (disjoining pressure) measurements suggest that the repulsive EDL forces create a force barrier that can keep clay particles dispersed, which is beneficial for liberation. By virtue of this novel process, we have obtained REE concentrates assaying ~1800 ppm total rare earth element (TREE) from a feed containing only ~300 ppm TREE. These REE concentrates have been characterized using SEM and EDS and the results suggest that REE-bearing particles in this clay sample are likely to be monazite.

5.2 Introduction

Rare earth elements (REEs) encompass a subset of chemical elements, consisting of all fourteen naturally-occurring lanthanides, with the exception of promethium. These elements can be further classified into distinct groups based on their respective atomic numbers. The first group comprises the "light" rare earth elements (LREEs), namely lanthanum (La), cerium (Ce), praseodymium (Pr), and neodymium (Nd). The second group encompasses the "middle and heavy" rare earth elements (HREEs), encompassing samarium (Sm), europium (Eu), gadolinium (Gd), terbium (Tb), dysprosium (Dy), holmium (Ho), erbium (Er), thulium (Tm), ytterbium (Yb), and lutetium (Lu). It is noteworthy to include yttrium (Y) and scandium (Sc) within the rare earth

classification, as they share similar properties with lanthanides and coexist in the same mineral deposits (Balaram, 2019; Moldoveanu, 2021).

Numerous industries such as aerospace, defense, healthcare, clean energy, electronics, transportation, vehicles, oil refining, and chemical manufacturing depend on Rare Earth Elements (REEs) (Feng et al., 2021; Binnemans et al., 2013; Wang et al., 2017). The 21st century has witnessed a growing global demand for these elements. In 2021, global production of rare earth oxides (REOs) was 280,000 metric tons, with China leading the production (60%), followed by the U.S. (15.36%), Burma (9.3%), Australia (7.8%), and other countries (7.54%) (USGS Mineral Commodity Summary, 2022). Remarkably, China controls over 80% of the global production as U.S. mines and many products are processed there.

Bastnaesite, monazite, and xenotime are globally distributed rare earth mineral (REM) sources known for their high rare earth element (REE) content. However, their extraction requires complex and costly hydrometallurgical processes. In contrast, ion adsorption clays (IACs) have lower REE content (0.05-0.3% rare earth oxides) but offer a more cost-effective extraction method due to the simplicity of the overall process (Feng et al., 2021; Moldoveanu and Papangelakis, 2012; Zhang et al., 2016). The weathering of granite gives rise to regolith containing IACs, which serve as the primary source of heavy rare earth elements (HREEs). Approximately 40-90% of the REEs are physically adsorbed on layer-structured minerals, facilitating their extraction through ion-exchange leaching without the need for aggressive processing of rare earth minerals (REMs) (Bao and Zhao, 2008; Sanematsu and Watanabe, 2016). Notably, a significant portion of the world's HREEs is produced from ion adsorption clays mined in South China (Foley and Ayuso, 2015a; Foley and Ayuso, 2015b).

Recent scholarly investigations have shed light on the potential of coal and its byproducts as promising alternative sources for rare earth elements (REEs), complementing the established primary sources such as bastnaesite, monazite, and xenotime (Seredin, 1996; McLellan et al., 2014; Hower et al., 2016; Zhang and Honaker, 2018; Huang et al., 2018). The abundance of coal reserves and the substantial volumes of byproducts resulting from coal mining and processing present compelling prospects for harnessing coal resources to address the challenges confronting the rare earth industry and potentially contribute to the economic vitality of the United States. However, it is noteworthy that the absence of a robust domestic supply chain exposes the country

to vulnerabilities arising from disruptions in the international market, thus underscoring the criticality of establishing a self-sustaining rare earth supply chain within the nation's borders.

A comprehensive nationwide survey conducted in the United States has identified viable domestic sources of rare earth elements (REEs) within major coal basins. These sources have exhibited REE grades reaching up to 1,500 ppm and have been notably linked to coal byproducts, particularly kaolinite clays, which serve as significant host materials for ion adsorption clays (IACs) (Bryan et al., 2015). Research findings indicate that rare earth element (REE) concentrations in coal and coal byproducts range from 270 to 1,480 ppm (Blissett et al., 2014; Das et al., 2018). Several studies conducted across diverse geological regions have reported an average REE content of approximately 69 ppm in coal (Eskanazy, 1987; Ketris and Yudovich, 2009; Karayigit et al., 2000; Hu et al., 2006; Wagner and Matiane, 2018; Huang et al., 2019). Moreover, Das et al. examined 86 coal ash samples collected from the United States and observed a total rare earth concentration ranging from 98 to 525 ppm (Das et al., 2018). Consistent with these findings, Lin et al. (2018) and Ekmann (2012) suggest that the Appalachian region holds promise as a potential area for rare earth recovery. Yang et al. (2020) also discovered that coal refuse piles spanning over 10,000 acres exhibit rare earth concentrations between 200 and 500 ppm.

The occurrence of rare earth elements (REEs) within coal can be attributed to diverse mechanisms, encompassing micro-dispersed minerals, ion-adsorption clays, and chemical bonding with carboxyl and carbonyl groups (Jordens et al., 2013; Zhang et al., 2017; Finkelman et al., 2018). Particularly noteworthy is the observation made by Finkelman et al. (2018) that a substantial portion, ranging from 50% to 60%, of the REEs present in low-rank coals are associated with clay minerals.

Ion-adsorption clay deposits originate from the chemical weathering of granite, a prevalent silicate rock covering about 25% of the Earth's surface (Oliva et al., 2003). Kaolinite, a stable clay mineral, forms as a result of weathering of potassium feldspar by CO_2-rich meteoric water. Other components of granite, such as muscovite and biotite, undergo chemical changes to convert into different clay minerals. Quartz remains largely unchanged except for fragmentation, while silica released from feldspar can accumulate in chert or disperse into the oceans (Velde, 2008).

Borst et al. (2020) used X-ray absorption spectroscopy (XAS) to investigate the adsorption of Nd and Y onto kaolinite. They found that heavy and light Ln^{3+} ions adsorb onto the basal

surfaces of kaolinite as fully-hydrated ions, forming outer-sphere complexes. These complexes are held in place by electrostatic interactions with the $AlO_4(OH)_2$ octahedra and SiO_4 tetrahedra. On the edge surfaces, Ln^{3+} ions can adsorb as partially hydrated ions, forming inner-sphere complexes (Borst et al, 2020). However, extracting inner-sphere complexes through ion exchange mechanisms proves to be difficult (Velde, 2008).

The variations in weathering conditions, host rock characteristics, pH levels, temperature, pressure, and redox conditions are likely to result in differences in the degree of hydrolysis and the formation of colloidal phases on clay surfaces. Therefore, the formation processes of ion-exchange clays present in American coals, along with their associated mineral matter, are expected to diverge from those observed in the ion adsorption clays of South China. These dissimilar conditions contribute to the distinctive properties and characteristics exhibited by the respective types of clay.

The clay production industry developed a dispersive liberation technique called "blunging." Originally developed as a conditioning stage for the removal of impurities from pigment kaolinite, blunging involves the disaggregation of clay particles to enhance their individualization prior to flotation processes. In mineral processing, grinding is the conventional approach for achieving size reduction and liberation. However, it is crucial to note that the energy requirements associated with grinding operations are significantly high in comparison to the blunging technique. The dispersion technique employed in the context of clay liberation involves the utilization of a high percentage solids slurry combined with a potent dispersant, which is vigorously mixed under elevated temperature conditions (MacCormac, 2020).

In conclusion, to effectively achieve the liberation of rare earth elements (REEs) within the coal clay sample prior to the Hydrophobic-Hydrophilic Separation process (Yoon, 2016), the influence of different dispersants on the blunging technique and the significance of positive disjoining pressure have been substantiated. These findings contribute to the overall understanding of the optimal methods for REE liberation and pave the way for further advancements in extracting and processing these valuable elements from coal sources.

5.3 Experimental

5.3.1 Materials

The clay sample used in this study was obtained from the thickener underflow in a coal preparation plant in Grundy, VA. The as-received sample assaying 46.9% ash was subjected to a laboratory-scale hydrophobic-hydrophilic separation (HHS) process to recover the ultrafine coal first prior to recovering the REE-bearing particles from the reject. The reject material assaying 93.5% ash was used as the feed for REE recovery using a second-stage HHS process. Figure 5.1 shows the concentrations of each rare earth element in the feed for REE recovery. As shown, this feed was mostly dominated by light rare earth elements and the total REE content was around 300 ppm.

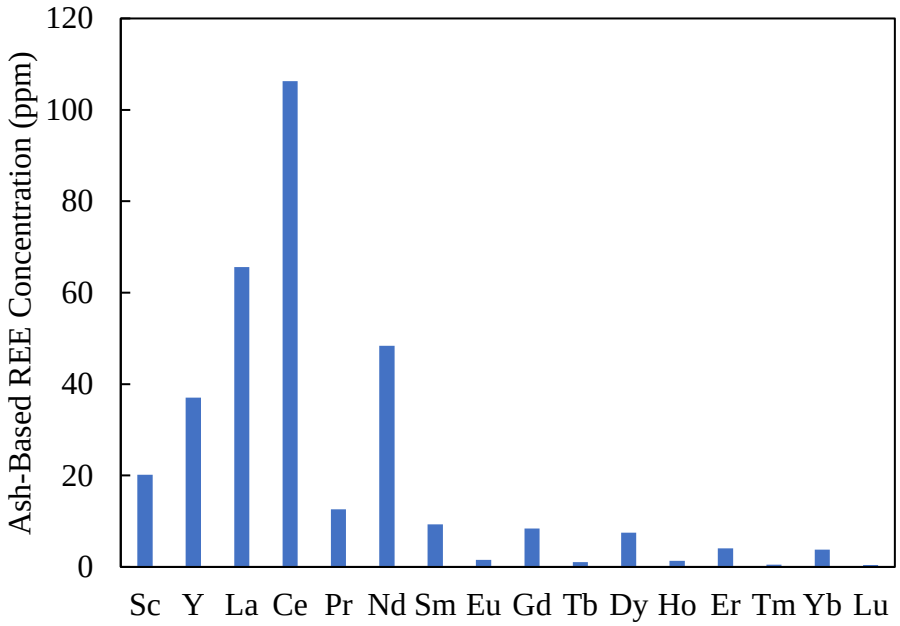

Figure 5.1 REE content (ash basis) in the clay sample before blunging, as determined by lithium metaborate fusion followed by ICP/MS analysis.

Reagent-grade sodium hydroxide from Fisher Scientific was used for pH regulations. The dispersants used in the blunging tests included sodium silicate, sodium phosphate, and ethylenediaminetetraacetic acid (EDTA), which were all purchased from Sigma Aldrich. Octyl hydroxamate acid (OHA, TCI America) was used as the collector to increase the hydrophobicity of REE-bearing particles. In some experiments, poly-methylhydrosiloxane (PMHS) was also used to further enhance the hydrophobicity of REE-bearing particles to improve the separation

efficiency of the HHS process. *n*-heptane used in the HHS tests was purchased from Alfa Aesar. Tap water is used for all the blunging and HHS tests. Deionized water with a resistivity of 18.2 MΩ·cm at 298.15 K was used for preparing solutions for the disjoining pressure measurement.

5.3.2 Blunging

To improve the degree of liberation of the REE-bearing particles, a series of dispersive liberation (blunging) tests have been carried out using the clay samples prepared by the HHS process as described in Section 5.3.1. The blunging test was conducted in a 500 mL Ninja blender as shown in Figure 5.2. In each test, around 100 grams of the clay sample was mixed with water to obtain a desired pulp density, *i.e.*, %solids in the slurry. A dispersant was then added to the slurry to keep the clay particles dispersed in the aqueous phase. In each test, pH was controlled between 10.5 and 11 using sodium hydroxide (NaOH). The slurry was extensively agitated in the Ninja blender for 5 minutes. The effects of %solids and different dispersants on the blunging process were investigated.

Figure 5.2 The Ninja blender used for the blunging process.

5.3.3 Hydrophobic-Hydrophilic Separation (HHS)

The blunged clay sample was subjected to the HHS process for REE recovery by using a high-shear Xtreme Waring blender as shown in Figure 5.3 a. Prior to each HHS test, the blunged clay sample containing high %solid was diluted to form a 900 ml slurry with 5 %solids. 0.4 kg/ton

octyl hydroxamate acid (OHA) was added as REE collectors to render the REE-bearing particles selectively hydrophobic. 150 ml *n*-heptane was used as the hydrophobic liquid (oil) to collect the hydrophobic REE-bearing particles. After agitation, the resulting mixture was transferred into a 2 L separatory funnel and left to settle for 15 minutes to allow for phase separation as shown in Figure 5.3b. The fine oil drops selectively collected the hydrophobic REE-bearing particles and slowly floated to form an oil phase on top of the aqueous phase containing hydrophilic gangue particles. Note that the oil phase was in dark color due to the fact that some residual coal particles were also floated due to their natural hydrophobicity. The aqueous phase at the bottom was then discharged as rougher tails, while the oil phase containing REE-bearing particles was rougher concentrate, which was further cleaned in the cleaner stages by water washing. In the present work, the rougher concentrate was washed with 500 ml tap water three times to obtain the final REE concentrate. After each HHS test, the rougher tails, cleaner tails, and cleaner concentrate were dried, weighted, and assayed using ICP-MS. The recovery *vs.* grade curves for each HHS test were constructed so that the performance of blunging could be evaluated.

Figure 5.3 a) The high-shear Waring blender for the HHS process; b) phase separation in the separatory funnel after one HHS test.

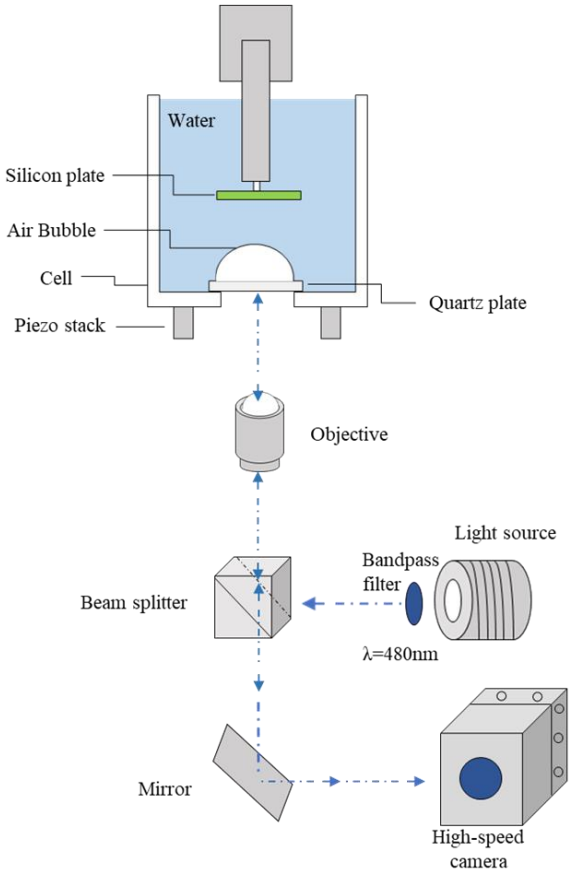

Figure 5.4 Schematic representation of the force apparatus for deformable surfaces (FADS).

5.3.4 Disjoining Pressure Measurement

To better understand the role of dispersant in the clay blunging process, a series of disjoining pressure measurements have been carried out in the wetting films formed between silica surface and air bubble. Sheets of silicon wafers were purchased from University Wafer, Boston, MA, with one side polished. Each sheet was cut into small plates of 10x10x0.5 mm in dimension for the disjoining pressure measurement. The plates were cleaned in a piranha solution, *i.e.*, a mixture of hydrogen peroxide (H_2O_2, Fisher Scientific, 30–35%) and sulfuric acid (H_2SO_4, Spectrum Chemical, 98%) at 90 ^oC for 5 min. After cleaning, a thin layer of silica formed on top of the silicon surface. The measurements were conducted in the presence of various dispersants, including sodium silicate (Na_2SiO_3, Sigma Aldrich) and ethylenediaminetetraacetic acid (EDTA, Sigma Aldrich). Sodium hydroxide (NaOH, Sigma Aldrich) was used for pH adjustment.

Figure 5.4 shows a schematic representation of the force apparatus for deformable surfaces (FADS), which has been designed to measure the disjoining pressures in the thin liquid films (TLFs) confined between a solid surface and a deformable subject, *e.g.*, an oil droplet or an air bubble. The measurement was conducted in a liquid (water) cell, in which a flat plate was suspended and an air bubble attached to a hydrophobic quartz surface is placed at the bottom. The quartz surface was hydrophobized by silylation to achieve a 90^o contact angle so that an air bubble could stay in place during the force measurement.

The force measurement was initiated by pushing the silica surface against the air bubble by means of piezo crystals at a ~330 nm/s approach speed. The air bubble deformed near the point of contact as it encountered resistance due to hydrodynamic and surface forces. The changes in local curvatures were monitored by recording the optical fringes using a high-speed camera. The recorded optical fringes were then analyzed offline using the micro-interference technique to reconstruct the spatiotemporal film profiles (Sheludko, 1962), from which one could determine hydrodynamic (p), capillary (p_c), and disjoining (Π) pressures. Π represents the surface forces per unit film area (Pan and Yoon, 2016; Huang and Yoon, 2019).

In the present work, p was determined using Reynolds lubrication theory as shown in Eq. [1] (Pan *et al.*, 2011),

$$p = 12\mu \int_{r=\infty}^{r} \frac{1}{rh^3} \left[\int_{r=0}^{r} r \frac{\partial h}{\partial t} dr\right] dr \qquad [1]$$

in which h is the film thickness, t is the time, μ is the liquid viscosity, and r is the radial location. According to a pressure balance in the direction perpendicular to the film, p can be also written as follows,

$$p = p_c - \Pi \qquad [2]$$

where p_c is the capillary (or Laplace) pressure, and Π is the disjoining pressure. The former can be calculated using the Young-Laplace equation (Pan *et al.*, 2011),

$$p_c = \frac{2\gamma}{R} - \frac{\gamma}{r}\frac{\partial}{\partial r}\left(r \frac{\partial h}{\partial r}\right) \qquad [3]$$

while the latter can be modeled using the DLVO theory,

$$\Pi = \Pi_d + \Pi_e$$

$$= -\frac{A_{132}}{6\pi h^3} - \frac{\varepsilon\varepsilon_0\,\kappa^2}{2sinh(\kappa h)}[(\psi_1^2 + \psi_2^2)cosech(\kappa h) - 2\psi_1\psi_2 coth(\kappa h)] \quad [4]$$

in which Π_d are Π_e are disjoining pressures due to van der Waals (vdW) and electrical double-layer (EDL) forces, respectively. A_{132} is the Hamaker constant for the interaction between solid **1** and air bubble **2** in water **3**, which can be determined using the combining rule (Israelachvili, 2011). Π_e can be readily predicted using the Hogg-Healey-Fuerstenau (HHF) approximation (Hogg *et al.*, 1966), in which ε_0 is the permittivity of vacuum, ε the dielectric constant of water, κ the reciprocal Debye length, ψ_1 the double-layer potential of the solid surface, and ψ_2 is the same of the air bubble.

5.4 Result and Discussion

5.4.1 Blunging and HHS

A series of blunging tests were conducted at varied pulp densities, *i.e.*, 30, 50, and 60% solids. In each test, pH was controlled at 11 by adding sodium hydroxide. 3 kg/ton sodium silicate was added to the clay slurry to keep the clay particles dispersed in the aqueous phase. After blunging, the clay samples were subjected to the HHS process for REE recovery. 0.4 kg/ton octyl hydroxamate acid (OHA) was added as REE collectors to render the REE-bearing particles

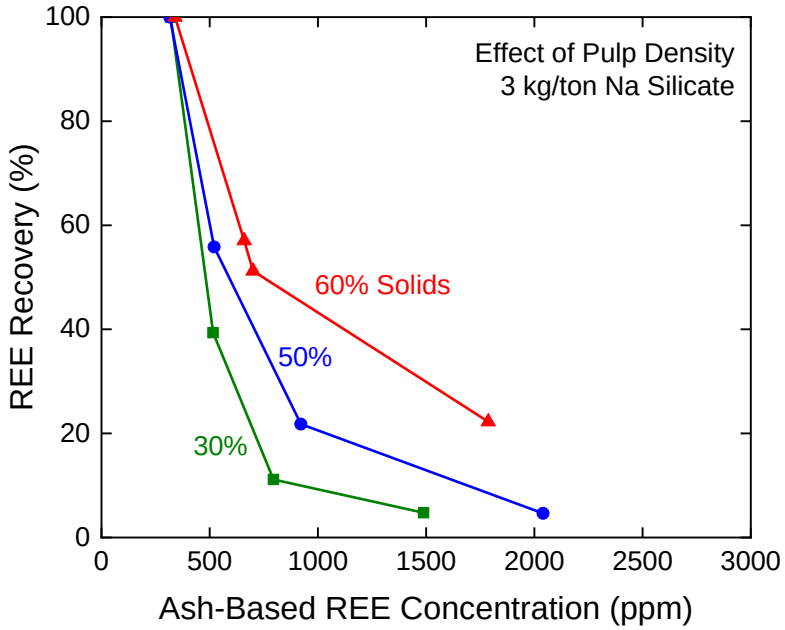

Figure 5.5 Effect of pulp density on blunging.

selectively hydrophobic. A secondary hydrophobizing reagent, PMHS, was added to further improve the hydrophobicity of the OHA-coated REE-bearing particles. *n*-heptane was used as the hydrophobic liquid (oil) to collect the hydrophobic REE-bearing particles.

The grade *vs.* recovery curves were plotted based on the data obtained in the HHS tests. These curves were then used to evaluate the effectiveness of blunging and the degree of liberation for REE-bearing particles. Figure 5.5 shows the effect of pulp density on the blunging. As shown, the grade *vs*. recovery curves shifted up when increasing %solids in the blunging, suggesting that more REE-bearing particles were liberated from barren clay particles at higher pulp densities in the blunging. Therefore, the blunging should be conducted at high % solids. This finding is consistent with the practice in the kaolin industry in Georgia and South Carolina, of which blunging process is routinely operated at 50-70 % solids.

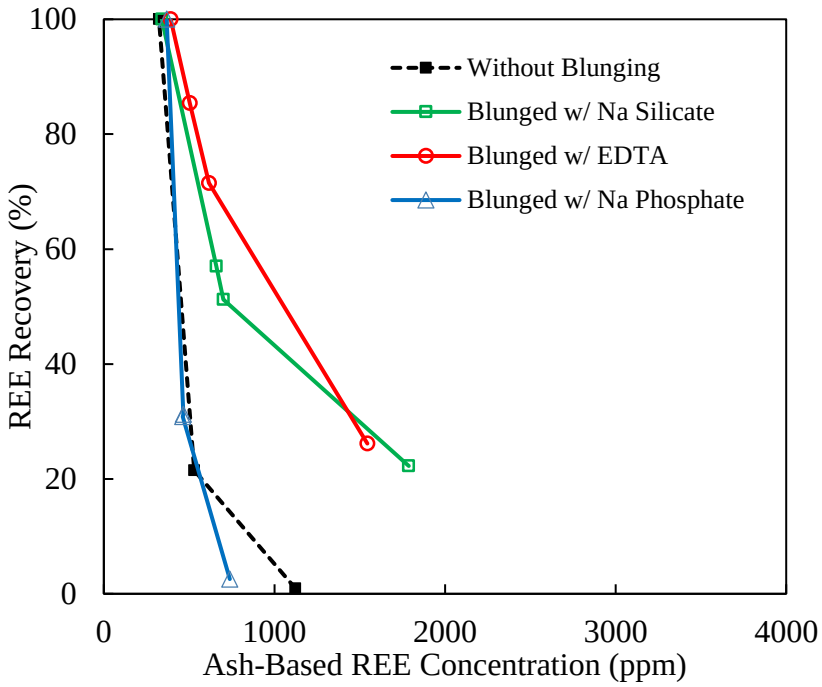

Figure 5.6 Effect of different dispersants on blunging.

An additional set of blunging experiments were performed to examine the influence of various dispersants on the blunging procedure. In this part of the study, three dispersants were studied, *i.e.*, sodium silicate, sodium phosphate, and ethylenediaminetetraacetic acid (EDTA). The former two were polyelectrolytes, while EDTA was a complexing agent that could be

partially/fully deprotonated at neutral/alkaline pH. The role of these polyelectrolytes is to increase the electrical double-layer (EDL) potentials of the clay particles so that they can be fully dispersed in the aqueous phase. The fully deprotonated EDTA ions, $EDTA^{4-}$, had four negative charges. In each blunging test, the pulp density was controlled at 60 %solids and the dosage of the dispersant was controlled at 3 kg/ton.

The grade *vs.* recovery curves obtained with different dispersants were shown in Figure 5.6. Remarkably, sodium silicate substantially outperformed sodium phosphate, although they both were polyelectrolytes. A possible explanation is that sodium phosphate might hinder the adsorption of OHA onto the REE-bearing particles, making the REE-bearing particles less hydrophobic and leading to a lower separation efficiency. It is well known that phosphate ions can readily hydrolyze in aqueous solutions and form different species that have different affinities for REE-bearing particles (Zhang and Honaker, 2017). Species like hydrogen phosphate (HPO_4^{2-}) and dihydrogen phosphate ($H_2PO_4^-$) can be readily formed under alkaline conditions. These species can react with REE-bearing particles by forming complexes with REE ions and REE hydroxides presented on the particle surface (Espiritu *et al.*, 2018). As a result, the OHA adsorption was prohibited, leading to low surface hydrophobicity. The grade *vs.* recovery curve obtained with EDTA was comparable to the one obtained with sodium silicate, suggesting that EDTA was also a good candidate for dispersants. The good performance of EDTA may be due to its high negative charges under alkaline conditions. When negatively charged EDTA ions adsorbed onto the clay surface, the clay became more negatively charged, which in turn increased the repulsive electrical double layer (EDL) force between two clay particles and hence improved the degree of liberation.

Also shown in Figure 5.6 is the recovery *vs*. grade curve for the HHS tests conducted with the clay sample without blunging process. The cleaner concentrate assayed 1123 ppm total REE content at 0.9% recovery, which was substantially lower than those obtained with sodium silicate and EDTA. The low REE recovery might be due to the fact that the most REE-bearing particles in the clay were not liberated from barren ones without the blunging process.

In the mineral processing industry, liberation of the valuable minerals from the gangue is mostly achieved by size reduction via grinding or crushing (Wills and Finch, 2015). It is, therefore, interesting to compare the performance of different liberation methods, *i.e.*, grinding and blunging. In the present work, we also conducted HHS tests on the ground clay sample. The grinding was conducted using an attrition mill purchased from Union Process, Inc. The clay sample was ground for 10 hours at 15% solid content to obtain an 80% passing size (d80) of 4 μm. The mill discharge was conditioned with 0.4 kg/t octyl hydroxamate acid (OHA) at pH 10 to render the REE-bearing minerals selectively hydrophobic prior to the second-stage HHS test. The relationship between REE Recovery and REE concentration (ash-based) is presented in Figure 5.7.

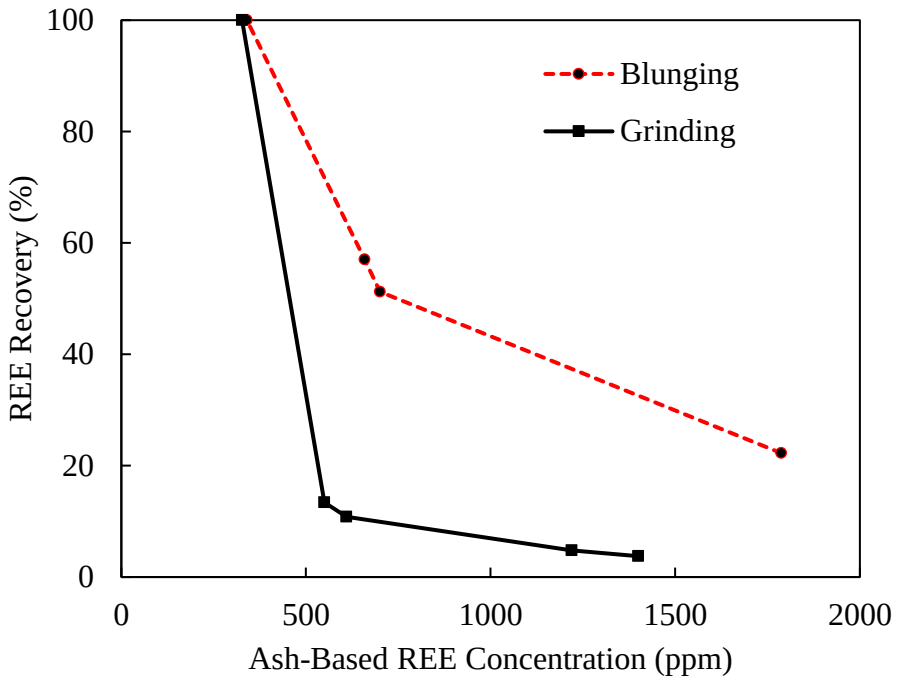

Figure 5.7 REE recovery vs. ash-based REE concentration curves for HHS tests conducted using clay samples liberated using different approaches, i.e., grinding (black) and blunging (red).

The REE recoveries obtained with the ground sample were poor, although the REE grades for concentrate products were substantially higher than the feed, *i.e.*, the concentrate assayed 1400 ppm REE with only 3.7% recovery. However, the blunged clay sample showed substantial improvement in both recovery and grade. The HHS concentrate after blunging assayed 1788 ppm REE with 22.3% recovery. The increase in recoveries and product grade may be due to the

improved liberation of the REE-bearing particles from the gangue materials by blunging. The results presented in Figure 5.7 suggest that blunging may be more effective than grinding in liberating REE-bearing particles from clays. Note also that blunging is also less energy intensive than grinding. The chemical potentials are used to induce the liberation in the blunging, while the liberation is achieved by size reduction due to the breakage of particles in the grinding, which requires large amount of mechanical energies.

5.4.2 Disjoining Pressure Measurement

In the blunging process, a clay slurry is intensely agitated at high solids content in the presence of polyelectrolytes to impart the particulate materials with high negative charges (ζ-potentials) so that the impurities are dispersed. To better understand the role of dispersants in the blunging process, especially the role of different surface forces, a series of disjoining pressure measurements have been conducted in the thin liquid film between air bubble and silica surface. The results have been analyzed using the DLVO theory as shown in Eq. [4].

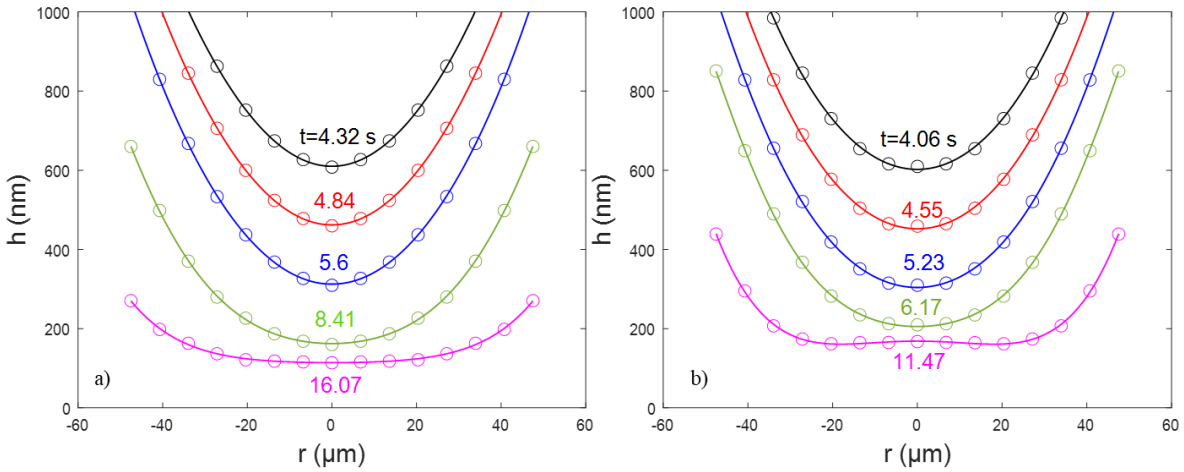

Figure 5.8 The spatiotemporal film profiles of an air bubble approaching the bare silica surface at pH 10 in a) water and b) 10-5M EDTA solution.

Figures 5.8 a and -b show the spatiotemporal profiles of the wetting film formed on the hydrophilic silica surface in water and 10^{-5} M EDTA at pH 10, respectively. In both cases, the wetting film thinned quickly initially at a film thickness of ~600 nm, while film thinning slowed down when the film thickness was below 200 nm. The reduction in the kinetics of film thinning was probably due to the repulsive surface forces operating in the wetting film, *i.e.*, repulsive van

der Waals (vdW) and electrical double layer (EDL) forces. As shown in Figure 5.8a, the center of the wetting film became flat as the air bubble approached to the silica surface and thinning stopped at an equilibrium film thickness (h_e) of 114 nm, at which the capillary pressure (p_c) is balanced by the disjoining pressure (Π) resulting a zero hydrodynamic pressure (p) according to Eq. [2]. In the presence of 10^{-5} M EDTA, a stable wetting film was formed at 11.47 s with h_e = 168 nm. Note here that h_e obtained with EDTA was higher than the same obtained with pure water, suggesting that the repulsive force, *i.e.*, EDL force, between air and silica became stronger when adding EDTA in the pure water. Note also that a dimple was observed at the end of film thinning in Figure 5.8b, which was also an indicator of strong repulsive force operating in the wetting film.

The spatiotemporal film profiles, *i.e.*, film thickness (h) as a function of time (t) and radial location (r), shown in Figure 5.8 were further used to calculate the $\partial h/\partial r$ and $\partial h/\partial t$ in Eqs. [1] and [3] to determine hydrodynamic (p) and capillary (p_c) pressures, respectively. The disjoining pressure isotherms ($\Pi(h)$) were then determined using Eq. [2] and plotted in Figure 5.9. As shown, Π became more and more positive with decreasing h, suggesting the repulsive force became stronger during the film thinning. The magnitude of positive Π obtained with 10^{-5} M EDTA was a

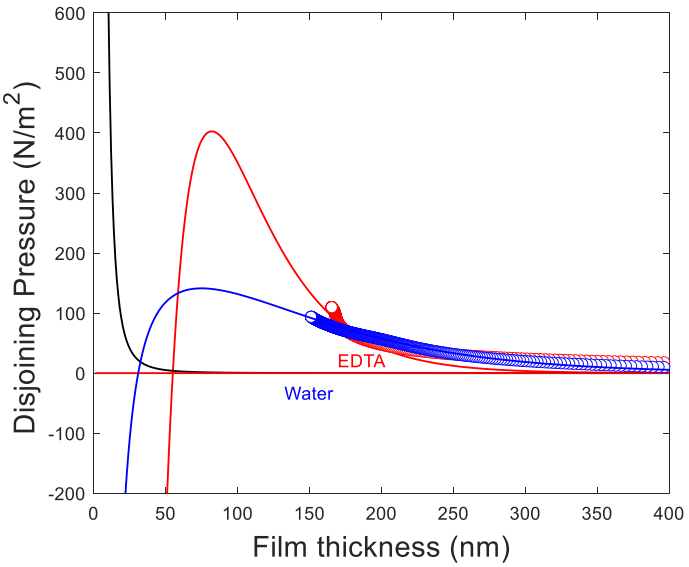

Figure 5.9 $\Pi(h)$ between air bubble and silica surface in pure water (blue) and 10^{-5} M EDTA (red). The points represented Π determined from the spatiotemporal film profiles. The curves represented Π calculated using the DLVO theory.

little higher than the one obtained with pure water, suggesting the repulsive force was stronger in the presence of EDTA.

To obtain a better understanding of the role of different surface forces, Π determined from the spatiotemporal profiles was further analyzed using DLVO theory (Eq. [4]), in which van der Waals force (vdW) (Πd) and electrical double-layer (EDL) (Π e) forces were considered. The surface force parameters used in the calculation are presented in Table 5.1. The Hamaker constant (A132) was determined using the combining rule and had a value of -1.2x10-20 J (Israelachvili, 2011). ζ-potentials (ψ1) of the silica surface were measured using Malvern Zetasizer, while the same of air bubbles (ψ2) were estimated based on the work published by Yoon and Yordan (1986).

Debye length (κ^{-1}) was determined by fitting the DLVO calculations to the experimental data. As shown in Figure 5.9, Π predicted using the DLVO theory (Eq. [4]) matched reasonably well with the same determined from Eq. [2]. A huge barrier was created in the presence of 10^{-5} M EDTA due to the repulsive EDL force, which was not shown in the pure water. This barrier kept the wetting film stable. It is, therefore, suggested that in the blunging process the dispersant may play the same role, *i.e.*, increase the repulsive EDL forces between clay particles and keep them dispersed, resulting in successful liberation.

Table 5.1 Surface force parameters used for calculating Π

Sample	Ψ_1* (mV)	Ψ_2† (mV)	κ^{-1} (nm)
Water	-125	-30	50
EDTA	-110	-51	40

A_{132} = -1.2×10^{-20} J; *Measured; †Estimated from Yoon and Yordan (1986); pH 10.

5.4.3 Characterization of Rare Earth Concentrate

The REE concentrate samples obtained from the HHS process were subjected to SEM and EDS characterizations. The SEM analysis aims to determine the type of REE-bearing minerals in this coal clay sample. Figure 5.10a shows an SEM image of an REE-bearing particle in the REE concentrate obtained in the HHS process. The total REE content in this concentrate was 1788 ppm.

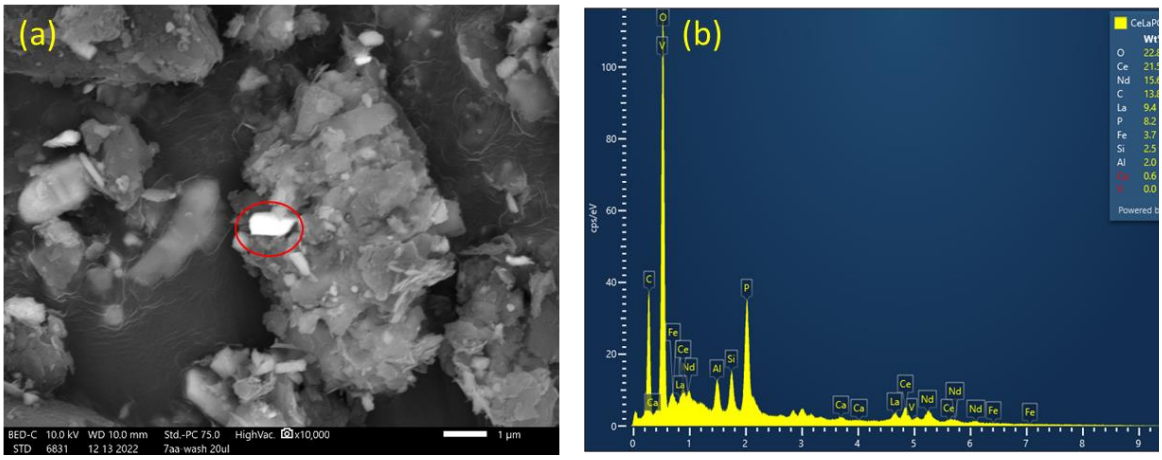

Figure 5.10 SEM image of a REE-bearing particle (a) and its corresponding EDS spectrum (b).

The corresponding EDS spectrum and elemental analysis were shown in Figure 5.10b. As shown, the particle contains 21.5% cerium (Ce), 15.6% neodymium (Nd), 9.4% lanthanum (La), and 8.2% phosphorous (P). Based on the EDS spectrum and elemental compositions, this REE-bearing particle is likely to be a monazite mineral with a chemical formula $(Ce,Nd,La)PO_4$. Note also that the REE-bearing particle has a particle size around 1 µm as shown in Figure 5.10a. The small particle size of REE-bearing particles may be one of the reasons for low REE recoveries in the HHS process as shown in Figures 5.5 and 5.6.

5.5 Conclusion

In the present work, we have developed a novel process that can be used to concentrate the rare earth elements (REEs) presented in the clayey materials. The process consists of two stages, dispersive liberation (blunging) and hydrophobic-hydrophilic separation (HHS) process. The former was used to improve the degree of liberation of REE-bearing particles, while the latter was used to recover the liberated REE-bearing particles with small particle size. This process has been validated by a series bench-scale blunging and HHS tests conducted on a clay sample obtained from a coal preparation plant. The results suggested that blunging could substantially improve the degree of liberation of REE-bearing particles at high pulp density and with right dispersants. A comparison between blunging and grinding has been evaluated. The results suggest that blunging was superior to grinding in the performance liberating REE-bearing particles. It is also found that the driving force for liberation in the blunging process is the repulsive electrical double layer force between clay particles, which implies that blunging should be more energy and cost efficient than

grinding. Lastly, the REE concentrates produced by this process have been characterized using SEM-EDS. Monazite was detected as the REE-bearing minerals in this clay sample.

Bibliography

Balaram, V. Rare earth elements: A review of applications, occurrence, exploration, analysis, recycling, and environmental impact. Geosci. Front. 2019,10, 1285–1303.

Bao, Z., Zhao, Z., 2008. Geochemistry of mineralization with exchangeable REY in the weathering crusts of granitic rocks in South China. Ore Geol. Rev. 33, 519–535.

Borst, A. M., Smith, M. P., Finch, A. A., Estrade, G., Villanova-de-Benavent, C., Nason, P., & Geraki, K. (2020). Adsorption of rare earth elements in regolith-hosted clay deposits. *Nature communications*, *11*(1), 1-15.

Binnemans, K., Jones, P., Blanpain, B., Gerven, T., Yang, Y., Walton, A., & Buchert, M. (2013). Recycling of Rare Earths: A Critical Review. Journal of Cleaner Production, 1-22.

Bryan, R. C., Richers, D., Andersen, H. T., & Gray, T. (2015). Assessment of rare earth elemental contents in select United States coal basins. *United States National Energy Technology Laboratory*.

Blissett RS, Smalley N, Rowson NA. An investigation into six coal fly ashes from the United Kingdom and Poland to evaluate rare earth element content. Fuel. 2014 Mar 1; 119:236-9.

Das, S., Gaustad, G., Sekar, A., & Williams, E. (2018). Techno-Economic Analysis of Supercritical Extraction of Rare Earth Elements from Coal Ash. *Journal of Cleaner Production*.

Ekmann, J. (2012). Rare Earth Elements in Coal Deposits - A Prospectivity Analysis. *Search and Discovery*.

Eskanazy, G. (1987). Rare Earth Elements and Yttrium in Lithotypes of Bulgarian Coals. *Org. Geochem.*, 83-89.

Espiritu, E. R. L., Naseri, S., & Waters, K. E. (2018). Surface chemistry and flotation behavior of dolomite, monazite and bastnäsite in the presence of benzohydroxamate, sodium oleate and phosphoric acid ester collectors. *Colloids and Surfaces A: Physicochemical and Engineering Aspects*, *546*, 254-265.

Feng, X., Onel, O., Council-Troche, M., Noble, A., Yoon, R. H., & Morris, J. R. (2021). A study of rare earth ion-adsorption clays: The speciation of rare earth elements on kaolinite at basic pH. *Applied Clay Science*, *201*, 105920.

Finkelman, R.B., Palmer, C.A., Wang, P., 2018. Quantification of the modes of occurrence of 42 elements in coal. Int. J. Coal Geol. 185, 138–160.

Foley, N., & Ayuso, R. (2015a). REE enrichment in granite-derived regolith deposits of the Southeastern United States: prospective source rocks and accumulation processes. *Geol. Surv. Pap*, *3*, 131-138.

Foley, N., Ayuso, R., Hubbard, B., Bern, C., & Shah, A. (2015b). Geochemical and mineralogical characteristics of REE in granite derived regolith of the Southeastern United States. In *Mineral resources in a sustainable world. Proceedings of the 13th Biennial SGA Meeting* (Vol. 2, pp. 725-729).

Huang, Q., Noble, A., Herbst, J., & Honaker, R. (2018). Liberation and Release of Rare Earth Minerals from Middle Kittanning, Fire Clay, and West Kentucky No. 13 Coal Sources. *Powder Technology*, 242-252.

Hu, J., Zheng, B., Finkelman, R., Wang, B., Wang, M., Li, S., & Wu, D. (2006). Concentration and Distribution of Sixty-One Elements in Coals from DPR Korea. *Fuel*, 679-688.

Hower, J., Granite, E., Mayfield, D., Lewis, A., & Finkelman, R. (2016). Notes on Contributions to the Science of Rare Earth Element Enrichment in Coal and Coal Combustion Byproducts. *Minerals*, 1-9.

Huang, Q., Talan, D., Restrepo, J., Baena, O., Kecojevic, V., & Noble, A. (2019). Characterization Study of Rare Earths, Yttrium, and Scandium from Various Colombian Coal Samples and Non-Coal Lithologies. *International Journal of Coal Geology*, 14-26.

Huang, K., & Yoon, R. H. (2019). Surface forces in the thin liquid films (TLFs) of water confined between n-alkane drops and hydrophobic gold surfaces. *Langmuir*, *35*(48), 15681-15691.

Hogg, R.; Healy, T.; Fuerstenau, D., Mutual coagulation of colloidal dispersions. Transactions of the Faraday Society 1966,62, 1638-1651.

Israelachvili, J. N., Intermolecular and surface forces: revised third edition. Academic press: 2011.

Jordens A, Cheng YP, Waters KE. A review of the beneficiation of rare earth element bearing minerals. Minerals Engineering. 2013 Feb 1; 41:97-114.

Karayigit, A., Gayer, R., Querol, X., & Onacak, T. (2000). Contents of Major and Trace Elements in Feed Coals from Turkish Coal-Fired Power Plants. *International Journal of Coal Geology*, 169-184.

Ketris, M., & Yudovich, Y. (2009). Estimations of Clarkes for Carbonaceous Biolithes: World Averages for Trace Element Contents in Black Shales and Coals. *International Journal of Coal Geology*, 135-148.

Lin, R., Soong, Y., & Granite, E. (2018). Evaluation of Trace Elements in U.S. Coals Using the USGS COALQUAL Database Version 3.0. Part I: Rare Earth Elements and Yttrium (REY). *International Journal of Coal Geology*, 1-13.

MacCormac, B. L. (2020). *Concentration and Recovery of Rare Earth Elements from Eastern US Coal Refuse* (Doctoral dissertation, Virginia Tech).

McLellan, B., Corder, G., Golev, A., & Ali, S. (2014). Sustainability of the Rare Earths Industry. *Procedia Environmental Sciences*, 280-287.

Moldoveanu, G.A., & Papangelakis, V.G. (2021). Chelation-Assisted Ion-Exchange Leaching of Rare Earths from Clay Minerals. *Metals*.

Oliva, P., Viers, J., & Dupré, B. (2003). Chemical weathering in granitic environments. *Chemical geology*, *202*(3-4), 225-256.

Pan, L.; Jung, S.; Yoon, R.-H., Effect of hydrophobicity on the stability of the wetting films of water formed on gold surfaces. Journal of colloid and interface science 2011,361(1), 321-330.

R.-H. Yoon, "Method for separating and de-watering fine particles," United States Patent 9,518,241, 2016.

Sanematsu, K., & Watanabe, Y. (2016). Characteristics and genesis of ion adsorption-type rare earth element deposits.

Seredin, V. (1996). Rare Earth Element-Bearing Coals from the Russian Far East Deposit. *International Journal of Coal Geology*, 101-129.

Sheludko, A. In Certain peculiarities of foam lamellas, Parts I− III, Proc. Koninkl. Ned. Akad. Wetenschap. B, 1962; pp 76-108.

USGS. (2022). Mineral Commodity Summary

Velde, B. B., & Meunier, A. (2008). *The origin of clay minerals in soils and weathered rocks*. Springer Science & Business Media.

Wills, B. A., & Finch, J. (2015). *Wills' mineral processing technology: an introduction to the practical aspects of ore treatment and mineral recovery*. Butterworth-heinemann.

Wang, L., Huang, X., Yu, Y., Zhao, L., Wang, C., Feng, Z., Long., Z. (2017). Towards Cleaner Production of Rare Earth Elements from Bastnaesite in China. Journal of Cleaner Production, 231-242.

Wagner, N., & Matiane, A. (2018). Rare Earth Elements in Select Main Karoo Basin (South Africa) Coal and Coal Ash Samples. *International Journal of Coal Geology*, 82-92.

Yang, X., Honaker, R., 2020. Leaching kinetics of rare earth elements from fire clay seam coal. Minerals 10.

Yoon, R.-H.; Yordan, J. L., Zeta-potential measurements on microbubbles generated using various surfactants. Journal of Colloid and Interface Science 1986,113(2), 430-438.

Zhang W, Honaker R, Groppo, J. Concentration of rare earth minerals from coal by froth flotation. Minerals & Metallurgical Processing. 2017 Feb 28, 34(3):132-137.

Zhang, W., & Honaker, R. (2017). Surface charge of rare earth phosphate (monazite) in aqueous solutions. *Powder Technology*, *318*, 263-271.

Zhang, W., & Honaker, R. (2018). Rare Earth Elements Recovery Using Stages Precipitation from A Leachate Generated from Coarse Coal Refuse. *International Journal of Coal Geology*, 189-199.

Zhang, J., Zhao, B., Schreiner, B., 2016. Rare Earth Beneficiation and Hydrometallurgical Processing, Separation Hydrometallurgy of Rare Earth Elements. Springer International Publishing, Cham, Switzerland, pp. 19-54.

Chapter 6. Conclusions & Original Contributions

6.1.1 Conclusions

The research conducted in this study helped improve our understanding of the behavior of rare earth elements (REEs) adsorbed onto clays, and helped us develop new approaches to extract them into solution. The studies significantly extended our understanding of the nature of ion-adsorption clays and helped us develop more efficient extraction processes.

It has been found that REE ions adsorbed on the surface of kaolinite surface at pH < 7 can be readily extracted into solution by an ion-exchange mechanism using $(NH_4)_2SO_4$ lixiviant. At pH >7, the REE ions adsorb on the clay mineral surface as hydroxo-complexes or as colloids. However, they can be readily extracted into solution at pH below 7 *via* an ion-exchange leaching mechanism using ammonium sulfate $(NH_4)_2SO_4$ as lixiviant.

During the examination of co-adsorption of REEs and Fe onto kaolinite at basic pH conditions, we found that the adsorbed iron forms FeOOH, which impede the ion-exchange mechanism. It has been discovered, however, that the passivating species can be dissolved away at pH <7 in the presence of a reducing agent. This treatment made it possible to extract the REEs using $(NH_4)_2SO_4$ as lixiviant.

While $(NH_4)_2SO_4$ is recognized as the best lixiviant for ion-adsorption clays, its driving force for ion-exchange leaching is the difference in hydration enthalpies between those of Ln^{3+} and NH_4^+ ions, which are in the range of 3,000 kJ/mole. In the present work, we used alkylammonium ions with varying chain lengths ($C_nH_{2n}NH_4^+$) as noble lixiviants. It has been found that these reagents gave comparable results with those obtained by using $(NH_4)_2SO_4$ as lixiviant. A rationale for using these reagents was that the hydrocarbon chains would facilitate the movement of these reagents toward the clay mineral surface and improve the kinetics. In general, the longer the hydrocarbon chain lengths, the higher the kinetics of ion-exchange leaching. The best results were obtained using hexadecyltrimethylammonium chloride (HTAC).

A novel process of reducing the cost of REE extraction has been developed. In this process, we subjected a coal byproduct to blunging to liberate REE-bearing minerals (*e.g.*, monazite) from clay materials and subsequently increase the population density of the liberated REE-bearing minerals using the hydrophobic-hydrophilic separation (HHS) process. Extracting REEs from the

higher-grade REE concentrate would greatly reduce the cost of extracting REEs from coal byproducts and minimizing waste products.

The SEM-EDS examination of the HHS products showed substantially higher population of REE-bearing minerals.

Surface force measurements were conducted on a silica surface in the presence and absence of a polyelectrolyte. The results showed that the role of polyelectrolyte in blunging is to increase the energy barrier created by the electrical double-layer (EDL) force.

6.1.2 Original Contributions

- REE speciation on clay surfaces was determined as REE-Hydroxides at alkaline pH values which is the colloidal phase. To address this problem ion-exchange leaching was applied at ~ pH 5 and the colloidal phase was extracted by ion-exchange leaching method with ~80-90 % recovery values.
- In the presence of Fe, the Ln^{3+} species on the clay surface were identified as REE-Fe-OOH. The results show that REEs can be readily passivated in the presence of Fe^{3+} and created a colloidal phase on the clay surface. Methods for overcoming the harmful effects of such species were investigated and results show that reductive leaching is a highly effective method to solve the negative effect of Fe.
- The results of the ion exchange leaching experiments using novel lixiviants were compared with those obtained using the conventional lixiviant, i.e., NH_4^+ ions. The findings revealed that the novel lixiviants can serve as a viable alternative to NH_4^+ ions, achieving comparable recovery rates of approximately 80% but at ten times lower concentrations.
- It has been proved that a comparison between blunging and grinding demonstrates the superior performance of blunging in liberating REE-bearing particles. The study also reveals that the repulsive electrical double layer force between clay particles drives the liberation process in blunging, suggesting that it is a more energy and cost-efficient alternative to grinding.